Modification of Multiwall Carbon Nanotubes

by *grafting from* Controlled Polymerization

and their Dispersion in a Block Copolymer Matrix

Dissertation

zur Erlangung des akademischen Grades

Doktor der Ingenieurwissenschaften

(Dr. -Ing.)

der Technischen Fakultät

der Christian-Albrechts-Universität zu Kiel

Julio Albuerne

Kiel

2009

1. Gutachter	Prof. Dr. Volker Abetz
2. Gutachter	Prof. Dr. Rainer Adelung
3. Gutachter	Dr. Mady Elbahri
Datum der mündlichen Prüfung	14.12.2009

Table of Contents

			Page
Table of Content…….....			**i**
List of Tables…….....			**iv**
List of Figures……..			**v**
Chapter 1	**Introduction**……...		**1**
Chapter 2	**Theoretical Background**……...		**9**
2.1	Carbon Nanotubes……..….		**9**
	2.1.1	Introduction……	**9**
	2.1.2	Synthesis…….	**11**
		2.1.2.1 Arc discharge and laser ablation……	**11**
		2.1.2.2 Chemical vapor deposition…….	**13**
	2.1.3	Properties of carbon nanotubes……...	**14**
	2.1.4	Chemistry of carbon nanotubes……..	**17**
		2.1.4.1 *Grafting onto* carbon nanotubes…….	**19**
		2.1.4.2 *Grafting from* carbon nanotubes…….....	**22**
		2.1.4.3 Other reactions……...	**27**
	2.1.5	Health considerations…….....	**28**
2.2	Atom Transfer Radical Polymerization (ATRP)…….		**31**
2.3	Block Copolymer…….....		**35**
2.4	Nanocomposites based on Block Copolymers……		**39**
2.5	References……...		**43**
Chapter 3	**Experimental Part**……		**47**
3.1	Materials…….....		**47**
3.2	Surface functionalization of multiwall carbon nanotubes……...		**48**
	3.2.1	Oxidation of MWCNTs……..	**48**
	3.2.2	Acid to Acid Chloride Conversion and Esterification I: Glycol Spacer.....	**49**
	3.2.3	Anchoring of initiator groups…….	**50**
	3.2.4	*Grafting from* styrene under atom transfer radical polymerization (ATRP) conditions…….....	**51**
3.3	Preparation of the nanocomposite films……..		**53**
3.4	Characterization……...		**54**
	3.4.1	Size Exclusion Chromatography (SEC)…….....	**54**
	3.4.2	Elemental Analysis…….	**55**
	3.4.3	Nuclear Magnetic Resonance Spectroscopy (^{1}H-NMR)……	**55**
	3.4.4	Fourier transform infrared Spectroscopy (FTIR)……...	**55**
	3.4.5	Thermogavimetric analysis (TGA)…….....	**56**
	3.4.6	Differential Scanning Calorimetry (DSC)…….....	**56**
	3.4.7	Optical Microscopy (OM)……..	**56**
	3.4.8	Scanning Electron Microscopy (SEM)……...	**56**
	3.4.9	Transmission Electron Microscopy (TEM)……...	**57**
	3.4.10	TappingMode^{TM} Atomic Force Microscopy……..	**57**
	3.4.11	AC conductivity measurements……..	**58**
	3.4.12	Dynamical Mechanical Thermal Analysis (DMTA)……..	**58**
	3.4.13	Viscosity measurements…….	**58**
	3.4.14	Strain-stress experiments……	**58**

	3.4.15 Simultaneous Small Angle X-ray Scattering (SAXS) and strain-stress experiments…….	**59**
3.5	References……...	**59**
Chapter 4	**Modification of Multiwall Carbon Nanotubes by *Grafting from* Controlled Polymerization of Styrene: Effect of the Characteristics of the Nanotubes**……	**61**
4.1	Introduction…….	**61**
4.2	Results and Discussion……	**63**
	4.2.1 Oxidation of the MWCNTs……	**63**
	4.2.2 Acid to Acid Chloride Conversion and Esterification I: Glycol Spacer…….	**66**
	4.2.3 Esterification II: ATRP Initiator…….	**72**
	4.2.4 ATR Polymerization…….....	**75**
4.3	Conclusions…….....	**83**
4.4	References……...	**84**
Chapter 5	**Block Copolymer Nanocomposites based on $MWCNT_{BMS}$[95]: Effect of the Functionalization of Multiwall Carbon Nanotubes on the Morphology of the Block Copolymer**……..	**87**
5.1	Introduction…….	**87**
5.2	Results and Discussions……..	**89**
	5.2.1 Characteristic of the carbon nanotubes grafted with polystyrene……..	**89**
	5.2.2 Morphology of the nanocomposites……...	**91**
	5.2.3 Mechanical Properties of the nanocomposites……...	**100**
	5.2.4 Thermal properties of the nanocomposite……..	**103**
	5.2.5 Morphology of the nanocomposites: behavior of the carbon nanotubes in the block copolymer under an applied deformation…….	**104**
5.3	Conclusions…….	**110**
5.4	References……...	**111**
Chapter 6	**Block Copolymer Nanocomposites based on $MWCNT_{FC}$[99]: Effect of the Functionalization of the Multiwall Carbon Nanotubes and the film preparation on the Morphology and Properties of the Nanocomposites**…….	**113**
6.1	Introduction…….	**113**
6.2	Results and Discussions……..	**114**
	6.2.1 Characteristic of the carbon nanotubes after the oxidation and the *grafting from* polymerization reactions……	**114**
	6.2.2 Optical dispersion of the carbon nanotubes in the nanocomposites: effect of the fractionation of the carbon nanotubes and the casting temperature……...	**117**
	6.2.3 Thermal properties of the nanocomposites…….	**120**
	6.2.4 Morphology of the AS-SB_{26}: effect of the casting temperature.	**122**
	6.2.5 Mechanical properties of the nanocomposites……	**124**
	6.2.6 Morphology of the nanocomposites: effect of the carbon nanotubes and the casting temperature in the block copolymer microstructure…….	**129**
	6.2.7 Electrical properties of the nanocomposites……...	**133**
6.3	Conclusions…….	**136**
6.4	References……...	**138**

Chapter 7 Summary…… **139**
Chapter 8 Acknowledgments…….. **143**
APPENDIX……... **145**
List of Publications…….. **147**

List of Tables

		Page
Chapter 3		
Table 3.1	Experimental conditions employed for the esterification with glycols and 2BriBr of $MWCNT_{BMS}^{95}$ and $MWCNT_{FC}^{99}$……...	**50**
Table 3.2	Experimental conditions employed for the styrene *grafting from* reaction at $MWCNT_{BMS}^{95}$ and $MWCNT_{FC}^{99}$……...	**52**
Chapter 4		
Table 4.1	Viscosity of the dispersion of carbon nanotubes in ethylene glycol (1 % wt/v). Values obtained at 500 s^{-1}……	**72**
Table 4.2	Concentration of initiator groups after the esterification reaction of hydroxyl functionalized carbon nanotubes……	**73**
Table 4.3	Conditions and polymer content on the styrene *grafting from* reaction on $MWCNT_{BMS}^{95}$ and $MWCNT_{FC}^{99}$……...	**76**
Chapter 5		
Table 5.1	Molecular and thermal characterization of the polystyrene grafted carbon nanotubes prepared by *grafting from* polymerization……	**90**
Table 5.2	Mechanical and thermal properties of the $MWCNT_{BMS}^{95}$/AS-SB_{26} nanocomposites……..	**101**
Chapter 6		
Table 6.1	Molecular and thermal characterization and recovery after the centrifugation of the dispersed nanoparticles of the acid treated and polystyrene grafted $MWCNT_{FC}^{99}$…….	**115**
Table 6.2	Glass transition temperatures of the polystyrene microphase of the AS-SB_{26} and its nanocomposites……..	**121**
Table 6.3	Mechanical properties of the nanocomposite as a function of the casting temperature…….	**125**

Figure Caption

Page

Chapter 1

Figure 1.1 Number of publications (**J**ournal, **R**eview, **L**etters, **P**reprints), patents, conference abstracts and books vs. publication year related with the carbon nanotube research……... **3**

Chapter 2

Figure 2.1 **(**a) Geometry of a graphene sheet using a coordinate system based on the unit vectors $\vec{a}$ and $\vec{b}$. The highlighted points (orange) indicate the integers for metallic nanotubes. (b)-(d) Examples of SWCNT with different (n, m) structures: (b) zig-zag (10,0), (c) arm chair (7,7) and (d) achiral (10,5)……. **10**

Figure 2.2 Sketches of the experimental setups for the synthesis of carbon nanotubes following the (a) arc-discharge and (b) laser ablation methods…….. **11**

Figure 2.3 Sketch of the experimental setup for the synthesis of carbon nanotubes using the CVD method……..... **13**

Figure 2.4. Correlation between the measured Young's modulus of MWCNTs and the amount of disorder (defects) present within the walls…… **15**

Figure 2.5 Schematic representation of the *grafting onto* approach on carbon nanotubes…… **20**

Figure 2.6 Schematic representation of the *grafting onto* approach on carbon nanotubes of polymers with functional groups along their backbone…….. **22**

Figure 2.7 Schematic representation of the *grafting from* approach from carbon nanotubes…… **23**

Figure 2.8 General mechanism of ATR polymerizations……. **32**

Figure 2.9 Schematic representation of the dependence of the conversion against time on linear and semilogarithmic scale…… **35**

Figure 2.10 Morphology and the expected mechanical properties for different styrene based block polymers……..…… **37**

Figure 2.11. Mechanical properties of multigraft copolymers compared with commercial TPEs Kraton (20 % v/v of polystyrene) and Styroflex (58 % v/v of polystyrene)…….… **38**

Figure 2.12 TEM image of PS grafted MWCNT sequestered in a polystyrene-*block*-polyisoprene diblock copolymer. The polyisoprene phase was stained with OsO_4…… **43**

Chapter 3

Figure 3.1 SEC trace of the AS-SB_{26}……... **48**

Figure 3.2 Schematic representation of the oxidation reaction carried out on the MWCNTs…… **49**

Figure 3.3 Schematic representation of the oxidation reaction between oxidized $MWCNT_x^y$ with thionyl chloride and ethylene glycol/poly(ethylene glycol)……. **50**

Figure 3.4 Schematic representation for the anchoring of initiator groups for ATR polymerization…… **51**

Figure 3.5 Schematic representation for the *grafting from* reaction of polystyrene…… **52**

Figure 3.6 Film casting strategy employed in Chapter 5……. **53**
Figure 3.7 Film casting strategy employed in Chapter 6……. **54**

Chapter 4
Figure 4.1 Fourier transform infrared spectra of multiwall carbon nanotubes from different sources before and after the oxidation reaction: (a) pristine and (b) oxidized $MWCNT_{BMS}^{95}$, (c) pristine and (d) oxidized $MWCNT_{FC}^{99}$……..... **64**
Figure 4.2 Transmission electron micrographs of (a) pristine and (b) oxidized $MWCNT_{BMS}^{95}$. Scale bar = 100 nm, insert = 10 nm……... **66**
Figure 4.3 Glycol grafting content (left axes, filled symbols) and concentration of hydroxyl groups (right axes, open symbols) vs. glycol molecular weight for $MWCNT_{BMS}^{95}$ (●, ○) and $MWCNT_{FC}^{99}$ (■, □)……... **67**
Figure 4.4 Carbon nanotube length distribution (nm) of (a) pristine MWCNTs and (b) oxidized MWCNTs, calculated from SFM phase images. Filled bars (black) correspond to $MWCNT_{BMS}^{95}$ and contour bars (orange) correspond to $MWCNT_{FC}^{99}$……... **68**
Figure 4.5 Infrared spectra of multiwall carbon nanotubes from FutureCarbon GmbH after different sequential modification steps (a) PEG_{400} grafted $MWCNT_{FC}^{99}$, (b) $MWCNT_{FC}^{99}$-Br^4, (c) $PS_{44}{}^3MWCNT_{FC}^{99}$ and (d) $PS_{85}{}^{24}MWCNT_{FC}^{99}$……. **72**
Figure 4.6 Length distribution (nm) for MWCNTs after the grafting of the ATRP initiator…… **74**
Figure 4.7 H^1NMR spectra of the polystyrene grafted carbon nanotube $PS_{91}{}^{20}MWCNT_{BMS}^{95}$……... **78**
Figure 4.8 Scanning and transmission (inserts) electron micrographs of PS grafted MWCNT, synthesized under the conditions indicated in Table 3.2 (a) $PS_9{}^1MWCNT_{FC}^{99}$, (b) $PS_{44}{}^3MWCNT_{FC}^{99}$, (c) $PS_{47}{}^{11}MWCNT_{BMS}^{95}$, (d) $PS_{70}{}^4MWCNT_{BMS}^{95}$ and (e) $PS_{91}{}^{20}MWCNT_{BMS}^{95}$. TEM scale bar = 20 nm….. **79**

Chapter 5
Figure 5.1 Selected scanning electron micrographs of the cryogenic fracture cross sections of: (a) $AS\text{-}SB_{26}$, (b) $MWCNT_{BMS}^{95}/AS\text{-}SB_{26}$, (c) $PS_{47}{}^{11}MWCNT_{BMS}^{95}/AS\text{-}SB_{26}$, (d) $PS_{70}{}^4MWCNT_{BMS}^{95}/AS\text{-}SB_{26}$ and (e) $PS_{91}{}^{20}$ $MWCNT_{BMS}^{95}/AS\text{-}SB_{26}$. The content of the carbon nanotubes is approximately 1 wt %. The samples were sputtered with a layer of Au/Pd….. **93**
Figure 5.2 Selected transmission electron micrographs (stained with OsO_4; black: polybutadiene, gray: polystyrene) of: (a) $AS\text{-}SB_{26}$, (b) $MWCNT_{BMS}^{95}/AS\text{-}SB_{26}$, (c) $PS_{47}{}^{11}MWCNT_{BMS}^{95}/AS\text{-}SB_{26}$, (d) $PS_{70}{}^4MWCNT_{BMS}^{95}/AS\text{-}SB_{26}$ and (e) $PS_{91}{}^{20}MWCNT_{BMS}^{95}/AS\text{-}SB_{26}$. The carbon nanotubes are highlighted. Ultra thin sections were obtained from the nanocomposite films. Scale bar = 100 nm…… **95**
Figure 5.3 Representative sketch of the simultaneous 2D-SAXS/stress-strain measurements…….. **105**
Figure 5.4 Orientation factor (P_2) versus δ (%) for the different $MWCNT_{BMS}^{95}/AS\text{-}SB_{26}$ nanocomposites……... **106**
Figure 5.5 Transmission electron micrographs of (a) $MWCNT_{BMS}^{95}/AS\text{-}SB_{26}$, (b) and (c) $PS_{91}{}^{20}MWCNT_{BMS}^{95}/AS\text{-}SB_{26}$ after the stress-strain experiments. Ultra thin cuts were obtained from the films embedded in an epoxy resin. The samples are not stained. The arrows indicate the direction of the applied deformation……..... **109**

Figure 5.6 Sketch of the deformation process of the $PS_{91}{}^{20}MWCNT/AS\text{-}SB_{26}$ nanocomposites (a) before and (b) after the strain-stress experiments……... **110**

Chapter 6

Figure 6.1 Optical microscopy images of the 0.1 wt % carbon nanotubes/$AS\text{-}SB_{26}$ films prepared at different casting temperatures: (a), (b) and (c) $^{oxid}MWCNT_{FC}{}^{99}$; (d) and (e) $PS_{14}{}^{2}MWCNT_{FC}{}^{99}$; (f) and (g) $PS_{85}{}^{24}MWCNT_{FC}{}^{99}$. The casting temperatures are indicated on the images. Scale bar = 20 µm…….…… **119**

Figure 6.2 Differential scanning calorimetry scans (first heating runs, 20°C/min, N_2) of the nanocomposites films prepared at 60 °C……... **122**

Figure 6.3 Transmission electron micrographs (stained with OSO_4; black; polybutadiene, gray; polystyrene) of the $AS\text{-}SB_{26}$ cast at (a) 60 °C and (b) 90 °C. Ultra thin sections were obtained at approximately -120 °C. Scale bar = 200 nm. (c) Lamellae thickness distribution of the $AS\text{-}SB_{26}$ at the indicated casting temperatures. The solid lines are the Gaussian distribution estimations of the lamellae thickness……... **124**

Figure 6.4 Selected scanning electron micrographs of the cryogenic fracture cross sections of the 0.5 wt % carbon nanotubes/$AS\text{-}SB_{26}$ films prepared at different casting temperatures: (a) and (b) $^{oxid}MWCNT_{FC}{}^{99}$; (c) and (d) $PS_{22}{}^{4}MWCNT_{FC}{}^{99}$; (e) and (f) $PS_{85}{}^{24}MWCNT_{FC}{}^{99}$; The casting temperatures are indicated on the images……. **128**

Figure 6.5 Transmission electron micrographs (stained with OSO_4; black; polybutadiene, gray; polystyrene) of the 0.5 wt % carbon nanotubes/$AS\text{-}SB_{26}$ films prepared at different casting temperatures: (a) and (b) $^{oxid}MWCNT_{FC}{}^{99}$; (c) and (d) $PS_{14}{}^{2}MWCNT_{FC}{}^{99}$; (e) and (f) $PS_{85}{}^{24}MWCNT_{FC}{}^{99}$. Ultra thin sections were obtained at approximately -120 °C. The casting temperatures are indicated on the images. Scale bar = 200 nm…….. **131**

Figure 6.6 Electrical conductivities measurements of the samples containing (a) 0.1 wt% and (b) 0.5 wt% of the different functionalized $MWCNT_{FC}{}^{99}$. (c) Electrical conductivities at 1 MHz, filled points indicate the films casted at 60 °C, contour points represent the films casted at 90 °C…….. **134**

APENDIX

Figure A.1 Model of carbon nanotubes……. **145**

Chapter 1. Introduction

Nowadays, polymers are of paramount importance on the development of new consumable products. The advantages of polymers over metal or ceramic based materials arise from the low production cost and the relative easy processability, which allows the creation of almost every imaginable form. The polymers have unique molecular definable properties due to the wide variety of structure, molecular weights, and functionalities available by different synthesis processes. According to the 2006 annual report of the European Union (EU), the chemical, rubber and plastic manufacturing sector of the EU countries generated €250 billion of added value in 2004. This number corresponds to 28.4% of the world market, just overcome by Asia. Among the EU countries, Germany is the principal producer of chemicals, rubbers and plastics. Particularly, the manufacturing of plastics and rubbers generated more than €75 billion of the reported added value. The products are focused in sectors related with packaging, construction and automotive applications.

Unfortunately, for certain applications, polymers are not able to substitute other materials like metals or ceramics due to their poorer mechanical properties, electric and thermal conductivity, thermal stability or fire resistance. Nevertheless, some of the shortcomings properties could be overcome through the addition of small quantities of fillers based on metals, glass, silica or carbon. The nature of the filler and the interaction with the polymer matrix determine the extent of improvement of the target property. The fillers are also classified according to their sizes and dimensions, where the most commonly used are the micron size fillers (microfillers). Microfillers refer to fillers where at least one of the dimensions is on the micrometer range.

Examples are the polyaramide and the carbon fibers used as mechanical reinforcers in epoxy resins for the fabrication of storage tanks. The drawback is that high contents of filler (30 to 40 wt %) are necessary to improve the stiffness of the material, which increases the weight, the brittleness, and worsens the surface finish of the compose material.

In this sense, the improvement of the properties of polymer based systems has been also achieved by the incorporation of fillers with smaller dimensions. These fillers are known as nanofillers. The nanofillers are defined as fillers that have at least one of their dimensions in the nanometer scale. Clay sheets (layered silicates), silica nanospheres, carbon based nanofibers or graphenes are common examples. Lower contents of the nanofillers are usually required (0.0025 to 5 wt %) to obtain polymer based materials with superior properties than with the use of microfillers. The main feature of nanofillers is their large surface-to-volume ratios compared with larger particles like microfillers. For example, the surface-to-volume ratio of a nanometer side cube is thousand times higher than in the case of a micrometer size cube.[1] These dimensions, comparable with the persistence length of a polymer chain, may further lead to significantly different properties and have initiated research and development activities known as “Nanoscience” and “Nanotechnology”.

Attention has been brought to the study of polymer nanocomposites based on nanospheres or layered silicates, especially for the improvement of the mechanical properties and the flammability resistance. Relative few works have been published about another upcoming class of nanofillers, which are known as carbon nanotubes. The carbon nanotubes are cylindrical graphite-like structures characterized by

diameters in the nanometer range and lengths of up to several micrometers. This confers a tremendous aspect ratio compared with spherical particles like fullerenes. The stiffness of the carbon nanotubes is predicted in the range of several TPa, making them interesting candidates for the manufacturing of polymer composites that might replace other commodity materials, like metal alloys.[2] Moreover, the graphitic structure allows the carbon nanotubes to conduct electricity, which makes them useful in applications where electrostatic discharges may cause damage to the environment. The carbon nanotubes can also increase the thermal conductivity of the typically isolating polymers. The increasing interest on the studies of carbon nanotubes can be observed by the incredible progression on the number of publications in journals, patents, conference abstracts and books (see Figure 1.1), since the first description of the carbon nanotubes by Ijima in 1991.[3]

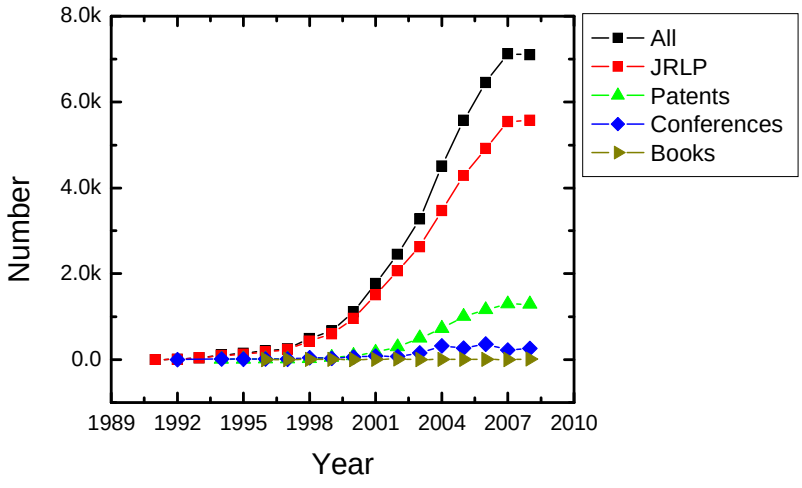

Figure 1.1. Number of publications (**J**ournal, **R**eview, **L**etters, **P**reprints), patents, conference abstracts and books vs. publication year related with the carbon nanotube research (source: Scifinder Scolar®).

The publications focused on carbon nanotubes have specially increased since the beginning of the twenty first century. Surprisingly, the works related with carbon nanotubes embedded in polymer matrices represent only 13% of the released publications and patents. One of the most recurrent problems attributed to the design

of composites based on carbon nanotubes is the difficulty to disperse these fillers in a polymer matrix. The rest of catalyst from the synthesis of the carbon nanotubes and the strong π-π stacking interaction between graphene sheets are the usually given reasons. The mass production of goods containing carbon nanotubes is nowadays limited due to these problems. For this reason, different strategies have been adopted for the improvement of the dispersion of these nanoparticles. Among these strategies, the grafting of polymer chains has shown good results regarding the dispersion of the carbon nanotubes in organic solvents and in some polymer matrices. However, the conclusions from these works are very limited because the purity and dimension of the carbon nanotubes depends mostly on the manufacturer (not on the manufacturing process). Several disagreements can be found in the literature regarding the grafting content and the molecular weight of the polymers using comparable reaction conditions but different sources of carbon nanotubes. These discrepancies open a series of questions that are important to be answered in order to clarify the limitations and advantages of these newcomer nanofillers: which factors regarding the characteristics of the carbon nanotubes (purity, dimensions, manufacturer) influence the surface grafting of polymer?, is it possible to control the polymer grafted independent of the source of the carbon nanotubes?, is it possible to describe a relation between the grafting of polymer from the carbon nanotubes taking into account only their dimension and carbon purity?.

Additionally, the anisotropic nature of these nanoparticles could represent an advantage if composites with anisotropic properties on the nanoscale are desired. The anisotropic reinforcement of a polymer could be then achieved by the appropriate functionalization of the carbon nanotubes, the preparation of the composite, or by the

selection of a polymer matrix that could induce the segregation of the nanoparticles. In this concern, block copolymers are potential candidates. Block copolymers are macromolecules that comprise two or more polymers covalently linked. The sequence, the affinity and the chain architecture of the constituent polymer chains determine the properties of the copolymer. The incompatibilities within polymer chains in the block copolymer lead to the assembly of the constituent blocks in different domains in the nanometer range. The importance of the block copolymer has been increasing during the last years, especially in areas related with medicine and water purification.

The ability of the block copolymers to selectively segregate sphere like nanoparticles has been used on the design of nonlinear optical materials, photonic crystals or magnetic composites.[4] In most of the cases, the size and the functional groups at the surface of the sphere like nanoparticle drive its segregation in the block copolymer matrix. The selective sequestering of carbon nanotubes in block copolymers is a more challenging task, because the length of the nanoparticle is approximately three orders of magnitude higher than the domain size of any known available block copolymer and the irregularity of the tubular structure limits its segregation in the polymer matrix. This challenge leads to different interrogations: which factors influence the preferential interaction of the carbon nanotube with one microdomain in a block copolymer?, can the carbon nanotubes induce the microphase separation of the block copolymer? and, if this is true, how is the morphology of the block copolymer affected by the shape of the carbon nanotubes?

The motivation of the present doctoral work is to discuss these open questions in a real scenario, i.e., taking into account commercially available carbon nanotubes and block copolymers. The goal of this work is to establish a common criterion for the functionalization of carbon nanotubes and on the understanding of the factors that govern the selective dispersion of carbon nanotubes in block copolymer matrices. The control on the selectivity of the carbon nanotubes and other high aspect ratio nanofillers in polymer matrices might lead to the creation of a fascinating new generation of materials, where their properties could be tuned at the nanoscale.

This doctoral work is organized as follows: in Chapter 2 a theoretical background gives some specific aspects regarding the process of synthesis and the properties of carbon nanotubes, the polymer surface grafting reactions on carbon nanotubes, basic concepts of block copolymer, and the actual status related with the nanocomposites based on carbon nanotubes. Chapter 3 details the experimental procedures employed for the polymer functionalization of the carbon nanotubes and the preparation of nanocomposites with a commercial block copolymer, as well as details regarding the characterization of the materials. The discussion of the work is divided in three chapters. On these chapters, a brief introduction is given related to the specific topic of study. Chapter 4 describes the different functionalization reactions until the polymer *grafting from* the surface of the two carbon nanotubes used, and compares them based on their characteristics. Chapter 5 and 6 are devoted to the preparation of nanocomposites composed of two types of carbon nanotubes obtained from different sources and a commercial block copolymer, and discuss the properties of the material as a function of the polymer grafting and the characteristics of the carbon nanotubes

along with the preparation of the nanocomposite. Finally, chapter 7 summarizes the conclusions obtained during these investigations.

1.1. References

1. Vollath, D. Nanomaterials, An Introduction to Synthesis, Properties and Applications; Wiley-VCH Verlag GmbH & Co. KGaA: Weinheim, 2008.
2. Schaefer, D. W.; Justice, R. S. Macromolecules 2007, 40, 8501-8517.
3. Iijima, S. Nature 1991, 354, 56-58.
4. Bockstaller, M. R.; Mickiewicz, R. A.; Thomas, E. L. Adv. Mater. (Weinheim, Ger.) 2005, 17, 1331-1349.

Chapter 2. Theoretical Background

2.1. Carbon Nanotubes

2.1.1. Introduction

Carbon nanotubes (CNTs) are defined as hollow cylinders of concentric graphite layers.[1] They have been considered as single molecules due to their dimensions (~nm in diameter and ~μm in length), or as quasi-one dimensional crystals with translational periodicity along the tube axis.[2] The carbon nanotubes are generally classified according to the number of graphene layers: single wall carbon nanotube (one roll up graphene, SWCNT), double wall carbon nanotube (two concentric roll up graphene cylinders, DWCNT), and multiwall carbon nanotube (three or more graphene sheets, MWCNT).

The electronic properties of the carbon nanotubes are closely related with the structure of the graphene, which is shown in Figure 2.1. The layer of graphene is described using a coordinate system with the unit vectors $\vec{a}$ and $\vec{b}$. The vector describing a carbon nanotube is called the "chiral vector" $\vec{c} = n\vec{a} + m\vec{b}$, where n and m are integers which describe the length of the coordinates in the directions $\vec{a}$ and $\vec{b}$. The chiral vector ($\vec{c}$) defines the circumference of the carbon nanotube. Two types of chiral vectors provide the carbon nanotube with a specific arrangement of the carbon atoms; these are called "zig-zag nanotubes" $\vec{c} = (n,0)$ and "armchair nanotubes" $\vec{c} = (n,n)$. It is also possible to calculate the diameter of a carbon nanotube with the integers using the following equation:

$$d = \frac{\sqrt{3}}{\pi} l_{c-c} \left(n^2 + m^2 + nm\right)^{0.5} \qquad \text{Eq. 2.1}$$

where $l_{c\text{-}c}$ = 0.14 nm is the distance between two neighbor carbon atoms.[1,3,4]

The chiral angle, this means, the angle between the vectors $\vec{a}$ and $\vec{c}$, is given by:[2]

$$\delta = \arctan\left[\sqrt{3}\frac{m}{2n+m}\right] \qquad \text{Eq. 2.2}$$

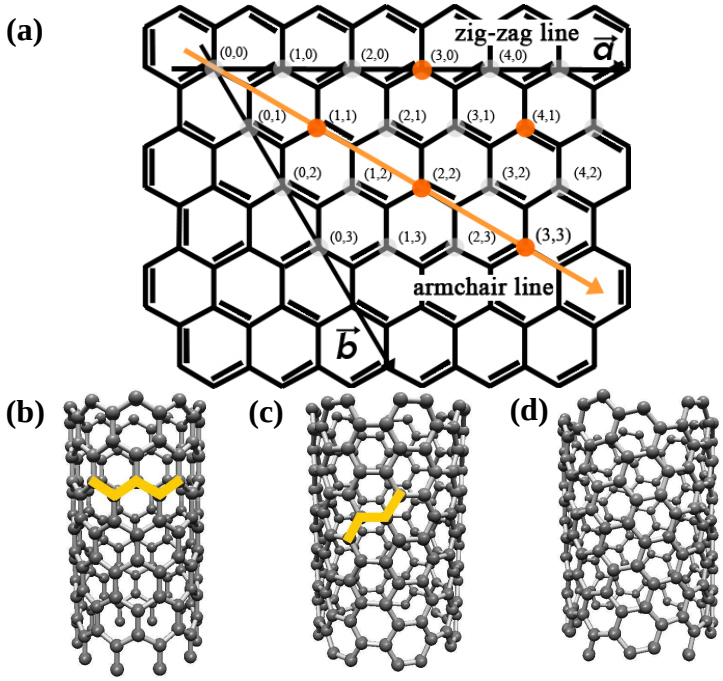

Figure 2.1. (a) Geometry of a graphene sheet using a coordinate system based on the unit vectors $\vec{a}$ and $\vec{b}$. The highlighted points (orange) indicate the integers for metallic nanotubes. (b)-(d) Examples of SWCNT with different (n, m) structures: (b) zig-zag (10,0), (c) arm chair (7,7) and (d) achiral (10,5).[1-4]

The chiral angle for armchair nanotubes is 30° and for zig-zag ones is 0°. Single wall carbon nanotubes (SWCNTs) with a chirality vector that fulfills the condition $\frac{2n+m}{3} = q = \text{integer}$ show metallic electrical conductivity.[2] In the case of double wall carbon nanotubes (DWCNTs) and multiwall carbon nanotubes (MWCNTs), the

control of the chirality along the graphene layers is complicated. For this reason, it is difficult to classify these carbon nanotubes according to their chirality.

2.1.2. Synthesis

Different methods for the production of multiwall carbon nanotubes (MWCNTs) have been published over the past 15 years. Among them, the most successful methods are the arch-discharge, the laser ablation, and the chemical vapor deposition.

2.1.2.1. Arc discharge and laser ablation

The arc-discharge and laser ablation were the first successful methods used for the production of carbon nanotubes in gram scales. They consist of the condensation of hot gaseous carbon atoms generated from the evaporation of solid carbon.[5,6] Both methods are sketched in Figure 2.2.

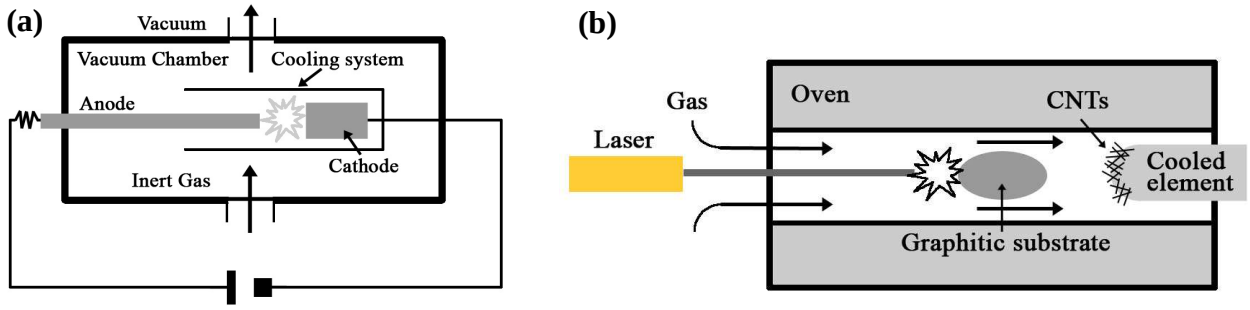

Figure 2.2. Sketches of the experimental setups for the synthesis of carbon nanotubes following the (a) arc-discharge and (b) laser ablation methods.

The synthesis of carbon nanotubes by the arc-discharge method consists in the evaporation of carbon atoms from the anode using plasma of an inert gas ignited by high currents passed through opposed graphite-based anode and cathode (see Figure 2.2(a)). The carbon nanotubes are built during the condensation of the carbon atoms on the cathode electrode and another colder part of the reaction chamber.[4,6] The

synthesis of MWCNTs using the arc-discharge method produces nanoparticles with high quality in gram scale. The MWCNTs have a high crystallinity, which makes them very straight.[5,6] The byproducts of the arc-discharge MWCNTs are multilayered graphitic particles in polyhedron shapes.

The evaporation of carbon atoms from the anode electrode and not from the cathode is because the cathode is dimensionally more stable and is cooled during operation. The replacement of the consumed anode must be controlled in order to avoid that both electrodes touch each other. The quality of the MWCNTs produced by this method will depend on the temperature of the cathode, the inert gas used (helium, argon, nitrogen, hydrogen/nitrogen mixture), the gas pressure and the difference in voltage employed.[4-6]

The synthesis of MWCNTs by laser ablation is similar to the arc-discharge method, and is schematically presented in Figure 2.2(b). In this process, a laser source evaporates carbon atoms from a graphitic substrate and the atoms deposit on a cooled element, usually base on copper. The process is performed at about 1200 °C in a cylindrical shape chamber made of quartz. The MWCNTs are then found on the cooled element or at the wall of the quartz chamber. Usually the MWCNTs produced by this method have between 4 and 25 walls, their lengths are of a few hundred nanometers (making them the shorter carbon nanotubes produced among the common techniques), have minor structural defects and their ends are usually capped.[4]

2.1.2.2. Chemical vapor deposition

The chemical vapor deposition (CVD) is the method used for the industrial production of carbon nanotubes. The method consists of the decomposition of gaseous or volatile compounds of carbon through a tube reactor for a period of time. The reaction is catalyzed by metallic nanoparticles, which also act as nucleation agents for the nucleation and growth of the carbon nanotubes. The synthesis can be carried out between 500 °C and 1000 °C.[5] The synthesized particles are collected upon cooling the system to room temperature. The precipitation of carbon from the saturated metal particles leads to the formation of tubular carbon solids in sp^2 structure. The key parameters for the synthesis of MWCNT by CVD growth are the carbon source, the catalysts and the temperature.[6] One advantage of the CVD method is that it allows the deposition of the carbon atoms over pre-designed lithographic structures, making possible the preparation of ordered arrays of carbon nanotubes or dense arrays of carbon nanotube forest films. A general sketch of the method can be appreciated in Figure 2.3. Different methods based on CVD have been implemented for the synthesis of carbon nanotubes. Among these methods, the most cited are methane, alcohol and plasma enhanced CVD, as well as high pressure catalytic deposition of carbon monoxide (HiPco).

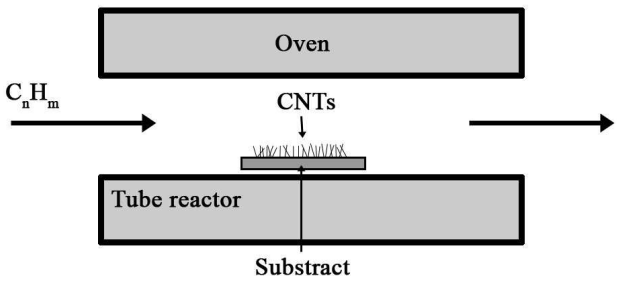

Figure 2.3. Sketch of the experimental setup for the synthesis of carbon nanotubes using the CVD method.

The upscaling production of carbon nanotubes has been limited due to the complicated experimental setups and the derived high costs of production. However, mass production of MWCNTs has been achieved through the so-called fluidized bed or floating-catalyst CVD synthesis. This system is ideal for the production of MWCNTs because the carbon nanotubes can grow laterally by the deposition of the carbon on the sidewalls of the chamber, and the catalyst particles are allowed to aggregate, which favors a high density of catalyst into the chamber. On the contrary, the production of SWCNTs is not possible by this method because of the aggregation of the catalyst during the synthesis. For this reason, the concentration of catalyst during the synthesis of SWCNTs needs to be minimized, increasing the costs of production.[5] Another difficulty of the production of SWCNTs relies on the fact that the MWCNTs are in the order of thousand times heavier than the SWCNTs, and thus the number of SWCNTs must be accordingly larger in order to synthesize the same amount.[6] One of the biggest worldwide producers of MWCNTs is Bayer AG, with reported productions 60 metric tons/year in 2007 and with an estimated expansion of 200 metric tons/year in the coming years.[7]

2.1.3. Properties of carbon nanotubes

Carbon nanotubes are extremely stiff. The reported Young's modulus fluctuates between 0.4 and 4.15 TPa; however, it is difficult to have an exact value due to the diversities of carbon nanotubes on the market. In the majority of the cases, the Young's modulus lies in the range of 1.0 - 1.25 TPa, which are the highest values ever reported for a material.[2,4] This strength is a consequence of the high elastic constant of the basal planes of the graphite. It is also worth mentioning that the mechanical properties of the carbon nanotubes depend on the quality of the material. For

SWCNTs with high concentration of defects produced through the catalytic degradation of acetylene, the Young's modulus decreases to 50 GPa.[4,8] The Young's modulus of catalytically grown MWCNTs (e.g. CVD process) is lower than the ones obtained for MWCNTs synthesized by the arc discharge method. Arc discharge MWCNTs, which contain very few defects, have a modulus comparable with the high values measured for individual SWCNTs.[9] Figure 2.4 shows a comparative correlation of the range of elastic modulus against the amount of order/disorder within the walls for arc discharge and catalytically grown MWCNTs.

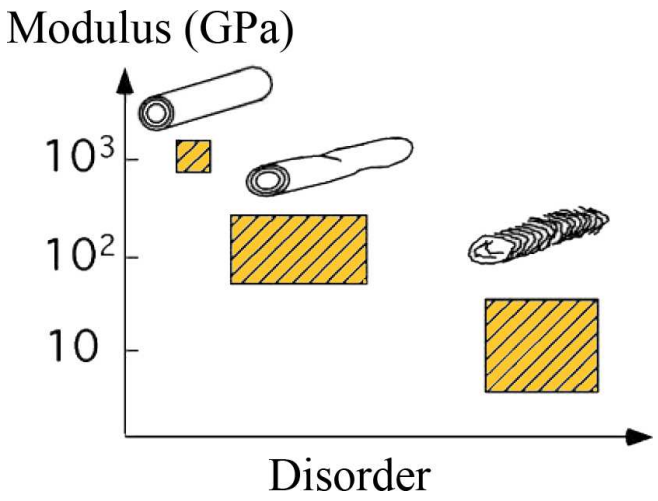

Figure 2.4. Correlation between the measured Young's modulus of MWCNTs and the amount of disorder (defects) present within the walls.[9]

Carbon nanotubes are known to possess high electrical conductivities (low electrical resistivity). For example, the electric resistance of a single MWCNT with low-ohmic contact is just 6 kΩ. In SWCNTs, the electrical resistance increases with the decrease in the temperature (Coulomb Blockade). This effect has not been observed for MWCNTs.[9] The delocalized electronic structure and the tubular dimension of the carbon nanotubes are responsible for current densities of approximately $10^9 A/cm^2$ or electrical current of the order of 1 mA, without destroying the structure. This proves

the ballistic transport of the carbon nanotubes. These values are two or three orders of magnitude higher compared to the ones corresponding to metals like aluminum or copper.[9,10] However, the presence of defects on the carbon nanotubes has also consequences on their electrical conductivity. The axial stresses under deformation from the bonds lead to changes in the band structure, aside from the problems related with the Stone-Wales-defect as well as other defects that reduce the electrical conductivity. These effects are related with two contiguous vacancies in the aromatic structure. For example, the electrical resistance of a SWCNT of about 400 nm in length increases a thousand times when the carbon nanotube has 0.03% of these double defects. Single defects do not show a dramatic change, they can just decrease the free path of the electrons a few nanometers through the nanotubes due to the huge number of available channels on the nanoparticle. The presence of rest of catalyst could change dramatically the resistivity of the carbon nanotubes at lower temperatures.[4]

Probably one of the most promising applications of carbon nanotubes is as field-effect transistor (FET). The carbon nanotubes have the ability to emit electrons when they are under an electrical field, as many other conductive materials. It is possible to build FET with just one carbon nanotube attached to two gold contacts. The geometry of the carbon nanotubes locally amplifies the electrical field, at voltages that can be handled. The carbon nanotubes can emit electrons under field strength below 1 V/µm, generating electrical densities of about 3 mA/cm^2.[2,4]

2.1.4. Chemistry of carbon nanotubes

The properties of carbon nanotubes have driven to the design of a new family of multifunctional nanomaterials. However, the manipulation of carbon nanotubes is one of its biggest drawbacks. The synthesized carbon nanotubes are usually strongly aggregated and are not stable in most of the common solvents. The π-π stacking interactions and the residues of catalyst from the synthesis are the main reasons for these problems. In this sense, a series of chemical treatments has been conducted in order to disaggregate the bundles and improve the dispersibility of isolated carbon nanotubes in common solvents. Tasis et. al.[11] have presented a review related with the chemistry of carbon nanotubes. They have categorized the modification on carbon nanotubes in three groups: the endohedral filling of their inner empty cavity, the noncovalent absorption or wrapping of various functional molecules, and the covalent attachment of chemical groups through reactions onto the π-conjugated skeleton of the carbon nanotubes. In the first case, the research has been focused on the production of nanowires or on the storage of liquid fuels. The works have been mainly related with the encapsulation of fullerenes, metalofullerenes, metal salts (subsequently reduced to metals), metal oxides, inorganic salts and biomolecules in SWCNTs and MWCNTs. The noncovalent absorption is based on van der Waals forces or π-π stacking interactions between the carbon nanotubes and the polynuclear species, generally pyrene modified reagents.[12] Different surfactants have been used in order to improve the dispersibility of the carbon nanotubes in different kinds of solvents. There are also examples of conjugated polymers that have the ability of wrapping the carbon nanotubes, usually, with a helical conformation.

Different strategies have been adopted for the covalent attachment of chemical groups onto the graphitic structure of the carbon nanotubes, amongst which the cycloaddition reactions and the radical addition are the most commonly used. These alternatives seek to improve the dispersion of the carbon nanotubes in organic solvents or polymer matrices. In order to obtain a good dispersion, the functionalization of the carbon nanotubes has to be maximized, which could worsen the properties of the nanoparticles. In this sense, the sidewall grafting of carbon nanotubes with polymer chains arise as an alternative for the improvement of the dispersion of the carbon nanotubes with low grafting contents, and for the creation of hybrids materials consisting on carbon nanotubes and other nanoparticles.

There are two main strategies for the covalent attachment of polymers on carbon nanotubes, known as *grafting onto* and *grafting from*. These approaches have been also applied on other micrometer and nanometer size particles. The *grafting onto* consists on the reaction between polymer chains end capped with functional groups and the carbon nanotubes. The surface of the carbon nanotubes could be treated previous to the grafting reaction. On the other hand, the *grafting from* approach relies on the creation of functional groups on the host surface that are able to promote a further polymerization reaction. Homenick et al.[13] have recently presented a review on the polymer grafting of carbon nanotubes using the described methods. Nevertheless, a selection of the most relevant findings will be discussed in the next sections.

2.1.4.1. *Grafting onto* carbon nanotubes

A summary of the reported pathways on the *grafting onto* reactions is schematized in Figure 2.5. The *grafting onto* reactions between polymers (or oligomers) with reactive groups at the chain ends and carbon nanotubes have been performed on pristine and pre-functionalized particles. The conditions of the reaction depend on the functional groups attached to the chain. Macromolecules end capped with nitroxyl[14] and nitrines[15] groups have shown high grafting efficiencies on pristine carbon nanotubes. Polymer chains functionalized with groups able to dissociate when they are heated (e.g., nitroxyl) produce polymer centered macroradicals that react with the graphitic structure of the carbon nanotubes. In the case of the nitrine functionalized polymers, it has been reported that the cycloaddition reaction with the double bond in the graphitic structure is successful in pristine[15] and alkyne functionalized SWCNTs (click coupling), under specific reaction conditions.[16]

Other approaches consist on the modification of the surface of the carbon nanotubes in order to create suitable groups for the grafting reaction. The most reported treatments start with the oxidation of the carbon nanotubes, followed by amidation or acyl chloride reactions. The amino or acyl groups on the carbon nanotubes are further functionalized with reactive oligomer or polymer chains.[17-26] For example, the functionalization of carboxyl or amine modified MWCNTs with polycarbonate (PC) has been reported. The oxidized MWCNTs showed a higher grafting content of PC than the amine counterpart. The reactions carried out in bulk conditions and under microwave irradiation showed the highest efficiencies, against the reactions in solutions or without microwave irradiation. The morphology of the PC grafted MWCNTs resembles a bead collar structure, with PC beads along the MWCNTs.

However, the grafting content of polymer is disproportionate (between 109 wt % and 300 wt %) may be due to the presence of absorbed polymer (nongrafted polymer).[23]

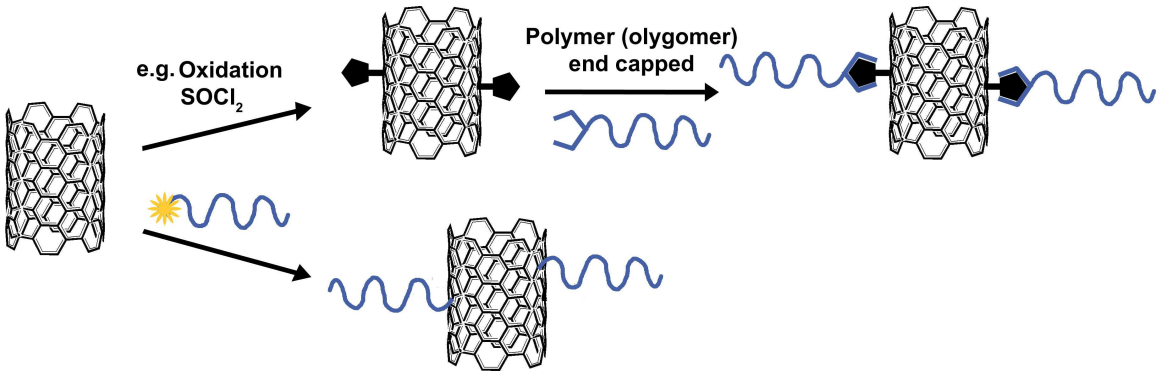

Figure 2.5. Schematic representation of the *grafting onto* approach on carbon nanotubes.

The grafting of end functionalized linear low molecular weight polymers (2 to 5 kg/mol) like poly(ethylene oxide) methyl ether (PEO-OH), monoamine terminated poly(ethylene oxide) (PEO-NH_2) and hydroxyl terminated poly(styrene) (PS-OH), or hyperbranched polymers like poly(amide-imide) to singlewall or multiwall carbon nanotubes has also been reported, in solution or under melt mixing conditions. However, the grafting efficiencies of these reactions are unknown because of the presence of absorbed polymers.[15,18,19,21] Baskaran and co-workers[17] have found that the presence of nongrafted polymer on MWCNT is reduced when the temperature of the reaction is increased and the time of the reaction decreased, during the *grafting onto* of hydroxyl terminated poly(methyl methacrylate) (PMMA-OH).

The *grafting onto* of poly(oxyalkylene)-diamine has been carried out by layer-by-layer (LbL) deposition on MWCNTs. This modification has shown higher proton conductivity in Nafion® based nanocomposites than the corresponding conductivity observed in Nafion® or in the pristine MWCNTs/Nafion® nanocomposite, at higher temperatures. This is attributed to a stronger binding of water molecules to the

sulfonic acid groups from the Nafion® and the amine groups *grafted onto* the MWCNTs.[27]

The *grafting onto* of polymers with functional groups along the backbone at carbon nanotubes has also been studied. A schematic representation of this type of reactions is presented in Figure 2.6. In this case, the polymer chains wrap the carbon nanotubes instead of forming the brush-like structure at the carbon nanotubes, as previously discussed. For example, the reaction between oxidized MWCNTs and high molecular weight poly(vinyl alcohol) (PVA, 70-100 kg/mol) have resulted in a relatively homogeneous coating of polymer on the surface of the carbon nanotubes and good dispersion in films with the same polymer as matrix.[28] The *grafting onto* of poly(styrene-*co*-p-(4-(4'-vinylphenyl)-3-oxabutanol) on singlewall and multiwall carbon nanotubes previously treated with HNO_3 and $SOCl_2$ results in an improvement of the dispersion in organic solvents and in blends with polystyrene.[29] The esterification reactions between the acyl chloride groups at the surface of the SWCNT and the hydroxyl pendant group from the p-(4-(4'-vinylphenyl)-3-oxabutanol were also used for the *grafting onto* of poly(*N*-vinyl carbazole) (PVK). A random copolymer of N-vinyl carbazole and low mol % of p-(4-(4'-vinylphenyl)-3-oxabutanol (~ 10 mol %) was synthesized. The nanocomposites showed a relatively homogeneous dispersion of functionalized SWCNTs.[30] A different route was reported by Blake and co-workers.[31] They have proposed the grafting of chlorinated polypropylene (CPP) to *n*-butyl lithium functionalized MWCNTs. Sedimentation experiments have shown that the MWCNTs form covalent bonds with the CPP.[31,32]

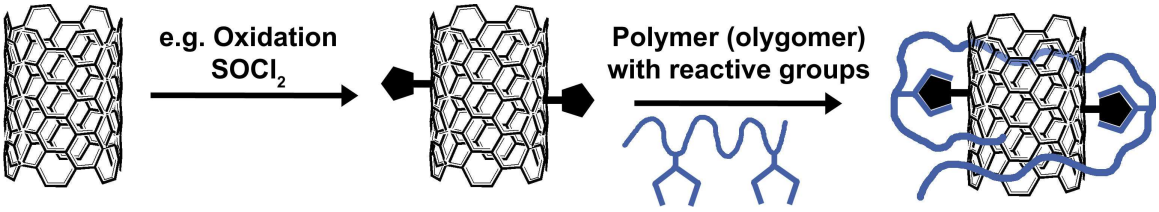

Figure 2.6. Schematic representation of the *grafting onto* approach on carbon nanotubes of polymers with functional groups along their backbone.

The reaction between carbon nanotubes and polymers with functional groups along their backbone has lead to the synthesis of comb-like structures grafted on the surface of the nanoparticles. Liu et al.[22] have proposed a two step reaction consisting of the grafting of poly(acyl chloride) and the subsequent reaction with poly(ethylene glycol) on MWCNTs. The high reactivity of the acyl chloride groups ensures the wrapping of the chain to the carbon nanotubes, leaving still functional groups for a further esterification with poly(ethylene glycol). The grafting of the comb-like copolymer has reached 80 wt %. A similar methodology was recently employed for the functionalization of MWCNTs with polyurethane (PU), obtaining around 90 wt % of polymer grafting.[33]

2.1.4.2. *Grafting from* carbon nanotubes

A schematic representation of the *grafting from* reactions of carbon nanotubes is presented in Figure 2.7. The first work related with the *grafting from* carbon nanotubes was published in 2003. The reaction consisted of the 1,3-dipolar cycloaddition between N-4-(hydroxyphenyl)glycine, octyl aldehyde and acid treated SWCNTs and the posterior esterification with 2-bromoisobutyryl bromide. The alkyl bromides groups were used as initiator moieties for the atom transfer radical polymerization (ATRP) of methyl methacrylate.[34] Although the infrared spectroscopy and calorimetric results showed that poly(methyl methacrylate) was successfully

grafted on SWCNTs, the TEM images illustrated that the coating of the SWCNTs was not homogeneously distributed. It was concluded that the polymerizations became uncontrolled after 2 hours of reaction.

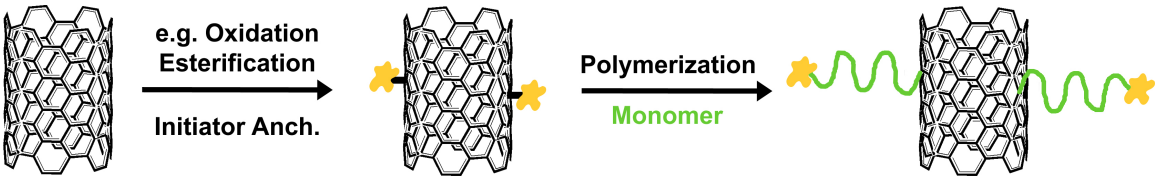

Figure 2.7. Schematic representation of the *grafting from* approach from carbon nanotubes.

The ATRP is the most used method for the *grafting from* carbon nanotubes. A brief description of this polymerization technique is given in section 2.2. The group of W. T. Ford has performed detailed studies regarding the functionalization of SWCNTs using *n*-butyl methacrylate[35] and styrene.[15] The initiator anchored SWCNTs were obtained after the esterification between 2-hydroxyethyl-2-bromopropionate and acyl chloride functionalized carbon nanotubes. The concentration of initiator obtained was relatively high (ca. 0.32 mmol of initiator groups per gram of SWCNT, about ~ 4 initiator groups per 1000 carbon atoms). The polymerizations were performed in the presence of nonbounded initiator, the so-called sacrificial or free initiator. The polymerization showed a controlled behavior. The molecular weight of the grafted polymers and the ones obtained in solution (from the free initiator) are comparable. The dispersibility of the SWCNTs in organic solvent improves with the increase of the content of polymer. Choi and co-workers[36] have proposed a method for the grafting of styrene from SWCNTs without previous acid treatment, which could be advantageous since the acid treatment might disrupt the graphitic structure of the carbon nanotubes. Hydroxyl groups were introduced on the surface of the SWCNTs by the electrophilic addition of $CHCl_3$, followed by hydrolysis. The initiator moieties

were anchored to the hydroxyl functionalized SWCNTs and styrene was polymerized under ATRP conditions. Although the grafted SWCNTs showed a thick polymer layer (approximately 6 nm), there is not given detailed information about the purification procedures after the polymerization reaction. Additionally, the Raman spectra are not conclusive regarding the preservation of the sp^2 graphitic structure of the SWCNTs after the reaction with $CHCl_3$.

More recently, Chochos et al.[37] reported the functionalization of SWCNTs with oligoquinoline chains using the *grafting from* approach. The initiator anchored SWCNTs were prepared following two different routes: the 1,3-cycloaddition of *p*-formaldehyde, and through the reaction with aminoethanol. In a second step, an esterification reaction with 2-chloropropionyl chloride was done, under suitable experimental conditions. These hybrid nanostructures are potential candidates for the design of materials that combine the electronic properties of the SWCNTs with the strong emission ability of the quinoline groups.

A similar methodology to the one applied by Ford in SWCNTs has been used in MWCNTs by Cheng et al.[38] They have presented the first example on the grafting of styrene from MWCNTs. The reaction was performed form 2-bromoacryl groups attached to the surface of the MWCNTs after the esterification reaction between 2-bromoacryl bromide and oxidized carbon nanotubes. The results showed control on the polymerization despite the relatively high temperature used during the reaction.

The same year, two independent groups presented more comprehensive investigations related with the synthesis of different (co)polymers from the surface of initiator

anchored MWCNTs. The anchoring of the initiator moieties on the MWCNTs has been achieved by following similar procedures as the ones used for SWCNTs (see Figure 2.7). The *grafting from* of styrene and (meth)acrylate monomers has generally shown an increase in the (co)polymer molecular weight, molecular weight distribution and grafting content with the increase of the concentration of monomer respect to the initiator groups anchored to the MWCNTs,[39-41] or to the presence of free initiator in the reaction media.[42-44]

These results have stimulated the research in this area over the past five years. For example, Gao et al.[45] have synthesized amphiphilic polymer brushes from the surface of MWCNTs by sequential polymerization of styrene and *tert*-butyl acrylate (tBA). The PtBA was further hydrolyzed, leading to poly(acrylic acid) (PAA). In a different work, the grafting of PAA and poly(sodium 4-styrenesulfonate) (PSS) from MWCNTs were successful used on the fabrication of carbon nanotubes/polyelectrolyte nanocomposites via LbL deposition.[46] The assembly of polycations resulted in higher loading, uniform, and stable polymer layers between the functionalized MWCNTs, compared to previous reported methods.

The design of hybrid structures consisting of metal nanoparticles and MWCNTs has been achieved through the *grafting from* polymerization on the carbon nanotubes. For example, nanohybrids composed of poly(glycerol monomethacrylate) (PG2MA) grafted MWCNTs and different metal ions (Ag^{+}, Co^{2+}, Ni^{2+}, Au^{3+}, La^{3+} and Y^{3+}) have been prepared. The concentration of metal nanoparticles could be controlled by adjusting the polymer grafting density. The metal loaded MWCNTs are relative stable due to the protective nature of the polymer layer.[42] The assembly of cadmium selenide

(CdSe) nanoparticles with poly(ether imide)-*graft*-poly(acrylonitrile) (PEI-*g*-PAN) grafted MWCNTs has been also reported. The Cd^{2+} ions were immobilized with the acrylonitrile groups present in the polymer chains.[47]

The grafting of branched structures from the surface of MWCNTs was done through self-condensing vinyl copolymerization (SCVP), combining monomers and inimers under ATRP conditions. High grafting efficiencies were obtained during the synthesis of hyperbranched polymers using 2-((bromobutyryl)oxy)ethyl acrylate (BBEA) as inimer.[44] The *grafting from* reactions of linear and hyperbranched glycopolymers were described for initiator anchored MWCNTs, in the absence or presence of a free initiator. The glycopolymers used were sugar-containing polymers, biocompatible and water soluble. The polymerization of 3-O-methacryloyl-1,2,:5,6-di-O-isopropylidene-D-glucofuranose (MAIG) and 2-(2-bromoisobutyryloxy)ethyl methacrylate (BIEM) lead to hyperbranched polymer chains with controllable degree of branching. These types of hyperbranched nanostructures with a high concentration of reactive groups might offer new alternatives on the design of multifunctional nanodevices.

As well as with SWCNTs, one step reactions for the functionalization of MWCNTs with initiator groups have been studied. Different works have focused on the reaction between carbon radicals and the double bonds of the graphene structure at the surface of the MWCNTs. For example, the reaction between 1-bromoethylbenzene (BEB) and MWCNTs leads to the formation of initiator groups at the surface of the nanoparticle. The labile halide is able then to initiate the polymerization reaction of polystyrene and polystyrene-*block*-poly(N-isopropyl acrylamide).[48] Polystyrene end capped with bromine groups was also used as precursor for the surface polymerization of

MWCNTs, combining the *grafting onto* and *grafting from* functionalization methods. In a first step, polystyrene end functionalized with bromine groups were radically coupled on the surface of MWCNT (*grafting onto*). The polymer could be used as precursor for the polymerization reaction through the labile halide atom at the free chain end.[49] The anchoring of halide atoms have been achieved through the electrochemical reduction of brominated aryl diazonium salts on the surface of MWCNTs. The polymerization of styrene and methyl methacrylate has proved the activity of the initiator moieties.[50]

2.1.4.3. Other reactions

Beside the grafting approaches, other strategies have been used for the coating of carbon nanotubes with polymer chains. These approaches include the in situ polymerization in the presence of pristine and pre-functionalized carbon nanotubes, the physisorption of polymer chains at the surface of carbon nanotubes, and the use of surfactants.

Thermostable nanocomposites have been prepared by pre-dispersion of pristine[51-55] or pre-functionalized[56-59] carbon nanotubes in epoxy based monomers. For example, epoxy polymers reinforced with triethylene-tretamine (TETA) decorated MWCNTs have shown notorious improvements on the mechanical properties compared with those nanocomposites based on pristine MWCNTs and the neat epoxy resin. The behavior is attributed to a homogeneous dispersion and the strong interfacial addition between the TETA functionalized MWCNTs and the epoxy matrix.[58]

The in-situ polymerization of thermoplastic nanocomposites has been also done following different strategies. One of the first strategies consisted in the synthesis of PMMA in the presence of MWCNTs, using 2,2'-azoiso-butyronitrile (AIBN) as the initiator. The spectroscopy results support that covalent bonds were formed between the MWCNTs and the PMMA chains.[60] Linear and hyperbranched poly(ether ketone)s were grafted on MWCNTs and carbon fibers through Friedel-Crafts acylation reactions in a mixture of phosphoric acid and phosphorous pentoxide (PPA/P_2O_5). This method provides a controlled functionalization without the damage of the carbon nanotubes due to the mild reaction conditions.[61,62] Singlewall and multiwall carbon nanotubes were grafted with functionalized polyoxadiazoles through the in-situ polycondensation reaction between hydrazine sulfate and aromatic dicarboxylic acid. The grafting of the polyoxadiazole on the surface of the carbon nanotubes was demonstrated through the improvement of the thermal stability, the storage modulus, and the antistatic properties of the nanocomposites.[63,64]

2.1.5. Health considerations

The needle like shape of the carbon nanotubes has opened a series of discussions regarding the similarities with the asbestos fibers. The inhalation of asbestos fibers causes asbestosis (a progressive fibrotic disease of the lung), lung cancer, and malignant mesothelioma of the pleura.[65]

The potential toxicity of a particle increases with the increment of the surface area per unit mass. Particles with a relatively inert surface could be harmful just by decreasing their dimensions. For this reason, a major concern has been taken because of the nanometer dimensions of the carbon nanotubes. Nevertheless, the toxicity of the

particles is also determined by their reactivity. On this concern, care must be taken on doing the comparisons between asbestos fibers and carbon nanotubes.[66] Donaldson et al.[67] have recently reviewed the toxicological risks that represent the handling of nanoparticles or micron sized fibers and compared them with the ones corresponding to carbon nanotubes. It was suggested that the carbon nanotubes may harm cells through a mechanism called oxidative stress.

Magrez and coworkers[65] were the first group that studied the toxicity of the carbon based nanomaterials (CBNs) as a function of their dimension. They studied the influence on the toxicity of different CBNs like MWCNTs, carbon nanofibers and carbon black in human lung tumor cells. The results from the *in vitro* experiments lead to the conclusion that the CBNs studied promote the cell death. Surprisingly, under the experimental conditions described, the MWCNTs were less toxic than the carbon black. The behavior is attributed to a higher concentration of dangling bonds on the carbon black. This was corroborated with the cell proliferation studies on acid treated MWCNTs and carbon fibers, where the defects induced at the carbon structure increase their toxicity. Other *in vitro* experiments take into account the surface functionalization of the carbon nanotubes on immune system cells. The carbon nanotubes were grafted with amine capped oligomers. The results showed that the coated carbon nanotubes neither disturb the cell function nor induce cell death or activation of lymphocytes and macrophages.[66]

The size of the carbon nanotubes is one important factor to consider for the determination of the toxicity. Poland et al.[68] recently reported that long MWCNTs injected directly into the abdominal cavity of mice induce inflammation, formation of

granulomas and early fibrosis or scarring in the mesothelial lining. Shorter MWCNTs have shown minimal influence, similar to short chopped fibers and carbon black particles. The carbon nanotubes did not cause mesothelioma after seven days of exposure, but the early inflammatory and granulomatous lesions are similar to the ones induced by long asbestos based fibers. Prolonged exposures (25 weeks) to the high aspect ratio MWCNTs have lead to the conclusion that the MWCNTs are potential carcinogenic agents on the basis of their fibrous geometry, biopersistence and ability to generate tissue-damaging free radicals.[69]

Based on these works, Kane et al.[70] recognized the critical issues regarding the toxicity of these materials: the length and the biopersistence. Generally, longer fibers cannot be covered by the macrophages. The incomplete phagocytosis stimulated the production of radicals that induce oxidative stress. The *in vivo* studies have introduced carbon nanotubes directly into the mice in relative high concentrations. The spontaneous inhalation of carbon nanotubes would require more extensive and expensive studies that, so far, have not been published. It is also unclear if the concentration required to produce cell damage can be reached by simple inhalation, because the state of aggregation of the carbon nanotubes is different compared with asbestos fibers and the diffusion of the carbon nanotubes in the respiratory system is still unknown.

The presented evidences open the debate about the right handling of these materials. There are different governmental and private initiatives that seek to classify the carbon nanotubes, regulate the creation of safety data sheets and find new strategies for the handling and disposal of carbon nanotubes in workspaces.

2.2. Atom Transfer Radical Polymerization (ATRP)

The *grafting from* polymerization on carbon nanotubes is regularly conducted under controlled radical polymerization (CRP) conditions. The CRP has the advantages that it does not required elaborated setups, accepts higher levels of impurities[71] compared with other polymerization techniques (like ionic polymerization) and the architecture and composition of the (co)polymer can be easily controlled. On the contrary, the near diffusion-controlled bimolecular radical coupling and the disproportion reactions that occur during the CRP are drawbacks of this polymerization technique.

The most common CRP methods are based on the establishment of a rapid dynamic between free radicals and dormant species, where the equilibrium is displaced to the dormant species during the reaction. These methods are the atom transfer radical polymerization (ATRP), the reversible addition fragmentation chain transfer (RAFT) polymerization, and the nitroxide mediated radical polymerization (NMP), where the dormant chains are alkyl halides, thioesters, and alkoxyamines, respectively. Among these methods, ATRP is the most cited in the literature, probably because the catalysts are commercially available and comparatively inexpensive.[72] Other CRP strategies include iniferters, other degenerative transfer systems, alkyl iodides, oligomers with methacrylate functionality, various types of non-nitroxide stable free radicals, and other transition metal mediators, which are also very efficient under specific conditions.

The mechanism for ATRP is sketched in Figure 2.8. The active species (radicals) are generated through a reversible redox reaction of a transition metal complex (M_t^n-Y/Ligand, where Y may be another ligand or the counterion) which undergoes a one

electron oxidation with concomitant abstraction of a (pseudo)halogen atom (X) from a dormant species, R-X. This process occurs with a rate constant of activation "k_{act}" and deactivation "k_{deact}". Polymer chains propagate by the addition of intermediate radicals to monomers in a manner similar to a conventional radical polymerization, with the rate constant k_p. Termination reactions (k_t) occur in ATRP, mainly through radical coupling and disproportionation. However, in a well controlled ATRP, only a few percent of the polymer chains undergo termination.[73]

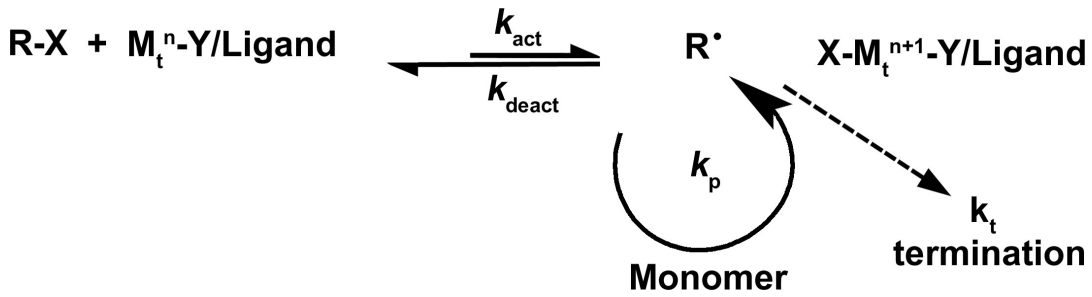

Figure 2.8. General mechanism of ATR polymerizations.[73]

The success of the ATRP reaction depends on the combination between the components and the polymerization conditions. Different monomers have shown control over the rate, the molecular weight and polydispersity. These include styrenes, (meth)acrylates, (meth)acrylamides, acrylonitrile and some cyclic monomers. The equilibrium constant ($K_{eq} = k_{act} / k_{deact}$) determines the polymerization rate when no (or negligible) side reactions occur. Each monomer possesses its own intrinsic radical propagation rate. For this reason, the control of the polymerization depends on the adjustments of the concentration of propagating radicals and the rate of radical deactivation as a function of the monomer. In ATRP, alkyl halides (RX) are typically used as the initiator. To obtain well-defined polymers with narrow molecular weight distributions, the halide groups (X) must rapidly and selectively migrate between the growing chains and the transition-metal complex. When this condition is fulfilled, the

theoretical degree of polymerization (*DP*) follows a first order kinetics as a function of the initial concentration of monomer ($[M]_o$) and initiator ($[I]_o$), and the conversion. This is expressed in equation 2.3.

$$DP = \frac{[M]_o}{[I]_o} * \text{conversion} \qquad \text{Eq. 2.3}$$

A better control of the molecular weight has been achieved when either bromine or chlorine based halides are used as initiators. Alkyl halide with activating substituent on the α-carbon, such aryl, carbonyl, or allyl groups, and polyhalogenated compounds are the most common initiators used in the literature.[73]

The control of the ATRP reactions depends not only on the reactivity of radical (monomer), but on the transition-metal catalyst. The growing radicals are generated through the abstraction of the (pseudo)halogen for the metal center, which expands its coordination sphere. The oxidized transition metal must then deactivate the propagating polymer chains rapidly and form the dormant species. The employed transition-metal are usually salt halides. While copper salts are the most common used transition-metal; others transition-metal based on molybdenum, chromium, rhenium, ruthenium, iron, rhodium, nickel or palladium have also been used. One of the major drawbacks of the ATRP is, precisely, the presence of the metal salt at the end of the reaction. Therefore, different efforts have been done during the last years in order to reduce the quantity of catalyst and (or) to find more efficient ways of purification of the polymer at the end of the reaction.[73-76]

The ligands are, together with the transition-metal salts, of primary importance during the ATRP. The solubilization of the transition-metal salt in the organic media during the polymerization depends on the ligand. The right selection of the ligand is also responsible for shifting the equilibrium between the transition-metal and alkyl halide to the dormant species, the fast deactivation of the active radicals by halogen transfer (control over the molecular weight distribution) and the relative fast activation of the dormant species (control over the polymerization rate).[73] The ligands more commonly used are based on nitrogen[77,78] and phosphorus.[73]

The kinetics of the ATRP depends on the combination of all the factors previously mentioned. The rate of polymerization can be expressed as follows:[73]

$$R_p = k_p[M][P^\bullet] = k_p K_{eq}[M][I]_o \text{ x } [M_t^n]/[X\text{-}M_t^{n+1}] \qquad \text{Eq. 2.4}$$

The conversion of the polymerization as a function of the time is linear in semilogarithmic coordinates, as shown in Figure 2.9. This behavior is typical of a first order kinetics of the polymerization with respect to the monomer and indicates a constant concentration of propagating species during the reaction. Usually, polymerizations carried out under homogeneous conditions showed that the rate of polymerization is first order with respect also to the initiator and the concentration of the transition-metal complex. The precise kinetic law for the deactivator ($X - M_t^{n+1}$) is more complex due to the spontaneous generation of deactivator (M_t^{n+1}), consequence of the persistent radical effect. Radical termination occurs rapidly until a sufficient amount of deactivator is formed and the radical concentration is low enough. Typically, termination occurs during the earliest stages of polymerization on a small fraction of the total growing polymer chains, but the majority of the chains

will propagate. If a deactivator is added initially to the polymerization, then the proportion of terminated chains can be greatly reduced.[79,80]

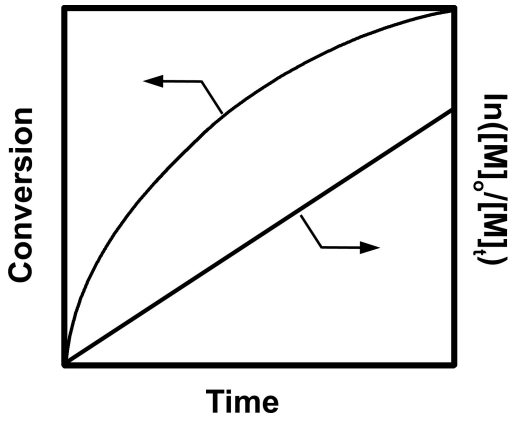

Figure 2.9. Schematic representation of the dependence of the conversion against time on linear and semilogarithmic scale.[73]

The ATRP can be carried out either in bulk, in solution, or in a heterogeneous system (e.g., emulsion, suspension). A solvent is sometimes necessary, especially when the polymer is insoluble in its monomer. Two principal factors affect the choice of solvent: the chain transfer between solvent and growing radical, and the interaction between solvent and the metal/ligand complex system. The temperature is another factor to be taken into consideration during the ATRP reaction. As a result of the higher activation energy for the radical propagation than for the radical termination, higher k_p/k_t ratios and better control are usually observed at higher temperatures. However, the increase of the temperature leads to chain transfer and other side reactions, or to catalyst decomposition. The optimal temperature depends mostly on the monomer, the catalyst and the targeted molecular weight.[72]

2.3. Block Copolymers

Copolymers are polymers obtained from the synthesis of two or more monomeric units. The copolymers are categorized according to the sequence of the monomeric

units along the polymer chain. They are classified as random, alternate, graft and block copolymers.[81]

Block copolymers consist of two or more polymer chains of different chemical structures linked together through a common junction bond. Copolymers with different physical properties can be designed by varying the chain architecture and the sequence of the constituent blocks. The synthesis of these well defined structures has been possible after the development of controlled polymerization techniques, such as anionic, cationic and controlled radical polymerization.[82]

The preparation of block copolymers has opened new possibilities on the design of materials that were very difficult to obtain by simple blending. The properties of these new materials depend on factors related with the physical properties of the polymer chains, the block sequence and their state of segregation.[81,83-87] For example, it is possible to prepare spherical micelles where the insoluble block forms the core and the soluble block the shell.[88] This structure can be used for the encapsulation and selective delivery or removal of inorganic/organic compounds.

One important characteristic of the block copolymers is their ability to self-assemble. The segregation of the polymer blocks will depend on their characteristics (polarity, molecular weight and microstructure).[81,82,86,87] Usually, the constituent polymer chains in a block copolymer are immiscible and tend to macrophase separate. However, the macrophase separation is hindered due to the covalent bond(s) that link together the polymer chains. The only possibility is then to phase separate into microdomains with the intersegmental bonds lying at the interphase. The size and periodicity of these

domains are determined by the molecular weight and architecture of the block copolymer and will determine its morphology.

One of the most known applications of block copolymers is as thermoplastic elastomers (TPEs).[82,89] The TPEs exhibit generally the characteristics of chemically crosslinked elastomers at ambient temperature, but, at elevated temperatures, they behave as thermoplastics. This means that the TPEs can be moldable using regular methods for processing (i.e., extrusion, injection, melt pressing). The thermoplastic elastomers are usually the result of the sequential polymerization of a "soft" polymer chain (T_g or T_m < ambient temperature) and a "hard" polymer chain that does not flow at ambient temperature (T_g or T_m > ambient temperature). The architecture of the TPEs consists typically on external hard segments and a soft core segment. Typical examples of thermoplastic elastomers are based on butadiene, isoprene, urethane, styrene, ester, ether and amides.

Styrene based thermoplastic elastomers have been well studied because of their defined microstructure and relative low polydispersity. The mechanical properties depend on the composition of the comonomers and the chain architecture. For example, for a defined polystyrene-*block*-polybutadiene or polyisoprene-*block*-polystyrene copolymer, the mechanical properties vary as a function of the comonomer composition. A schematic representation can be appreciated in Figure 2.10.[90]

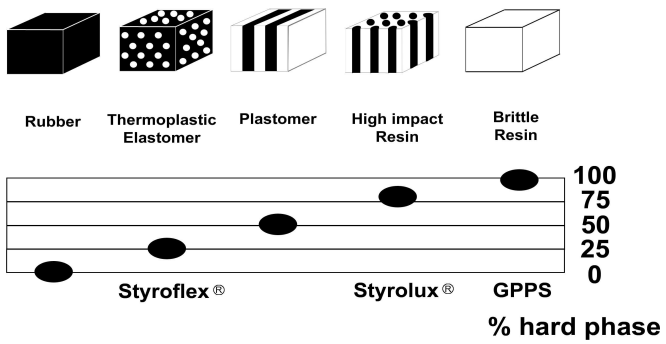

Figure 2.10. Morphology and the expected mechanical properties for different styrene based block copolymers.[90]

The architecture and the topology of the polymer chains influence the properties of the TPEs. The mechanical properties drastically change if one compares polymers with the same chemical composition but with different chain architectures and polymer sequences.[89,90] For example, Figure 2.11 illustrates the differences in mechanical properties between block copolymers based on polystyrene and polybutadiene with different chain architectures, like a commercial linear polystyrene-*block*-polybutadiene-*block*-polystyrene with 20 % v/v of polystyrene (Kraton, Shell), a commercial polystyrene-*block*-poly(styrene-*co*-butadiene)-*block*-polystyrene with 58 % v/v of polystyrene (Styroflex, BASF), and two tetrafunctional multigraft copolymers with the same polystyrene content but different number of branch points.[82]

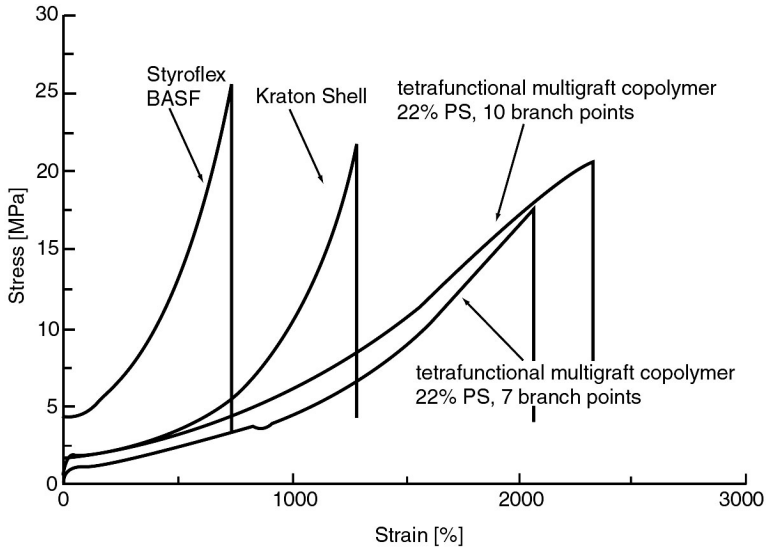

Figure 2.11. Mechanical properties of multigraft copolymers compared with commercial TPEs Kraton (20 % v/v of PS) and Styroflex (58 % v/v of polystyrene).[82]

2.4. Nanocomposites based on Block Copolymers

The creation of new materials based on the combination of materials with different properties is a practice that goes back to the Egyptians, who were the first ones that made bricks composed of straw and mud.[2] These materials are called composites.[91] One fascinating multicomponent system is the bone, which is a hierarchical composite built from ceramic tablets and organic binders.[92] Polymer science has thrown its interest over the past decades on the understanding of these complex systems for the design of new polymer based materials.

The use of polymers for high performance applications is restricted to certain areas. The combination of polymers and fillers for the design of new materials with enhanced mechanical (modulus, yield strength, toughness), optical (refractive index, luminescence, nonlinear properties), thermal, electrical, fire retardant, transport or ablative properties has been the focus of many research groups.

Polymer composites based on micrometer size fillers (particles) have been commercially used since decades. Nonetheless, the decrease of the size of the filler, from the micrometer to the nanometer-scale, is a current topic of study. Six characteristics, reviewed by Thomas et al.[93] are associated with the advantage of the materials based on nanometer fillers compared with micrometer size fillers. The characteristics are: 1) particle-particle correlation arises at low concentrations (approximately at 0.1 % v/v), 2) low percolation thresholds (below 1 % v/v), 3) large particle number densities up to ~10^{20} cm^{-3}, 4) extensive interfacial area per volume of particle (10^{7} $cm^{2}cm^{-3}$), 5) short particle-particle distance, and 6) comparable length

scales between the particle size, the distance between the particles, and the typical relaxation volume of a polymer chain (~ R_g^3, where R_g is the radius of gyration).

Nanometer size fillers (or nanoparticles) can be defined as materials where at least one of their dimensions is smaller than 100 nm.[2] Another accepted definition is that the nanoparticles have properties which depend inherently on the small grain size.[2] The nanoparticles are classified according to their dimensionality: zero dimensions refers to sphere like particles (e.g., silica, metals), one dimension to fiber like particles (e.g., nanotubes), and two dimensional to plate like particles (e.g., silica platelets).[93] Changes inherently to the polymer, like crystallinity, glass transition temperature, or mechanical strength, as well as changes related with the nanoparticles, like electrical conductivity, thermal conductivity or fire resistance, have been studied on nanocomposites based on homopolymers and different nanoparticles.[92] The most general conclusion among these works is that the highest enhancement of the properties is directly related with the control on the dispersion of the nanometer size inclusions.

In this sense, the use of block copolymers as matrices offers an alternative for the selective dispersion of the nanoparticles. If the dimension of the nanoparticles is on the range of the microdomain size of the block copolymer, the nanoparticles can be selectively arranged into a specific polymer phase.[93] Different examples have been reported related with the selective dispersion of spherical nanoparticles in block copolymers. Recently, Mendoza et al.[94] have selectively synthesized gold nanoparticles within the poly(4-vinyl pyridine) forming aligned hexagonally packed

cylinders in a polystyrene matrix. The etching of the organic phase in the nanocomposite could lead to the formation of gold nanowires.[95]

As another example, the selective incorporation of relative small gold nanoparticles (d_{core} = 3.5 ± 0.1 nm) and large diameter silica spheres (d_{core} ~ 22 ± 3 nm) has been done using a lamellar forming polystyrene-*block*-poly(ethylene propylene) copolymer as scaffold. Gold nanoparticles were found to segregate to the interphase between the polystyrene and poly(ethylene propylene) lamellae microdomains, whereas the silica nanoparticles were located at the center of the poly(ethylene propylene) domains.[96] Bates and coworkes[97] have studied the relation between the dispersion and the molecular weight of polystyrene grafted from silica nanoparticles embedded in polystyrene and symmetric polystyrene-*block*-polybutadiene matrices. They have found that the increase in the molecular weight of the block copolymer and the decrease in the molecular weight of the grafted polystyrene favor the dispersion of the silica particles in the polystyrene block copolymer.

The effect of tube or plate like nanoparticles on the morphology of block copolymer based nanocomposites is hard to find in the literature, compared with works where homopolymers or other types of copolymer are used as matrix. Ha et al.[98] analyzed the effect of clay platelets grafted with polystyrene on the morphology of a polystyrene-*block*-polybutadiene-*block*-polystyrene (SBS) copolymer. The nanocomposite samples were prepared by roll casting. They have found that the molecular weight of the grafted polystyrene is critical for the exfoliation of the clay sheets in the block copolymer, i.e., the exfoliation improves with the increase of the molecular weight of the grafted polystyrene. The authors claim that the individual

clay sheets serve to nucleate the orientation of the lamellae morphology during the phase separation of the block copolymer. Other studies related with the inclusion of modified clay platelets in a hydrogenated SBS triblock copolymer suggested that the clay templates the morphology of the block copolymer. The nanocomposites were prepared by compression molding after the melt mixing of organophilic montmorillonite intercalated with stearyl ammonium and a hydrogenated SBS. Based on experimental evidences, the authors proposed that the polystyrene chains are selectively absorbed on the silicate surfaces and form polystyrene domains on those surfaces. The poly(ethylene-*ran*-butylene) chains consequently segregate, forming a lamellae morphology from the clay platelet.[99] On the other hand, in the case of nanocomposites based on clay platelets and polystyrene-*block*-polyisoprene-*block*-polystyrene (SIS) copolymers with highly aligned hexagonally packed cylindrical microdomains, the nanoparticles distort the orientation of the cylinders, probably due to geometrical dissimilarities.[100]

In the specific case of nanocomposites based on block copolymers and carbon nanotubes, so far just two groups have discussed the influence of the carbon nanotubes on the morphology of the block copolymers.[101,102] Other works just considered the improvement on a desired property without paying attention to the final morphology of the nanocomposite.[103] Kenny and coworkers[101] have reported that octadecylamine functionalized SWCNTs stabilized with dodecanethiol switches the self-assembled microstructure of a lamellar forming SIS copolymer (Kraton) into a cylinder-like morphology. The selective sequestering of carbon nanotubes in block copolymer has been also observed on nanocomposites based on a lamellar polystyrene-*block*-polyisoprene copolymer with polystyrene grafted MWCNTs

prepared by film casting.[102] The TEM image can be appreciated in Figure 2.12. This is the only evidence that shows a MWCNT trapped into the polystyrene lamellae. The selective sequestering of the MWCNTs in a microdomain phase was attributed to the large block copolymer domain thickness, (compared to the diameter of the MWCNTs),[93] and the affinity of the nanotube to the polystyrene phase due to the polymer coating.

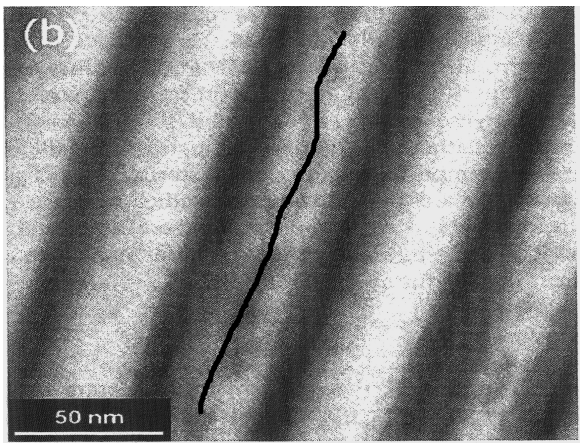

Figure 2.12. TEM image of PS grafted MWCNT sequestered in a polystyrene-*block*-polyisoprene diblock copolymer. The polyisoprene phase was stained with OsO_4.[102]

2.5. References

1. Reich, S.; Thomsen, C.; Maultzsch, J. Carbon Nanotubes, Basic Concepts and Physical Properties; Wiley-VCH, Berlin, 2004.
2. Vollath, D. Nanomaterials, An Introduction to Synthesis, Properties and Applications; Wiley-VCH Verlag GmbH & Co. KGaA: Weinheim, 2008.
3. Dresselhaus, M.; Avouris, P. In Carbon Nanotubes: Synthesis, Structure, Properties and Applications; Springer Berlin / Heidelberg, 2001, p 1-9.
4. Krueger, A. In Neue Kohlenstoffmaterialien; Vieweg+Teubner, 2007, p 125-286.
5. Joselevich, E.; Dai, H.; Liu, J.; Hata, K.; Windle, A. H. In Carbon Nanotubes; Springer Berlin / Heidelberg, 2008, p 101-164.
6. Dai, H. In Carbon Nanotubes: Synthesis, Structure, Properties and Applications; Springer Berlin / Heidelberg, 2001, p 29-53.
7. BayerMaterialScience. 2008.
8. Yakobson, B.; Avouris, P. In Carbon Nanotubes: Synthesis, Structure and Applications; Springer Berlin / Heidelberg, 2001, p 287-327.
9. Forró, L.; Schönenberger, C. In Carbon Nanotubes: Synthesis, Structure and Applications; Springer Berlin / Heidelberg, 2001, p 329-391.
10. Avouris, P. Acc. Chem. Res. 2002, 35, 1026-1034.
11. Tasis, D.; Tagmatarchis, N.; Bianco, A.; Prato, M. Chem. Rev. 2006, 106, 1105-1136.
12. Chen, R. J.; Zhang, Y.; Wang, D.; Dai, H. J. Am. Chem. Soc. 2001, 123, 3838-3839.

13. Homenick, C. M.; Lawson, G.; Adronov, A. Polym. Rev. (Philadelphia, PA, U. S.) 2007, 47, 265 - 290.
14. Liu, Y.; Yao, Z.; Adronov, A. Macromolecules 2005, 38, 1172-1179.
15. Qin, S.; Qin, D.; Ford, W. T.; Resasco, D. E.; Herrera, J. E. Macromolecules 2004, 37, 752-757.
16. Li, H.; Cheng, F.; Duft, A. M.; Adronov, A. J. Am. Chem. Soc. 2005, 127, 14518-14524.
17. Baskaran, D.; Dunlap, J. R.; Mays, J. W.; Bratcher, M. S. Macromol. Rapid Commun. 2005, 26, 481-486.
18. Baskaran, D.; Mays, J. W.; Bratcher, M. S. Polymer 2005, 46, 5050-5057.
19. Feng, Q.-P.; Xie, X.-M.; Liu, Y.-T.; Zhao, W.; Gao, Y.-F. J. Appl. Polym. Sci. 2007, 106, 2413-2421.
20. Wu, C.-S. J. Appl. Polym. Sci. 2007, 104, 1328-1337.
21. Sano, M.; Kamino, A.; Okamura, J.; Shinkai, S. Langmuir 2001, 17, 5125-5128.
22. Liu, Y.-X.; Du, Z.-J.; Li, Y.; Zhang, C.; Li, C.-J.; Yang, X.-P.; Li, H.-Q. J. Polym. Sci., Part A: Polym. Chem. 2006, 44, 6880-6887.
23. Mormann, W.; Lu, Y.; Zou, X.; Berger, R. Macromol. Chem. Phys. 2008, 209, 2113-2121.
24. Olalde, B.; Aizpurua, J. M.; Garcia, A.; Bustero, I.; Obieta, I.; Jurado, M., J. J. Phys. Chem. C 2008, 112, 10663-10667.
25. Chen, X.; Chen, X.; Lin, M.; Zhong, W.; Chen, X.; Chen, Z. Macromol. Chem. Phys. 2007, 208, 964-972.
26. Deng, J.; Cao, J.; Li, J.; Tan, H.; Zhang, Q.; Fu, Q. J. Appl. Polym. Sci. 2008, 108, 2023-2028.
27. Chen, W.-F.; Wu, J.-S.; Kuo, P.-L. Chem. Mater. 2008, 20, 5756-5767.
28. Lin, Y.; Zhou, B.; Shiral Fernando, K. A.; Liu, P.; Allard, L. F.; Sun, Y. P. Macromolecules 2003, 36, 7199-7204.
29. Hill, D. E.; Lin, Y.; Rao, A. M.; Allard, L. F.; Sun, Y. P. Macromolecules 2002, 35, 9466-9471.
30. Wang, W.; Lin, Y.; Sun, Y.-P. Polymer 2005, 46, 8634-8640.
31. Blake, R.; Gun'ko, Y. K.; Coleman, J.; Cadek, M.; Fonseca, A.; Nagy, J. B.; Blau, W. J. J. Am. Chem. Soc. 2004, 126, 10226-10227.
32. Blake, R.; Coleman, J. N.; Bryne, M. T.; McCarthy, J. E.; Perova, T. S.; Blau, W. J.; Fonseca, A.; Nagy, J. B.; Gun'ko, Y. K. J. Mater. Chem. 2006, 16, 4206-4213.
33. Wang, X.; Du, Z.; Zhang, C.; Li, C.; Yang, X.; Li, H. J. Polym. Sci., Part A: Polym. Chem. 2008, 46, 4857-4865.
34. Yao, Z.; Braidy, N.; Botton, G. A.; Adronov, A. J. Am. Chem. Soc. 2003, 125, 16015-16024.
35. Qin, S.; Qin, D.; Ford, W. T.; Resasco, D. E.; Herrera, J. E. J. Am. Chem. Soc. 2004, 126, 170-176.
36. Choi, J. H.; Oh, S. B.; Chang, J.; Kim, I.; Ha, C.-S.; Kim, B. G.; Han, J. H.; Joo, S.-W.; Kim, G.-H.; Paik, H.-j. Polym. Bull. 2005, 55, 173-179.
37. Chochos, C. L.; Stefopoulos, A. A.; Campidelli, S.; Prato, M.; Gregoriou, V. G.; Kallitsis, J. K. Macromolecules 2008, 41, 1825-1830.
38. Cheng, B.; Li, Y.; Shen, C. Polym. Prepr. (Am. Chem. Soc., Div. Polym. Chem.) 2004, 45, 653-654.
39. Baskaran, D.; Mays, J. W.; Bratcher, M. S. Angew. Chem., Int. Ed. 2004, 43, 2138-2142.
40. Kong, H.; Gao, C.; Yan, D. J. Am. Chem. Soc. 2004, 126, 412-413.
41. Kong, H.; Gao, C.; Yan, D. Macromolecules 2004, 37, 4022-4030.
42. Gao, C.; Vo, C. D.; Jin, Y. Z.; Li, W.; Armes, S. P. Macromolecules 2005, 38, 8634-8648.
43. Gao, C.; Muthukrishnan, S.; Li, W.; Yuan, J.; Xu, Y.; Muller, A. H. E. Macromolecules 2007, 40, 1803-1815.
44. Hong, C. Y.; You, Y. Z.; Wu, D.; Li, Y.; Pan, C. Y. Macromolecules 2005, 38, 2606-2611.
45. Kong, H.; Gao, C.; Yan, D. J. Mater. Chem. 2004, 14, 1401-1405.
46. Kong, H.; Luo, P.; Gao, C.; Yan, D. Polymer 2005, 46, 2472-2485.

47. Lei, Z.; Wei, X.; Zhang, L.; Bi, S. Colloids Surf., A 2008, 324, 131-136.
48. Liu, Y. L.; Chen, W. H. Macromolecules 2007, 40, 8881-8886.
49. Wu, H.-X.; Tong, R.; Qiu, X.-Q.; Yang, H.-F.; Lin, Y.-H.; Cai, R.-F.; Qian, S.-X. Carbon 2007, 45, 152-159.
50. Matrab, T.; Chancolon, J.; L'Hermite, M. M.; Rouzaud, J.-N.; Deniau, G.; Boudou, J.-P.; Chehimi, M. M.; Delamar, M. Colloids Surf., A 2006, 287, 217-221.
51. Sandler, J.; Shaffer, M. S. P.; Prasse, T.; Bauhofer, W.; Schulte, K.; Windle, A. H. Polymer 1999, 40, 5967-5971.
52. Liao, Y.-H.; Marietta-Tondin, O.; Liang, Z.; Zhang, C.; Wang, B. Mater. Sci. Eng., A 2004, 385, 175-181.
53. Martin, C. A.; Sandler, J. K. W.; Windle, A. H.; Schwarz, M. K.; Bauhofer, W.; Schulte, K.; Shaffer, M. S. P. Polymer 2005, 46, 877-886.
54. Moniruzzaman, M.; Du, F.; Romero, N.; Winey, K. I. Polymer 2006, 47, 293-298.
55. Zhou, Y.; Pervin, F.; Lewis, L.; Jeelani, S. Mater. Sci. Eng., A 2007, 452-453, 657-664.
56. Zhu, J.; Kim, J.; Peng, H.; Margrave, J. L.; Khabashesku, V. N.; Barrera, E. V. Nano Lett. 2003, 3, 1107-1113.
57. Gojny, F. H.; Schulte, K. Compos. Sci. Technol. 2004, 64, 2303-2308.
58. Li, S.; Wang, F.; Wang, Y.; Wang, J.; Ma, J.; Xiao, J. J. Mater. Sci. 2008, 43, 2653-2658.
59. Gojny, F. H.; Wichmann, M. H. G.; Fiedler, B.; Kinloch, I. A.; Bauhofer, W.; Windle, A. H.; Schulte, K. Polymer 2006, 47, 2036-2045.
60. Park, S. J.; Cho, M. S.; Lim, S. T.; Choi, H. J.; Jhon, M. S. Macromol. Rapid Commun. 2003, 24, 1070-1073.
61. Choi, J. Y.; Oh, S. J.; Lee, H. J.; Wang, D. H.; Tan, L. S.; Baek, J. B. Macromolecules 2007, 40, 4474-4480.
62. Oh, S.-J.; Lee, H.-J.; Keum, D.-K.; Lee, S.-W.; Wang, D. H.; Park, S.-Y.; Tan, L.-S.; Baek, J.-B. Polymer 2006, 47, 1132-1140.
63. Gomes, D.; Loos, M. R.; Wichmann, M. H. G.; de la Vega, A.; Schulte, K. Compos. Sci. Technol. 2009, 69, 220-227.
64. Loos, M. R.; Gomes, D. Mater. Lett. 2009, 63, 694-696.
65. Magrez, A.; Kasas, S.; Salicio, V.; Pasquier, N.; Seo, J. W.; Celio, M.; Catsicas, S.; Schwaller, B.; Forro, L. Nano Lett. 2006, 6, 1121-1125.
66. Brayner, R. Nano Today 2008, 3, 48-55.
67. Donaldson, K.; Aitken, R.; Tran, L.; Stone, V.; Duffin, R.; Forrest, G.; Alexander, A. Toxicol. Sci. 2006, 92, 5-22.
68. Poland, C. A.; Duffin, R.; Kinloch, I.; Maynard, A.; Wallace, W. A. H.; Seaton, A.; Stone, V.; Brown, S.; MacNee, W.; Donaldson, K. Nat. Nanotechnol. 2008, 3, 423-428.
69. Takagi, A.; Hirose, A.; Nishimura, T.; Fukumori, N.; Ogata, A.; Ohashi, N.; Kitajima, S.; Kanno, J. J. Toxicol. Sci. 2008, 33, 105-116.
70. Kane, A. B.; Hurt, R. H. Nat. Nanotechnol. 2008, 3, 378-379.
71. Matyjaszewski, K.; Coca, S.; Gaynor, S. G.; Wei, M.; Woodworth, B. E. Macromolecules 1998, 31, 5967-5969.
72. Matyjaszewski, K. Advance in Controlled/Living Radical Polymerization; American Chemical Society: Boston, Massachusetts, 2003.
73. Matyjaszewski, K.; Xia, J. Chem. Rev. 2001, 101, 2921-2990.
74. Hong, S. C.; Paik, H.-j.; Matyjaszewski, K. Macromolecules 2001, 34, 5099-5102.
75. Matyjaszewski, K.; Pintauer, T.; Gaynor, S. Macromolecules 2000, 33, 1476-1478.
76. Munirasu, S.; Deshpande, A.; Baskaran, D. Macromol. Rapid Commun. 2008, 29, 1538-1543.
77. Chu, J.; Chen, J.; Zhang, K. J. Polym. Sci., Part A: Polym. Chem. 2004, 42, 1963-1969.
78. Xia, J.; Matyjaszewski, K. Macromolecules 1997, 30, 7697-7700.
79. Munirasu, S. J.; Ruehe, J.; Dhamodharan, R. J. Polym. Sci., Part A: Polym. Chem. 2006, 44, 2848–2861.
80. Chen, Y.; Shen, Z.; Barriau, E.; Kautz, H.; Frey, H. Biomacromolecules 2006, 7, 919-926.
81. Hamley, I. W. The Physics of Block Copolymers; Oxford University Press, 1999.

82. Hadjichristidis, N.; Pispas, S.; Floudas, G. A. Block Copolymers. Synthetic Strategies, Physical Properties, and Applications; Wiley-VCH, 2002.
83. Müller, A.; Balsamo, V.; Arnal, M. In Block Copolymers II, 2005, p 1-63.
84. Thorsten Goldacker, V. A. Macromol. Rapid Commun. 1999, 20, 415-418.
85. Abetz, V.; Goldacker, T. Macromol. Rapid Commun. 2000, 21, 16-34.
86. Boschetti-de-Fierro, A.; Spindler, L.; Reiter, G.; Olmos, D.; Magonov, S.; Abetz, V. Macromolecules 2007, 40, 5487-5496.
87. Boschetti-de-Fierro, A.; Muller, A. J.; Abetz, V. Macromolecules 2007, 40, 1290-1298.
88. Duxin, N.; Liu, F.; Vali, H.; Eisenberg, A. J. Am. Chem. Soc. 2005, 127, 10063-10069.
89. Staudinger, U.; Satapathy, B. K.; Weidisch, R. Eur. Polym. J. 2008, 44, 1822-1833.
90. Knoll, K.; Niessner, N. Macromol. Symp. 1998, 132, 231-243.
91. Miles, I. S.; Rostani, S. Multicomponent Polymer Systems; Harlow: Longman Scientific & Technical, 1992.
92. Ajayan, P. M.; Schadler, L. S.; Braun, P. V. Nanocomposite Science and Technology; Wiley-VCH Weinheim, 2003.
93. Bockstaller, M. R.; Mickiewicz, R. A.; Thomas, E. L. Adv. Mater. (Weinheim, Ger.) 2005, 17, 1331-1349.
94. Mendoza, C.; Gindy, N.; Gutmann, J. S.; Frömsdorf, A.; Förster, S.; Fahmi, A. Langmuir 2009, 25, 9571-9578.
95. Mendoza, C.; Pietsch, T.; Gindy, N.; Fahmi, A. Adv. Mater. (Weinheim, Ger.) 2008, 20, 1179-1184.
96. Bockstaller, M. R.; Lapetnikov, Y.; Margel, S.; Thomas, E. L. J. Am. Chem. Soc. 2003, 125, 5276-5277.
97. Lan, Q.; Francis, L. F.; Bates, F. S. J. Polym. Sci., Part B: Polym. Phys. 2007, 45, 2284-2299.
98. Ha, Y.-H.; Kwon, Y.; Breiner, T.; Chan, E. P.; Tzianetopoulou, T.; Cohen, R. E.; Boyce, M. C.; Thomas, E. L. Macromolecules 2005, 38, 5170-5179.
99. Hasegawa, N.; Usuki, A. Polym. Bull. 2003, 51, 77-83.
100. Lee, J. Y.; Park, M. S.; Yang, H. C.; Cho, K.; Kim, J. K. Polymer 2003, 44, 1705-1710.
101. Peponi, L.; Valentini, L.; Torre, L.; Mondragon, I.; Kenny, J. M. Carbon 2009, 47, 2474-2480.
102. Park, I.; Lee, W.; Kim, J.; Park, M.; Lee, H. Sensor Actuat B-Chem 2007, 126, 301-305.
103. Lu, L.; Zhou, Z.; Zhang, Y.; Wang, S.; Zhang, Y. Carbon 2007, 45, 2621-2627.

Chapter 3. Experimental Part

3.1. Materials

Multiwall carbon nanotubes (MWCNTs) were obtained from Bayer MaterialScience® (Baytubes, purity > 95%, internal mean diameter = 4 nm, external mean diameter = 13-16 nm, length = 1-10 μm, number of walls = 3-15, denoted $MWCNT_{BMS}^{95}$) and FutureCarbon GmbH (purity > 99%, internal mean diameter = 6 nm, external mean diameter = 15 nm, length = 10-50 μm, number of walls ~ 10, denoted $MWCNT_{FC}^{99}$). In the notation here employed, i.e., $MWCNT_x^y$, the subscript *x* indicates the MWCNTs manufacturer and the superscript *y* the carbon purity of the carbon nanotube.

Styroclear GH62® is an asymmetric star block copolymer containing polystyrene external blocks with different lengths and a polybutadiene core, with a total styrene volume fraction of 0.74, an overall number molecular weight of 110 kg/mol and a polydispersity of approximately 1.4. The size exclusion chromatography trace can be appreciated in Figure 3.1. The block copolymer was synthesized under anionic polymerization conditions, as described elsewhere.[1] In order to simplify the writing, the block copolymer is denoted $AS\text{-}SB_{26}$, where AS stands for asymmetric star, S and B are the monomers, and the subscript is the volume fraction of the polybutadiene block.

Nitric acid (HNO_3, 65 % v/v), thionyl chloride ($SOCl_2$, ≥ 99%), ethylene glycol (EG), polyethylene glycol of 200 g/mol and 400 g/mol (PEG_{200} and PEG_{400}, respectively), 2-bromo-2-methylpropionyl bromide (2BriBr, 99%), triethyl amine

(Et_3N, ≥ 99.5%), dimethylaminopyridine (DMAP, 97%), copper I bromide (CuBr, 99%), N, N, N', N', N-pentamethyl diethylenetriamine (PMDETA, 97%), tetrahydrofurane (THF) and anisole were used as received. Chloroform ($CHCl_3$, ≥ 99%) and styrene (St, ≥ 99.9%) were dried over calcium hydride (CaH_2) and distilled before use. All the reagents were purchased from Aldrich.

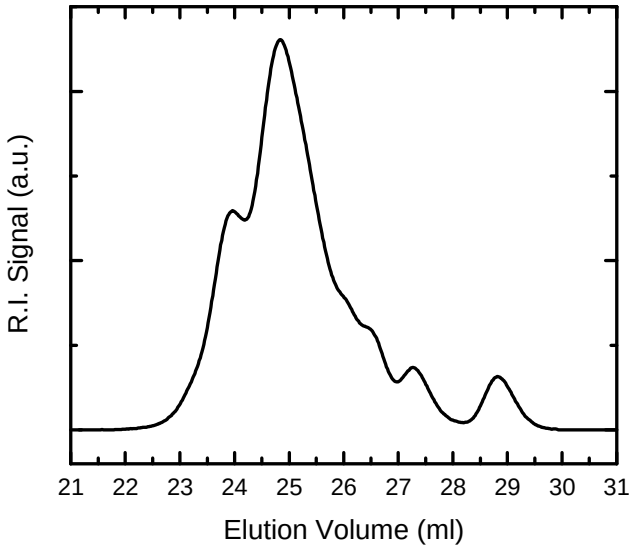

Figure 3.1. SEC trace of the AS-SB_{26}.

3.2. Surface functionalization of multiwall carbon nanotubes

Different functionalization reactions were performed on the surface of the MWCNTs, details of these reactions are described in this section.

3.2.1. Oxidation of MWCNTs

The schematic representation of the oxidation reactions can be appreciated in Figure 3.2. In a typical experiment, 1 g of $MWCNT_x^y$ was dispersed in 40 ml of HNO_3 (65 % v/v) in a round bottom flask. The dispersion was homogenized for 30 min in an ultrasonication bath (Bandelin SONOREX, f = 35 kHz) at ambient temperature. The round bottom flask was then placed in a silicon bath at 65 °C for 48 hours under

continuous stirring. After the reaction was completed, the dispersion was filtered and washed with copious amounts of deionized water until the pH reached constant values. Finally, the oxidized nanotubes were dried at 60 °C under vacuum for 72 hours. The carbon nanotubes after the oxidation treatments are denoted $^{oxid}MWCNT_x^y$.

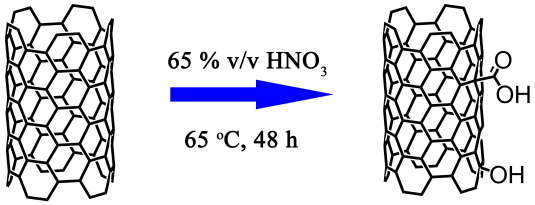

Figure 3.2. Schematic representation of the oxidation reaction carried out on the MWCNTs.

3.2.2. Acid to Acid Chloride Conversion and Esterification I: Glycol Spacer

The oxidized carbon nanotubes (400 mg) were chlorinated in the presence of $SOCl_2$ (28 ml) for 24 hours at 65 °C. After the reaction, the dispersion was generously washed with THF, filtered and dried at ambient temperature overnight. The acyl or alkyl chloride functionalized MWCNTs were refluxed with different amounts of EG or PEG at 120 °C for 48 hours. The hydroxyl decorated carbon nanotubes were passed through a Teflon® membrane (0.2 μm pore size), washed with THF and dried for 48 hours at ambient temperature. The products were repeatedly dispersed in THF, filtered and dried. The reaction is summarized in Figure 3.3. Details of the reaction conditions can be appreciated in Table 3.1.

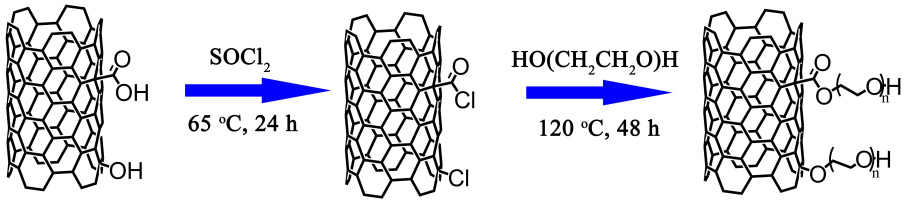

Figure 3.3. Schematic representation of the oxidation reaction between oxidized $MWCNT_x^y$ with thionyl chloride and ethylene glycol/poly(ethylene glycol).

Table 3.1. Experimental conditions employed for the esterification with glycols and 2BriBr of $MWCNT_{BMS}^{95}$ and $MWCNT_{FC}^{99}$.

Sample	Esterification I (EG or PEG)[a]		Esterification II (Initiator anchoring)	
	Type[a]	[glycol] (mol/g)[b]	[2BriBr] (µl/mg)[c,d]	[MWCNT] (mg/ml)[e]
$MWCNT_{FC}^{99}$-Br^1	EG	1.3	1.4	6.5
$MWCNT_{FC}^{99}$-Br^2	EG	1.3	2.7	6.9
$MWCNT_{FC}^{99}$-Br^3	PEG_{200}	1.3	2.7	6.9
$MWCNT_{FC}^{99}$-Br^4	PEG_{400}	1.3	5.4	6.9
$MWCNT_{FC}^{99}$-Br^5	PEG_{400}	0.6	2.7	6.0
$MWCNT_{FC}^{99}$-Br^6	PEG_{400}	1.3	2.7	6.9
$MWCNT_{FC}^{99}$-Br^7	PEG_{200}	1.3	2.7	6.9
$MWCNT_{BMS}^{95}$-Br^1	EG	1.3	1.4	15.6
$MWCNT_{BMS}^{95}$-Br^2	EG	1.3	2.7	16.0
$MWCNT_{BMS}^{95}$-Br^3	PEG_{200}	1.3	1.4	15.7
$MWCNT_{BMS}^{95}$-Br^4	PEG_{400}	1.3	1.4	15.6

a) EG: ethylene glycol; PEG_{200} and PEG_{400}: polyethylene glycol of 200 g/mol and 400 g/mol, respectively; b) relation between EG or PEG (mol) and MWCNT (g); c) relation between 2BriBr (µl) and MWCNT (mg); d) [Et_3N] = 0.3 mol%, [DMAP] = 0.05 mol% (respect to 2BriBr); e) relation between MWCNT (mg) and CH_3Cl (ml) used during the reaction.

3.2.3. Anchoring of initiator groups

The functionalization with initiator groups suitable for the grafting of styrene was done following the work of Kong et al.[2] In a typical reaction (see entry 1, Table 3.1), hydroxyl decorated carbon nanotubes (150 mg) were dispersed in $CHCl_3$ (9.2 ml) with a catalytic amount of Et_3N (228 µl) and DMAP (29 µl). The system was immersed in an ultrasonication bath for 10 min under Ar flow. Then, the dispersion

was cooled down in an ice bath and thrice vacuum filled with Ar. A diluted solution of 2BriBr (210 µl) in $CHCl_3$ (2.4 ml) was added drop wise for approximately 1 hour. The reaction was kept in the ice bath for three hours and after that at ambient temperature for 48 hours. The reaction scheme can be observed in Figure 3.4. After the reaction, the carbon nanotubes grafted with initiator groups were passed through a Teflon® membrane and washed with copious amounts of $CHCl_3$. The carbon nanotubes were redispersed in $CHCl_3$, filtered and dried three times. The notation employed here is $MWCNT_x^y$-Br, where the Br indicates the anchoring of the initiator. Details of the reactions are also shown in Table 3.1.

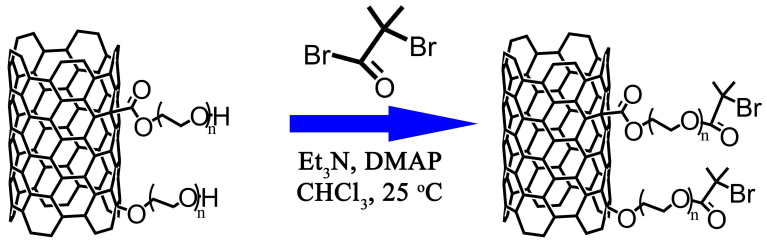

Figure 3.4. Schematic representation for the anchoring of initiator groups for ATR polymerization.

3.2.4. *Grafting from* styrene under atom transfer radical polymerization (ATRP) conditions

In a Schlenk tube, $MWCNT_{BMS}^{95}$-Br or $MWCNT_{FC}^{99}$-Br, 0.7 mol % of CuBr(I) (respect to the monomer) were dispersed in St and anisole (4 % v/v with respect to the monomer) under Ar flow for 60 min. After 3 freeze-pump-thawed cycles, 0.7 mol % of PMDETA (with respect to the monomer) was added and the tube was transferred into an oil bath at 90 °C. Detailed information regarding the reaction conditions are detailed in Table 3.2. When the reaction was completed, the solution was diluted with toluene and precipitated in methanol. The precipitated sample was filtered using a Teflon® membrane and dried for 48 hours. After drying, the polystyrene grafted carbon nanotubes were again dispersed in $CHCl_3$ for 24 hours, filtered and dried. This

procedure was repeated until no traces of polymer were collected from the filtered solution by precipitation in methanol. Figure 3.5 shows the schematic procedure for this reaction. The polystyrene grafted carbon nanotubes are denoted $PS_w^qMWNCNT_x^y$, where the subscript *w* represents the weight percent of polystyrene grafted, and the superscript *q* represents the molecular weight of the grafted polymer (in kg/mol).

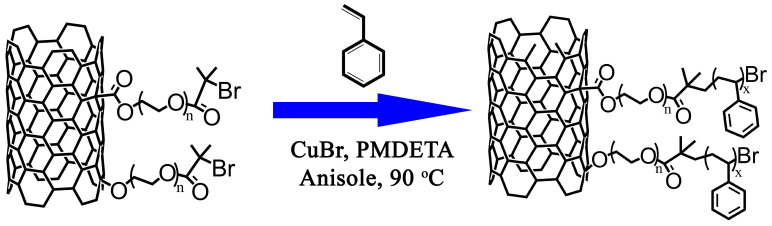

Figure 3.5. Schematic representation for the *grafting from* reaction of polystyrene.

Table 3.2. Experimental conditions employed for the styrene *grafting from* reaction at $MWCNT_{BMS}^{95}$ and $MWCNT_{FC}^{99}$

Sample	Source	St[a]		t_{rxn}
		(wt %)	(mol %)	(h)
$PS_{19}^{3}MWCNT_{FC}^{99}$	$MWCNT_{FC}^{99}$-Br^{1}	30	4000	20.0
$PS_{9}^{1}MWCNT_{FC}^{99}$	$MWCNT_{FC}^{99}$-Br^{2}	30	2200	20.1
$PS_{11}^{1}MWCNT_{FC}^{99}$	$MWCNT_{FC}^{99}$-Br^{3}	30	1300	20.2
$PS_{44}^{3}MWCNT_{FC}^{99}$	$MWCNT_{FC}^{99}$-Br^{4}	30	1200	20.1
$PS_{85}^{24}MWCNT_{FC}^{99}$	$MWCNT_{FC}^{99}$-Br^{4}	120	4700	19.4
$PS_{28}^{10}MWCNT_{FC}^{99}$	$MWCNT_{FC}^{99}$-Br^{5}	30	6700	23.7
$PS_{22}^{2}MWCNT_{FC}^{99}$	$MWCNT_{FC}^{99}$-Br^{6}	30	2100	20.1
$PS_{13}^{2}MWCNT_{FC}^{99}$	$MWCNT_{FC}^{99}$-Br^{7}	30	3800	20.0
$PS_{23}^{4}MWCNT_{FC}^{99}$	$MWCNT_{FC}^{99}$-Br^{7}	60	7700	20.0
$PS_{31}^{6}MWCNT_{FC}^{99}$	$MWCNT_{FC}^{99}$-Br^{7}	120	15400	20.1
$PS_{32}^{6}MWCNT_{FC}^{99}$	$MWCNT_{FC}^{99}$-Br^{7}	120	15400	20.2
$PS_{11}^{2}MWCNT_{FC}^{99}$	$MWCNT_{FC}^{99}$-Br^{7}	30	3800	20.2
$PS_{34}^{7}MWCNT_{BMS}^{95}$	$MWCNT_{BMS}^{95}$-Br^{1}	30	3400	21.0
$PS_{43}^{10}MWCNT_{BMS}^{95}$	$MWCNT_{BMS}^{95}$-Br^{1}	30	3400	26.0
$PS_{47}^{11}MWCNT_{BMS}^{95}$	$MWCNT_{BMS}^{95}$-Br^{1}	60	6800	20.0

Table 3.2. *cont'd*

Sample	Source	St[a]		t_{rxn}
		(wt %)	(mol %)	(h)
$PS_{91}{}^{20}MWCNT_{BMS}{}^{95}$	$MWCNT_{BMS}{}^{95}$-Br^2	30	430	20.0
$PS_{85}{}^{9}MWCNT_{BMS}{}^{95}$	$MWCNT_{BMS}{}^{95}$-Br^2	60	870	18.0
$PS_{70}{}^{4}MWCNT_{BMS}{}^{95}$	$MWCNT_{BMS}{}^{95}$-Br^2	60	870	7.0
$PS_{86}{}^{17}MWCNT_{BMS}{}^{95}$	$MWCNT_{BMS}{}^{95}$-Br^3	30	740	20.0
$PS_{49}{}^{7}MWCNT_{BMS}{}^{95}$	$MWCNT_{BMS}{}^{95}$-Br^4	30	2900	20.1

a. weight and mole percent of St respect to the $MWCNT_x{}^y$-Br

3.3. Preparation of the nanocomposite films

Nanocomposites based on AS-SB_{26} were prepared using different MWCNTs by film casting. Two different strategies were used to disperse the MWCNTs prior to the blending with AS-SB_{26}. In the approach used in Chapter 5, a given amount of MWCNTs were dispersed in toluene. After the dispersion was optically homogeneous, the AS-SB_{26} (5 % w/v) was added and the blend was continuously stirred for 24 hours at ambient temperature. The dispersions were homogenized with the use of an ultrasonic probe for 2 min (Bandelin SONOPULS®, *f* = 20 kHz), centrifuged for 10 min (SIGMA 3K15, rotor speed = 11000 rpm) and casted at 60 °C for 48 hours over Teflon® supports. This strategy is sketched in Figure 3.6. After casting process, the films were cut into stripes of approximately of 10 mm x 70 mm.

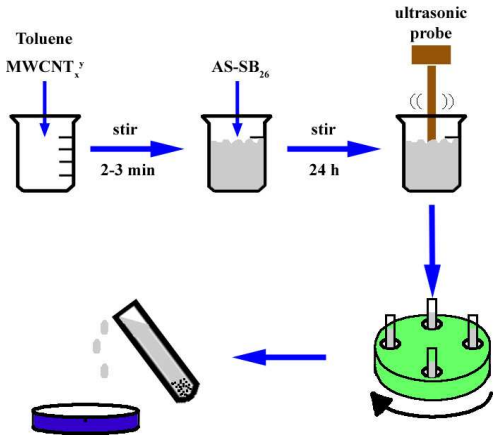

Figure 3.6. Film casting strategy employed in Chapter 5.

The strategy employed in Chapter 6 (see Figure 3.7) consisted of the preparation of a dispersion of the carbon nanotubes in $CHCl_3$ for 24 hours at ambient temperature. The dispersions were placed in an ultrasonic bath for 10 min (Bandelin SONOREX, f = 35 kHz) and centrifuged for 10 min (SIGMA 3K15, rotor speed = 11000 rpm). The supernatants were extracted and recovered by filtration. A solution of 5 % w/v of AS-SB_{26} containing a given amount of MWCNTs recovered from the supernatants was stirred in toluene at ambient temperature for 24 hours. The dispersions were then homogenized for 2 min with an ultrasonic probe (Bandelin SONOPULS®, f = 20 kHz), and directly poured on glass plates at 60 °C or 90 °C for 24 hours. After casting, the films were dried for 48 hours at 70 °C. Finally, the films were cut into stripes of approximately of 10 mm x 70 mm.

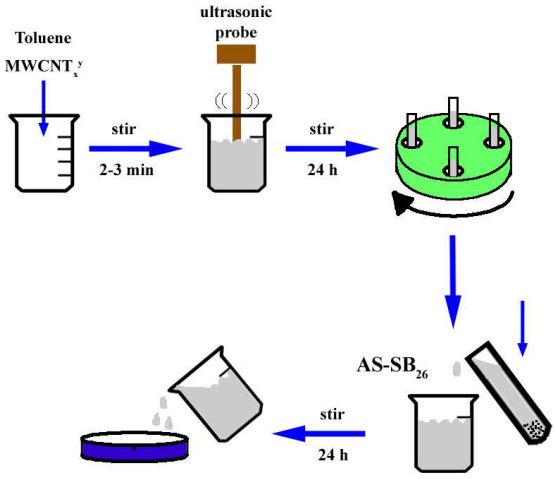

Figure 3.7. Film casting strategy employed in Chapter 6.

3.4. Characterization

3.4.1. Size Exclusion Chromatography (SEC)

SEC measurements were performed using a Waters instrument. The instrument is equipped with four PSS columns with a porosity range from 10^2 to 10^5 Å coupled with a differential refractometer (Waters™ 2410 RI) and a UV detector (Waters™ 486, at 254 nm). The samples were dissolved in THF (2 % wt/v) and measured at 30

°C with a flow rate of 1 ml/min using toluene as internal standard. The results were calibrated with polystyrene standards.

3.4.2. Elemental Analysis

The content of carbon, hydrogen, and bromine atoms was determined after the anchoring of the initiator groups at the surface of the $MWCNT_x^y$ (section 3.2.3). In the case of the carbon and hydrogen atoms, the carbon nanotubes were combusted and the oxidation gases produced were reduced and analyzed by gas chromatography. The bromine content was determined by potentiometric titration.

3.4.3. Nuclear Magnetic Resonance Spectroscopy (^{1}H-NMR)

The ^{1}H-NMR spectra of the polystyrene grafted carbon nanotubes were performed in a Bruker AV-300 at 300 MHz. The polystyrene grafted carbon nanotubes (0.1 % wt/v) were dispersed in $CDCl_3$ and placed in the ultrasonic bath (Bandelin SONOREX, f = 35 kHz) for 5 min before the measurements.

3.4.4. Fourier transform infrared Spectroscopy (FTIR)

Fourier transform infrared spectra (FTIR) were conducted on a Bruker Equinox 55. The samples were carefully dispersed in potassium bromide (KBr), placed in a vacuum oven at 60 °C for 24 hours. The content of carbon nanotubes in the KBr pellets varied from 0.025 wt %, in the case of the carbon nanotubes without polymer coating, to 0.05 wt % in the case of the polymer grafted carbon nanotubes. The infrared spectra were recorded in a spectral range of 400-4000 cm^{-1}, with a spectral resolution of 1 cm^{-1}.

3.4.5. Thermogavimetric analysis (TGA)

Thermal gravimetric analysis (TGA) measurements were carried out on a Netzsch TG209 F1 Iris. The experiments were conducted under a constant Ar flow (20 ml/min), from 25 °C to 900 °C, at a constant rate of 20 °C/min.

3.4.6. Differential Scanning Calorimetry (DSC)

Differential scanning calorimetry (DSC) experiments were performed using a Netzsch DSC Phoenix. The equipment was calibrated using indium and cyclohexane. Standard aluminum pans of 50 µl were used to encapsulate the samples of 10 mg ± 1 mg. Dynamic heating and cooling scans were performed. The samples were first heated to 150 °C, held for 3 min, cooled down to 25 °C, held for another 3 min, and finally heated to 150 °C. All the measurements were done under N_2 atmosphere at a constant rate of 20 °C/min.

3.4.7. Optical Microscopy (OM)

Optical microscopy (OM) studies were performed on a “Leica” DMLM microscope. The nanocomposite films were directly placed on a glass slide and observed in transmission mode at ambient temperature.

3.4.8. Scanning Electron Microscopy (SEM)

Scanning electron microscopy (SEM) studies were done on a Zeiss LEO Gemini 1550VP (1 kV). In the case of the MWCNTs, they were directly glued with conducted tape on the sample holders. The MWCNTs containing more than 40 wt % of grafted polymer were sputtered with a fine layer of Au/Pd, the other samples were observed without being sputtered. In the case of the nanocomposite films, the cross sections of

the samples were fractured under cryogenic conditions and were sputtered with a fine layer of Au/Pd before observation.

3.4.9. Transmission Electron Microscopy (TEM)

The TEM experiments were done using a FEI Tecnai G^2 F20 operated at 200 kV. The MWCNTs were dispersed in $CHCl_3$ (5 % w/v) for 24 hours at ambient temperature. After 24 hours, the dispersion were homogenized for 1 min with an ultrasonic probe (Bandelin SONOPULS®, *f* = 20 kHz) and one drop (5 µl) was placed on a TEM grid. The nanocomposite films were cut on thin sections (50 nm – 100 nm) at -130 °C with a Reichert-Jung Ultracut E microtome equipped with a diamond knife. Contrast between the microphases of the block copolymer was achieved by exposing the nanocomposites to OsO_4 vapor for approximately 1 min. The TEM analyses have the limitation that only specific areas of the sample can be observed. For this reason, several images of the nanocomposites were taken in order to verify the description given in the discussion, and selected representative images were chosen.

3.4.10. TappingMode™ Scanning Force Microscopy (SFM)

The SFM experiments were performed on a "Veeco" MultimodeTM AFM (NanoScope IV controller) operating in tapping mode at ambient temperature. Silicon TM AFM tips (model MPP-12100) with a free resonance of 150 kHz and spring constant of 5 N/m were employed. The MWCNTs were dispersed in $CHCl_3$ (5 % w/v) for 24 hours at ambient temperature. After 24 hours, the dispersion was homogenized for 1 min with an ultrasonic probe (Bandelin SONOPULS®, *f* = 20 kHz) and one drop (5 µl) was placed on a clean polished silicon wafer. The silicon wafers were previously cleaned in a water-saturated UV-ozone atmosphere for at least 24 hours.

3.4.11. AC conductivity measurements

AC conductivity measurements were studied by dielectric spectroscopy using a HP 4284a impedance analyzer. At least three films were evaluated with voltage amplitude of 1.0 V, on a frequency range between 20 Hz and 1 MHz, at ambient temperature. The conductivity was calculated from the complex impedance (Z^*) according to $\sigma = 1/\lfloor Z^*(\upsilon)\rfloor t/A$, where t represents the thickness of the sample and A the cross sectional area (~1 cm^2).[3]

3.4.12. Dynamical Mechanical Thermal Analysis (DMTA)

Dynamic mechanical thermal analysis experiments were performed on a RSAII from "TA Instruments". Films of AS-SB_{26} and the nanocomposites (10 mm x 5 mm x 100 µm) were cut with the help of a scalpel. Frequency scans were done between 0.01 rad/s and 100 rad/s with a constant strain of 0.5 % at two temperatures (25 °C and 90 °C). The samples have an average dimension of 5 mm x 80 mm x 100 µm.

3.4.13. Viscosity measurements

The viscosity measurements of the dispersed MWCNTs before and after the oxidation reactions were carried out in a Brookfield R/S rheometer. The experiments were performed at a constant rate (500 s^{-1}) for 2 min in a plate/plate geometry (C75-1). The MWCNTs (1 % w/v) were dispersed in ethylene glycol for 24 hours at ambient temperature. Before the measurements, the dispersions were then homogenized for 5 min with an ultrasonic probe (Bandelin SONOPULS®, f = 20 kHz).

3.4.14. Strain-stress experiments

The strain-stress experiments were carried out on a "Zwick" model Z020, with a load cell of 20 kN. The measurements were done with a crosshead speed of 5 mm/min at

ambient temperature, according to the standard ASTM D882. The samples have an average dimension of 10 mm x 80 mm x 100 µm.

3.4.15. Simultaneous Small Angle X-ray Scattering (SAXS) and strain-stress experiments

Simultaneous Small Angle X-ray Scattering (SAXS) and strain-stress experiments were performed at the BW4 beamline of DORIS III, HASYLAB at DESY in Hamburg, Germany. The sample to detector distance used was set to 4.04 m and the wavelength of the beam was 1.38 Å. The 2D-SAXS images were recorded with a marCCD165 detector. The tensile test equipment was available in the line. The tensile test equipment simultaneously moves the upper and lower clamps in opposite directions thus keeping the beam on the same position of the sample during its deformation. The straining rate was set to 5 mm/min. The 2D-SAXS images were collected every 5 % of deformation. The samples have an average dimension of 10 mm x 80 mm x 100 µm.

3.5 References

1. Knoll, K.; Niessner, N. Macromol. Symp. 1998, 132, 231-243.
2. Kong, H.; Gao, C.; Yan, D. Macromolecules 2004, 37, 4022-4030.
3. Gojny, F. H.; Wichmann, M. H. G.; Fiedler, B.; Kinloch, I. A.; Bauhofer, W.; Windle, A. H.; Schulte, K. Polymer 2006, 47, 2036-2045.

Chapter 4. Modification of Multiwall Carbon Nanotubes by *Grafting from* Controlled Polymerization of Styrene: Effect of the Characteristics of the Nanotubes

4.1. Introduction

The incorporation of carbon nanotubes in polymer matrices has become a challenge during the past decade.[1] The outstanding mechanical, electrical and thermal properties of the carbon nanotubes (reviewed in Chapter 2) have inspired the design of a new generation of light weight materials,[1-3] or even their use as biosensors or biocarriers,[4-7] although their biocompatibility is still questionable.[8-11]

The tendency of the carbon nanotubes to aggregate due to the strong π-π stacking interactions between graphene sheets is an important drawback for the inclusion of these nanofillers in polymer matrices. Several strategies have been used to reduce the size of the aggregates or to improve the dispersion of individual carbon nanotubes. Sonication, centrifugation, calendaring or intense stirring have shown promising results on SWCNT, DWCNT and MWCNT carbon nanotube dispersions in solvents and different polymer matrices.[2,3,12-14] The dispersion in different solvents has been also achieved through the interaction or physisorption of surfactants and polymers.[15] Other approaches aim for the tuning of the surface of carbon nanotubes through chemical modification. These include the reaction on the graphene sheet and the creation of new functional groups by the degradation of the structure or the attack on labile points as a consequence of the synthesis, like caps and defects.[16]

One alternative for the improvement of the dispersion of carbon nanotubes in polymer matrices is the grafting of polymers at their surface. The grafting of polymers at carbon nanotubes can be divided in two general cases: *grafting onto* and *grafting from*. Generally, the efficiency of the *grafting onto* reactions decreases with the increase of the molecular weight of the grafted polymer, because of the steric hindrance between polymer chains or the decrease in the accessibility of the functional groups.[17]

Higher molecular weights and grafting densities can be obtained through the grafting of polymer from the surface of carbon nanotubes because of the easier access of the monomer to the growing chain.[6,17-29] The most versatile technique used on the grafting of polymer from carbon nanotubes (and other substrates) is the controlled radical polymerization.[6,17-19,21-23,30-43] The advantage of the controlled radical polymerization compared with other polymerization techniques have been previously discussed. There are diverse references regarding the *grafting from* carbon nanotubes where the control on the polymerization is achieved by adjusting the concentration of monomer, initiator or deactivator.[6,20,21,30,32] However, the characteristics of the carbon nanotubes and how they could affect the surface functionalization has not been discussed until now, mainly because they vary depending on the supplier and the method of synthesis. In this chapter, a comparison between two commercially available multiwall carbon nanotubes ($MWCNT_{BMS}$[95] and $MWCNT_{FC}$[99]) subjected to functionalization reactions and their influence on the *grafting from* of styrene is presented for the first time.

4.2. Results and Discussion

4.2.1. Oxidation of the MWCNTs

The first step implies the oxidation of the pristine MWCNTs with HNO_3, the scheme of the reaction is shown in Figure 3.2. The FTIR spectra of the pristine and oxidized MWCNTs can be appreciated in Figure 4.1. Many authors attribute the signals between 1650 cm^{-1} and 1540 cm^{-1} to the C=C stretching mode of the aromatic ring.[44-47] Around 1460 cm^{-1}, the C-H bending alkyl vibrations can be observed. Besides these signals, other features in the pristine MWCNTs are interesting. A clear C-H stretching vibration in the vicinity of a carboxylic group (~1430 cm^{-1}) and a rocking vibration (~1380 cm^{-1}) could indicate the presence of quinones and aldehydes, respectively. The C=O vibration in both cases might be overlapped with the stretching mode of the aromatics. Another feature around 1160 cm^{-1} is related with the C-O-C stretching from aromatic esters. The described bands show that the MWCNT skeleton is not just composed of crystalline graphite layers but have also defects coming from the synthesis or the rest of catalyst. These imperfections might have consequences on the properties of the MWCNTs; however, they may also represent an advantage if reactions on these "weak points" can improve the dispersion of the MWCNTs in solvents or polymers. After oxidation, a C=O stretching vibration related with esters is easily identified for the $MWCNT_{FC}$[99]. In the case of the $MWCNT_{BMS}$[95], the C=O vibration is located at a lower wavenumber (broad peak) that would indicate the presence of carboxylic acid,[48] and a relative increase in the intensity at 1575 cm^{-1} is observed. This signal might be related with a keto-enol tautomerism. One interesting change due to the oxidation reaction is the appearance of a strong signal in MWCNTs from both suppliers around 1380 cm^{-1}. The assignment could be related again with the C-H rocking vibration of aldehydes, but this would imply a stronger signal at around

1700 – 1650 cm^{-1}, which is not observed. A second and more probable explanation could be the formation of phenols which present such strong signal due to the combination of O-H and C-O deformation vibrations. Another hypothesis is the formation of nitrobenzene groups along the nanotubes, which is plausible since the presence of nitrogen atoms after HNO_3 treatment has been previously reported.[49] The nitrobenzene group has a sharp signal around the mentioned wavenumber due to the symmetric stretching vibration of the NO_2 group, but, the FTIR spectra do not show the asymmetric vibration band at around 1550 cm^{-1}. Even though the reaction might lead to the grafting of nitroxy groups, the conditions used are not the most adequate.[50] The oxidation favors the formation of phenol groups in MWCNTs from both suppliers; esters groups seem more favorable in case of the $MWCNT_{FC}$[99], while in the case of the $MWCNT_{BMS}$[95] the presence of ketones and carboxylic acid groups is predominant.

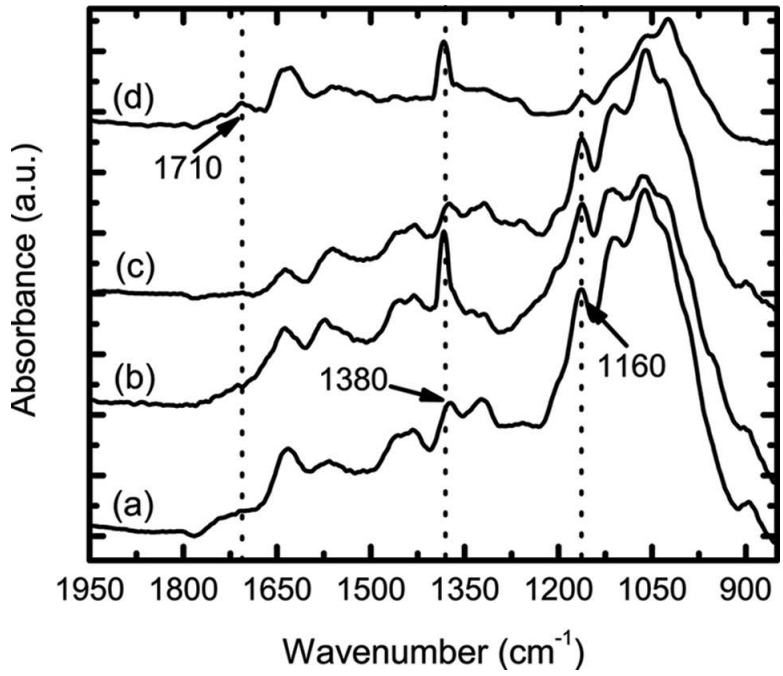

Figure 4.1. Fourier transform infrared spectra of multiwall carbon nanotubes from different sources before and after the oxidation reaction: (a) pristine and (b) oxidized $MWCNT_{BMS}$[95], (c) pristine and (d) oxidized $MWCNT_{FC}$[99].

It is known that, in order to obtain high concentrations of carboxylic acid groups (or their derivatives) on carbon nanotubes, treatments more aggressive than the one used here are required, such as combinations of HNO_3 with stronger acids (like sulfuric acid) or air oxidation at high temperatures.[51-53] Such treatments lead to the destruction of the graphitic structure, reduction on the length, disaggregation of the bundles, and improvement of the dispersion of the carbon nanotubes in organic solvents. The aim of the chosen acid treatment was to preserve the carbon nanotubes by aiming to attack defects already present in the structure and to dissolve the catalysts and the synthesis byproducts (e.g., amorphous carbon), without cutting the length of the carbon nanotubes or loosing any of the walls. The achieved disappearance of catalyst or amorphous carbon was appreciated by transmission electron microscopy, as shown in Figure 4.2 for the $MWCNT_{BMS}$[95]. Additionally, TEM images show that the numbers of walls are preserved (see inserts in Figure 4.2). In the case of the $MWCNT_{FC}$[99], catalyst residues were not appreciated in the pristine sample during the observations (results not shown). Some pioneering works have proposed correlation models between the nanotubes length against time for different oxidation systems on SWCNT.[51,54] Unfortunately, these results cannot be directly correlated to the ones presented here because the oxidation depends on factors related with the number of walls, purity, synthesis process and source of the carbon nanotubes.[53] A systematic study is required in order to understand the effect of the oxidation on identical MWCNT exposed to mild and aggressive oxidation conditions.

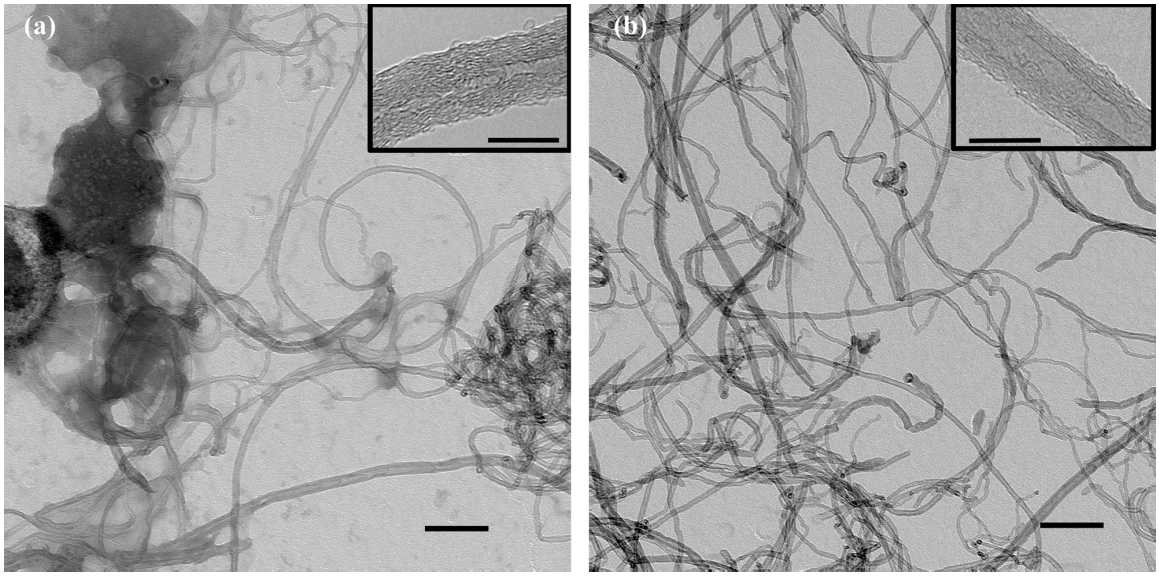

Figure 4.2. Transmission electron micrographs of (a) pristine and (b) oxidized $MWCNT_{BMS}$[95]. Scale bar = 100 nm, insert = 10 nm.

4.2.2. Acid to Acid Chloride Conversion and Esterification I: Glycol Spacer

Further reaction between the oxidized carbon nanotubes and thionyl chloride leads to the formation of alkyl and acyl chloride groups. Experimental and theoretical evidences have shown that carbon nanotubes could also absorb thionyl chloride and the presence of moisture gives rise to byproducts that could form C-Cl bonds on the structural defects.[55] The acyl or alkyl chloride groups are highly reactive and can further form esters or ethers, respectively, in the presence of an alcohol. Glycols of different molecular weights were used in this work. These α,ω-dihydroxy-functionalized telechelics will be used as spacers between the carbon nanotubes and the initiator moieties necessary for the *grafting from* of styrene. While increasing the glycol molecular weight from 62 g/mol (ethylene glycol) to 400 g/mol, the weight loss between 100 °C and 500 °C (determined by thermal gravimetric analysis) increases from approximately 5 % to more than 18 %, as can be observed in Figure 4.3.

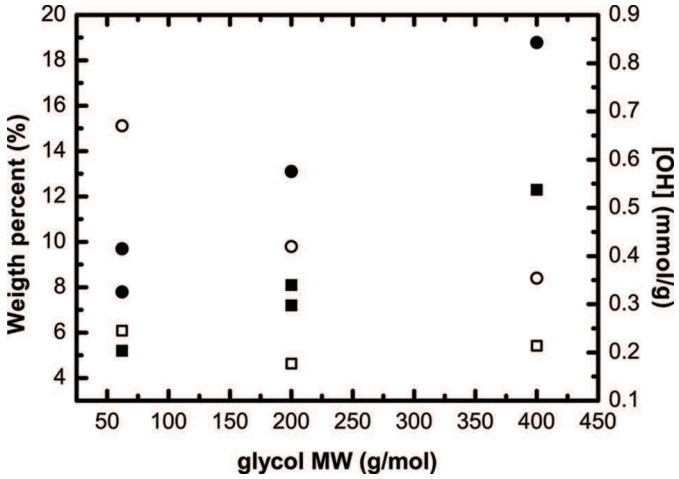

Figure 4.3. Glycol grafting content (left axes, filled symbols) and concentration of hydroxyl groups (right axes, open symbols) vs. glycol molecular weight for $MWCNT_{BMS}$[95] (●, ○) and $MWCNT_{FC}$[99] (■, □).

The MWCNT source also has an effect on the reaction product; since it was observed that the grafting content of ethylene glycol on $MWCNT_{BMS}$[95] is almost the double of the content obtained on $MWCNT_{FC}$[99]. On one hand, the concentration of reactive groups on $MWCNT_{BMS}$[95] and $MWCNT_{FC}$[99] could explain the difference in grafting efficiency; however, the characterization techniques available for the determination of the concentration are still not reliable. On the other hand, the difference in grafting could be also attributed to the differences in the dimension of the carbon nanotube and the quality of the dispersion during the reaction. The contour length of the pristine and the oxidized MWCNTs were examined by scanning force microscopy (SFM). The distribution of the MWCNTs contour lengths can be appreciated in Figure 4.4. Approximately one hundred independent length measurements were done on each case, from different positions on several silicon wafers.

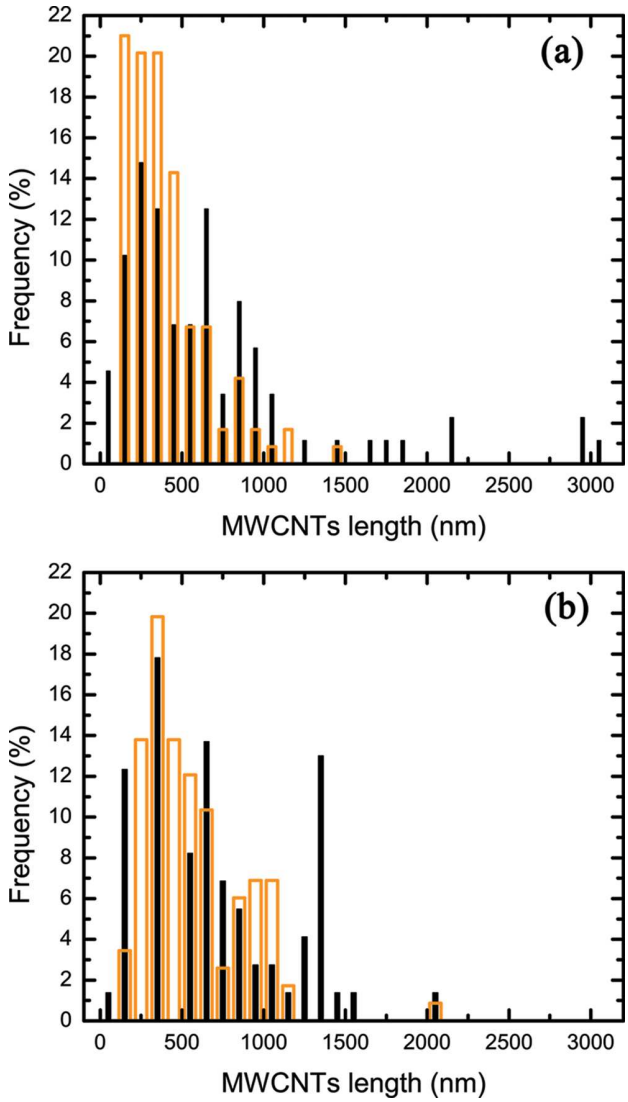

Figure 4.4. Carbon nanotube length distribution (nm) of (a) pristine MWCNTs and (b) oxidized MWCNTs, calculated from SFM phase images. Filled bars (black) correspond to $MWCNT_{BMS}^{95}$ and contour bars (orange) correspond to $MWCNT_{FC}^{99}$.

Although the reported information in the technical data sheets of the products indicates that the $MWCNT_{BMS}^{95}$ are on average shorter than the $MWCNT_{FC}^{99}$, the results in Figure 4.4 show the contrary. The length distribution of the pristine carbon nanotubes is 370 ± 60 nm and 225 ± 30 nm, for $MWCNT_{BMS}^{95}$ and $MWCNT_{FC}^{99}$, respectively. It has to be pointed out that just the carbon nanotubes dispersed on the silicon wafers were taken into account for the measurements, longer carbon nanotubes could be present in the form of aggregates that could not be dispersed under the

experimental conditions employed. The ultrasonic probe was used to disaggregate the carbon nanotubes before dropping the dispersion on the silicon wafer. The ultrasonic treatment could also induce the cleavage of the carbon nanotubes, especially if the graphitic structure has defects. In any case, comparison can be made between the $MWCNT_{BMS}$[95] and the $MWCNT_{FC}$[99] because the carbon nanotubes were dispersed under the same conditions. After the oxidation reaction, the population of carbon nanotubes with shorter lengths decreases in both cases, which evidences that the HNO_3 is also able to worsen the structure of the carbon nanotubes. The distribution of the length of the carbon nanotubes is slightly displaced to higher values after the acid treatment. This probably indicates that the acid treatment unbundled the long carbon nanotubes from the aggregates.

While the SFM measurements give an indication of the length of the isolate carbon nanotubes, the viscosity of the dispersion of carbon nanotubes could give evidences of the state of aggregation of the nanoparticles. Table 4.1 shows the viscosity of the dispersion of MWCNTs in ethylene glycol before and after the acid treatment. The viscosity of the MWCNTs dispersions in ethylene glycol increases after the acid treatment. The increase in viscosity can be associated with the deaggregation of the MWCNTs that leads to the presence of longer carbon nanotubes or looser aggregates in the dispersion. Additionally, the viscosity of the dispersion of the $MWCNT_{FC}$[99] is more than two times higher than the $MWCNT_{BMS}$[95]. These differences could be associated to the structure of the aggregates. It is known that the synthesis process of the $MWCNT_{BMS}$[95] leads to the formation of highly bundled nanoparticles, whereas the synthesis of the $MWCNT_{FC}$[99] to more loose aggregates. The viscosity results obtained could indicate that the highly aggregated MWCNTs have a minor incidence on the

viscosity of the dispersion while, on the contrary, the loose aggregate structure increases the relative viscosity of the dispersion. This assumption is corroborated after the acid treatment, where the viscosity of the dispersion $MWCNT_{BMS}^{95}$ and $MWCNT_{FC}^{99}$ increases approximately 20 % and 80 %, respectively. The oxidation reaction using HNO_3 unbundles more efficiently the $MWCNT_{FC}^{99}$ compared to the $MWCNT_{BMS}^{95}$. It is expected then that the low viscosity of the dispersion containing the acyl and alkyl chloride functionalized $MWCNT_{BMS}^{95}$ favors the grafting reaction more than the dispersion containing the acyl chloride functionalized $MWCNT_{FC}^{99}$. However, the relative low increase in viscosity of the dispersion of $MWCNT_{BMS}^{95}$ after the oxidation reaction might indicate that the disaggregation of these carbon nanotubes during the functionalization reactions is more difficult compare with the $MWCNT_{FC}^{99}$; as a consequence, the functionalization of the $MWCNT_{BMS}^{95}$ probably takes place rather on the surface of aggregates than on isolated carbon nanotubes.

Table 4.1. Viscosity of the dispersion of carbon nanotubes in ethylene glycol (1 % wt/v). Values obtained at 500 s^{-1}.

Sample	Description	η (MPas)
ethylene glycol		17
$MWCNT_{BMS}^{95}$	as received	63
	oxidized	75
$MWCNT_{FC}^{99}$	as received	154
	oxidized	280

Previous works have shown that noncovalent absorption of poly(ethylene glycol) may occur during grafting.[24,56] Although the reactions have been performed at high concentration of the glycols and in the absence of solvent, the poly(ethylene glycol)s used have relative low molecular weights, and due to the thorough washing processes no or negligible physisorption should be present.[57] From the difference in weight loss

between the MWCNTs after the acid treatment and after the *grafting onto* reaction of the glycols and the molecular weight of the glycols, one can estimate the concentration of hydroxyl groups ([OH]). This value is presented in the right axis in Figure 4.3. In the case of the $MWCNT_{BMS}$[95], the [OH] decreases dramatically when the glycol molecular weight increases. This suggests that even when the grafting content of the glycols increases with the molecular weight, the relative concentration of terminal hydroxyl group decreases. In the case of $MWCNT_{FC}$[99], the [OH] is lower compared with the $MWCNT_{BMS}$[95] and independent of the glycol used, in the range of molecular weights employed in the present study. Then, the MWCNTs can be more easily dispersed in organic solvent because of the longer grafted chains, but have fewer functional groups available for the successive reactions.

The difference in [OH] between the $MWCNT_{BMS}$[95] and the $MWCNT_{FC}$[99] can be attributed to different factors. The concentration of acyl (or alkyl) chloride groups present on the $MWCNT_{BMS}$[95] and the $MWCNT_{FC}$[99] could be responsible for the difference of the *grafting onto* of the glycols, unfortunately, these differences are difficult to quantify using any of the existing characterization method. The contour length of the MWCNTs estimated by the SFM measurements (Figure 4.4) showed no marked difference between the disperse nanoparticles that could infer any influence on the reaction efficiency.[58] However, the viscosity of the dispersion containing the MWCNTs seems to play a role on the grafting efficiency. The low viscosity of the dispersion of $MWCNT_{BMS}$[95] during the reaction might increase the accessibility of the hydroxyl groups to the acyl (or alkyl) chloride groups compared with the $MWCNT_{FC}$[99].

A representative infrared spectrum of the MWCNTs after grafting of PEG_{400} is presented in Figure 4.5. Even though the symmetric C-H stretching of the methylene groups is difficult to identify due to the alkyl groups of the MWCNTs, the C-H stretching deformations at approximately 1420 cm^{-1} and the C-O-C stretching deformation at 880 cm^{-1} are evident. These indicate the success of the reaction. An asymmetric C-H deformation is observed for this sample at 2970 cm^{-1}, which is only observed clearly in MWCNTs modified with poly(ethylene glycol) of 400 g/mol. The occurrence of any noncovalent interaction can be ruled out, since the reported shift to higher frequencies was not observed.[59]

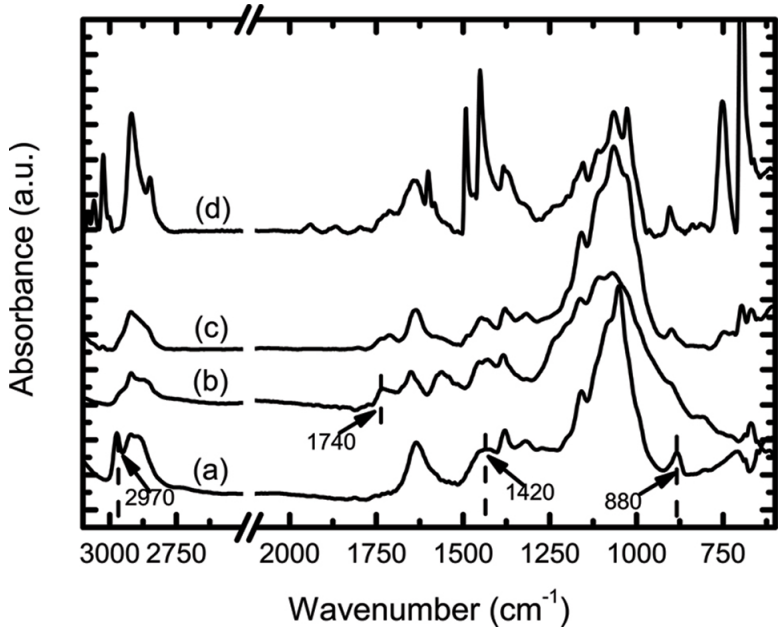

Figure 4.5. Infrared spectra of multiwall carbon nanotubes from FutureCarbon GmbH after different sequential modification steps (a) PEG_{400} grafted $MWCNT_{FC}^{99}$, (b) $MWCNT_{FC}^{99}$-Br^{4}, (c) $PS_{44}{}^{3}MWCNT_{FC}^{99}$ and (d) $PS_{85}{}^{24}MWCNT_{FC}^{99}$.

4.2.3. Esterification II: ATRP Initiator

The infrared spectrum after anchoring the initiator groups for the controlled radical polymerization to the MWCNTs is also shown in Figure 4.5. The carboxylic acid stretching vibration located at 1740 cm^{-1} indicates the successful grafting of the

initiator. Table 4.2 shows the initiator concentration estimated by elemental analysis. The reaction conditions were optimized in order to obtain comparable results of anchored initiator concentration [Br] for the MWCNTs from both used sources as a function of the 2BriBr concentration, as can be seen in Table 4.2 (entries 1 and 8). For this reason, the esterification reaction on the hydroxyl modified $MWCNT_{FC}^{99}$ was carried out at higher dilutions.

Table 4.2. Concentration of initiator groups after the esterification reaction of hydroxyl functionalized carbon nanotubes.

Entry	Sample	Esterification I (EG or PEG)[a]	Esterification II Initiator anchoring	
		Type[a]	[2BriBr] (µl/mg)[b]	[Br] (mmol/g)[c]
1	$MWCNT_{FC}^{99}$-Br^{1}	EG	1.4	0.071
2	$MWCNT_{FC}^{99}$-Br^{2}	EG	2.7	0.131
3	$MWCNT_{FC}^{99}$-Br^{3}	PEG_{200}	2.7	0.220
4	$MWCNT_{FC}^{99}$-Br^{4}	PEG_{400}	5.4	0.240
5	$MWCNT_{FC}^{99}$-Br^{5}	PEG_{400}	2.7	0.041
6	$MWCNT_{FC}^{99}$-Br^{6}	PEG_{400}	2.7	0.136
7	$MWCNT_{FC}^{99}$-Br^{7}	PEG_{200}	2.7	0.075
8	$MWCNT_{BMS}^{95}$-Br^{1}	EG	1.4	0.080
9	$MWCNT_{BMS}^{95}$-Br^{2}	EG	2.7	0.623
10	$MWCNT_{BMS}^{95}$-Br^{3}	PEG_{200}	1.4	0.364
11	$MWCNT_{BMS}^{95}$-Br^{4}	PEG_{400}	1.4	0.146

a) EG: ethylene glycol; PEG_{200} and PEG_{400}: polyethylene glycol of average number molecular weight of 200 g/mol and 400 g/mol, respectively; b) concentration of 2-bromo-2-methylpropionyl bromide (2BriBr, µl) respect to MWCNT (mg); c) [Br] determined by elemental analysis.

Figure 4.6 shows the distribution of the average contour lengths of two MWCNTs with a comparable concentration of initiator. The length distribution of the MWCNTs shorter than ~ 1 µm does not appreciably change with respect to the values obtained

after oxidation; however, longer carbon nanotubes were observed on the samples after the esterification, which confirms the assumption that the functionalization reaction helps to disaggregate the MWCNTs. In addition, longer carbon nanotubes were found in the sample $MWCNT_{FC}^{99}$-Br^{6} than in the sample $MWCNT_{BMS}^{95}$-Br^{4}. This could be also an indication that the $MWCNT_{FC}^{99}$ are effectively longer than the $MWCNT_{BMS}^{95}$ and that they are easier to disentangle due to the looseness of the aggregates.

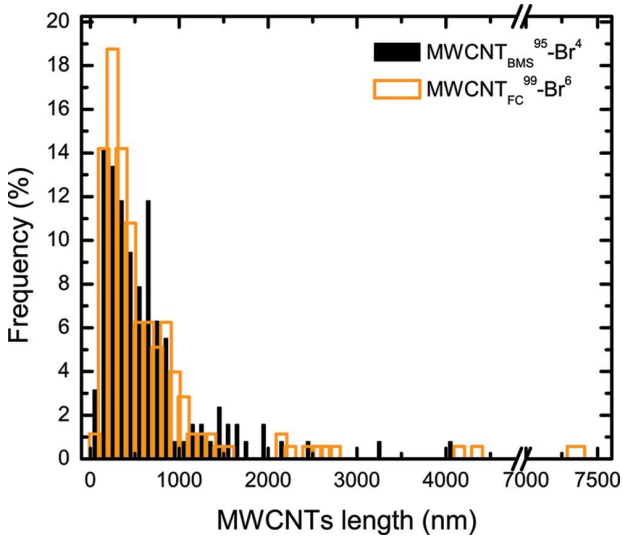

Figure 4.6. Length distribution (nm) for MWCNTs after the grafting of the ATRP initiator.

In the case of the ethylene glycol modified MWCNTs, the anchored initiator concentrations shown in Table 4.2 for $MWCNT_{BMS}^{95}$ and $MWCNT_{FC}^{99}$ are comparable when low 2BriBr concentrations are used. By increasing the concentration of 2BriBr, the [Br] increased in both cases, though it is five times higher for the $MWCNT_{BMS}^{95}$ (0.62 mmol/g) than for $MWCNT_{FC}^{99}$ (0.13 mmol/g). To the author's knowledge, the [Br] obtained for the $MWCNT_{BMS}^{95}$ under the described conditions is the highest value found on the grafting of initiator for surface initiated radical polymerizations on carbon nanotubes.[6,18-21,23,32,36,60,61]

The use of poly(ethylene glycol) spacers also affects the anchoring of the initiator. Under the same experimental conditions, the highest [Br] concentration is found on the MWCNTs grafted with PEG_{200}, followed by PEG_{400} and EG. Two effects are involved in this behavior. On one hand, it was previously discussed that the concentration of hydroxyl groups decreases if the molecular weight of the spacer increases (shown in Figure 4.3), in the case of the $MWCNT_{BMS}$[95], while the concentration is rather low in the case of the $MWCNT_{FC}$[99]. On the other hand, the stability of the carbon nanotube dispersions in organic solvents improves with the increment in spacer chain length, as well as the mobility of the hydroxyl end-groups. Therefore, as the molecular weight of the spacer increases, the esterification reaction takes place under conditions that resemble more those of a homogeneous reaction, which increases the feasibility of the reaction. Consequently, the observed tendency results from the competition between these two effects: the lower [Br] on the PEG_{400} modified carbon nanotubes is assumed to be due to lower hydroxyl concentration, while the lower [Br] on the EG modified MWCNTs is attributed to the heterogeneity of the reaction.

4.2.4. ATR Polymerization

Styrene (St) was chosen as a monomer for the "*grafting from*" the initiator anchored MWCNTs under controlled radical polymerization conditions. The results are summarized in Table 4.3. The decoration of carbon nanotubes and other substrates using this monomer has been well documented. St is able to solubilize its polymer, shows slower polymerization rate than other available monomers (i.e., meth(acrylates)),[62] and thermally polymerizes under the experimental conditions described.[63] These characteristics allow the study of the grafting without non-bonded

initiators (free initiator), or deactivator (e.g., $CuBr_2$)[64] and with reduced quantity of solvent, which may complicate the analysis. In the St *grafting from* polymerization reactions, some free chains are always generated in solution, which promotes the termination in the reaction medium rather than within the active species attached to the substrate, and supports a controlled polymer growth in the sense that crosslinking between different nanoparticles will unlikely occur. This has been described previously on polymerization from silica nanostructures.[63,65,66]

Table 4.3. Conditions and polymer content on the styrene *grafting from* reaction on $MWCNT_{BMS}^{95}$ and $MWCNT_{FC}^{99}$

Entry	Sample	Source	f_{PS}[b] (wt %)	$M_{n,TGA}$[c] (kg/mol)	T_d[d] (°C)
1	$PS_{19}{}^{3}MWCNT_{FC}{}^{99}$	$MWCNT_{FC}{}^{99}$-Br^{1}	19	3.3	352
2	$PS_{9}{}^{1}MWCNT_{FC}{}^{99}$	$MWCNT_{FC}{}^{99}$-Br^{2}	9	0.8	272
3	$PS_{11}{}^{1}MWCNT_{FC}{}^{99}$	$MWCNT_{FC}{}^{99}$-Br^{3}	11	0.6	344
4	$PS_{44}{}^{3}MWCNT_{FC}{}^{99}$	$MWCNT_{FC}{}^{99}$-Br^{4}	44	3.3	375
5	$PS_{85}{}^{24}MWCNT_{FC}{}^{99}$	$MWCNT_{FC}{}^{99}$-Br^{4}	85	24.0	410
6	$PS_{28}{}^{10}MWCNT_{FC}{}^{99}$	$MWCNT_{FC}{}^{99}$-Br^{5}	28	9.6	361
7	$PS_{22}{}^{2}MWCNT_{FC}{}^{99}$	$MWCNT_{FC}{}^{99}$-Br^{6}	22	2.0	348
8	$PS_{13}{}^{2}MWCNT_{FC}{}^{99}$	$MWCNT_{FC}{}^{99}$-Br^{7}	13	2.0	335
9	$PS_{23}{}^{4}MWCNT_{FC}{}^{99}$	$MWCNT_{FC}{}^{99}$-Br^{7}	23	3.9	356
10	$PS_{31}{}^{6}MWCNT_{FC}{}^{99}$	$MWCNT_{FC}{}^{99}$-Br^{7}	31	5.9	371
11	$PS_{32}{}^{6}MWCNT_{FC}{}^{99}$	$MWCNT_{FC}{}^{99}$-Br^{7}	32	6.3	370
12	$PS_{11}{}^{2}MWCNT_{FC}{}^{99}$	$MWCNT_{FC}{}^{99}$-Br^{7}	11	1.7	331
13	$PS_{34}{}^{7}MWCNT_{BMS}{}^{95}$	$MWCNT_{BMS}{}^{95}$-Br^{1}	34	6.6	393
14	$PS_{43}{}^{10}MWCNT_{BMS}{}^{95}$	$MWCNT_{BMS}{}^{95}$-Br^{1}	43	9.6	394

Table 4.3. *cont'd*

Entry	Sample	Source	f_{PS}[b] (wt %)	$M_{n,TGA}$[c] (kg/mol)	T_d[d] (°C)
15	$PS_{47}{}^{11}MWCNT_{BMS}{}^{95}$	$MWCNT_{BMS}{}^{95}$-Br^1	47	11.3	396
16	$PS_{91}{}^{20}MWCNT_{BMS}{}^{95}$	$MWCNT_{BMS}{}^{95}$-Br^2	91	20.0	420
17	$PS_{85}{}^{9}MWCNT_{BMS}{}^{95}$	$MWCNT_{BMS}{}^{95}$-Br^2	85	9.0	418
18	$PS_{70}{}^{4}MWCNT_{BMS}{}^{95}$	$MWCNT_{BMS}{}^{95}$-Br^2	70	3.9	406
19	$PS_{86}{}^{17}MWCNT_{BMS}{}^{95}$	$MWCNT_{BMS}{}^{95}$-Br^3	86	16.7	410
20	$PS_{49}{}^{7}MWCNT_{BMS}{}^{95}$	$MWCNT_{BMS}{}^{95}$-Br^4	49	6.6	387

a) weight and mole percent of St respect to the MWCNTs; b) Polystyrene grafting content; c) average molecular weight of the grafted polystyrene, calculated from TGA;[32] d) decomposition onset temperature calculated from TGA data.

The infrared spectra of polystyrene (PS) surface grafted MWCNTs under different reaction conditions are also shown in Figure 4.5. The bands corresponding to the polymer are clearly evident when the polymer content is over 70 wt %, e.g., the =C-H stretching vibrations between 3100-3000 cm^{-1}, the ring stretching vibration at ca. 1600 cm^{-1}, the overtones between 2000-1660 cm^{-1}, and the C-H out-of-plane vibration and ring out-of-plane deformation located at 760 cm^{-1} and 690 cm^{-1}, respectively. ^{1}H-NMR measurements also support the presence of the grafted PS at the MWCNTs. The ^{1}H-NMR of the $PS_{91}{}^{20}MWCNT_{BMS}{}^{95}$ can be observed in Figure 4.7. High polymer content is required also for the ^{1}H-NMR measurements, because the magnetization of the MWCNT promotes first the aggregation and then the sedimentation of the nanoparticles during the measurement.

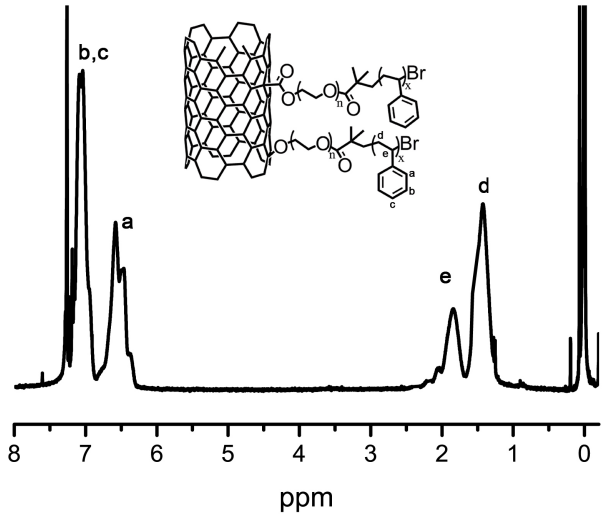

Figure 4.7. H^1NMR spectra of the polystyrene grafted carbon nanotube $PS_{91}{}^{20}MWCNT_{BMS}{}^{95}$.

Scanning electron micrographs are presented for a representative group of samples in Figure 4.8. Qualitatively, the PS grafted MWCNTs are similar, independent of the source ($MWCNT_{BMS}{}^{95}$ or $MWCNT_{FC}{}^{99}$). The scanning electron micrographs show that if the polymer content is below 50 wt %, the aspect ratio of the MWCNTs does not discern from the one of unmodified filler. When the polymer content is lower than approximately 20 wt % it is possible to analyze the sample without being sputtered, which indicates that the MWCNTs preserve their electrical conductivity characteristics after modification. This might represent an advantage in applications like conducting polymer films, where a relatively good dispersion ensures a low MWCNTs percolation threshold in the nanocomposite. The samples with polymer content higher than 50 wt % present a more homogeneous structure, where the carbon nanotubes look like they are embedded in polymer. This effect has been previously observed by other groups.[20,21]

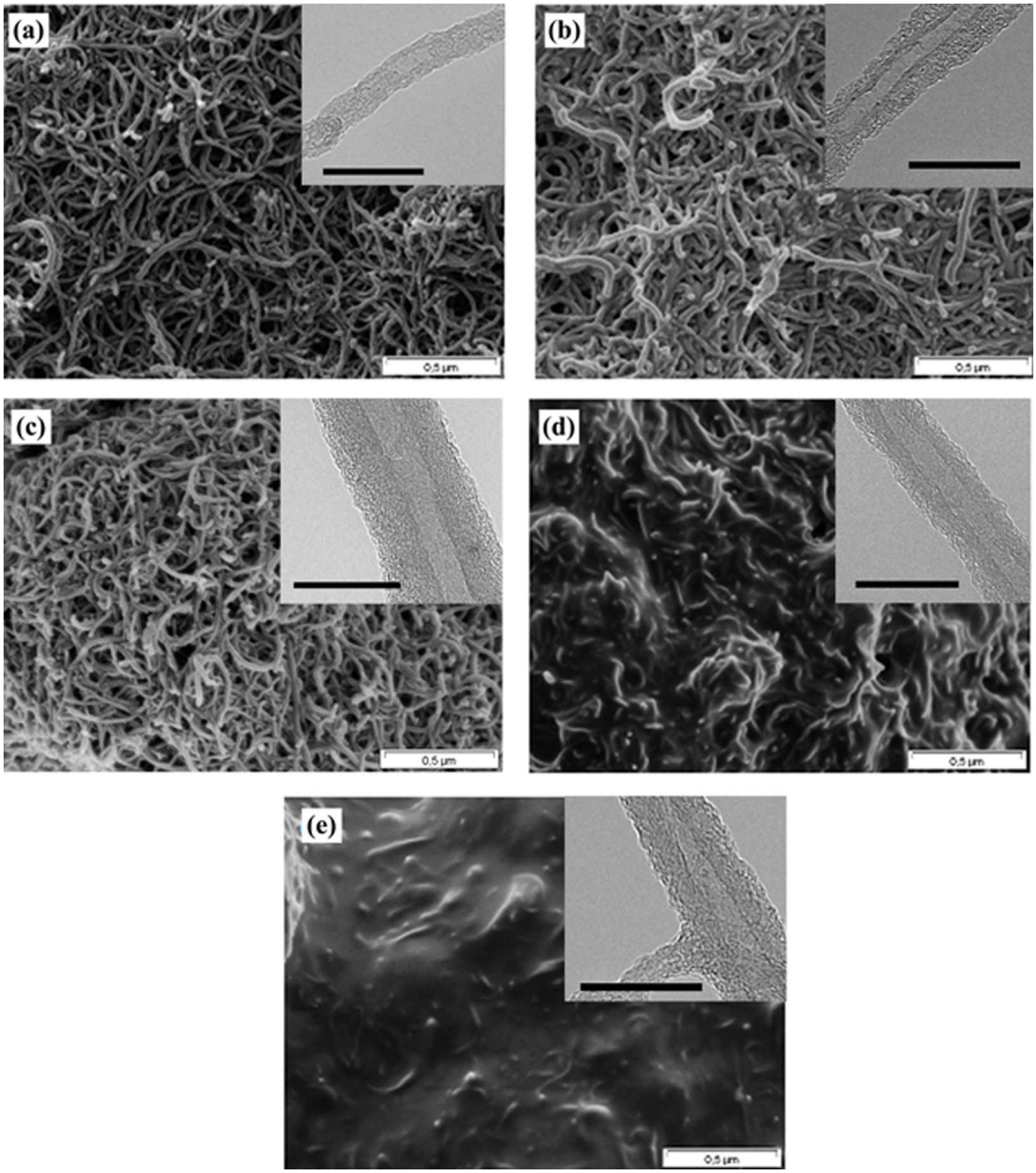

Figure 4.8. Scanning and transmission (inserts) electron micrographs of PS grafted MWCNT, synthesized under the conditions indicated in Table 3.2 (a) $PS_9{}^{1}MWCNT_{FC}{}^{99}$, (b) $PS_{44}{}^{3}MWCNT_{FC}{}^{99}$, (c) $PS_{47}{}^{11}MWCNT_{BMS}{}^{95}$, (d) $PS_{70}{}^{4}MWCNT_{BMS}{}^{95}$ and (e) $PS_{91}{}^{20}MWCNT_{BMS}{}^{95}$. TEM scale bar = 20 nm.

From the transmission electron micrographs (shown as inserts in Figure 4.8) one could assume that the graphitic-like structure of the carbon nanotubes is preserved after all the functionalization reactions. The grafting of polymer takes place along the MWCNTs, not just on their tips, where the highest initiator concentration is supposed

to be due to a major concentration of defects. However, as previously discussed, the infrared analysis on the pristine MWCNTs shows that defects are present along the structure. These potentially reactive locations enable the distribution of initiator groups along the MWCNTs.

The quantity of polymer grafted on the MWCNTs from both sources could be controlled by adjusting the weight ratio between the monomer and the nanofiller as a function of the initiator concentration. The results are summarized in Table 4.3. The weight ratios used in this work are comparable to the experimental conditions presented somewhere else,[20,40] although there is lack of agreement throughout the literature.[19,21,38]

The results presented in Table 4.3 show that, in general, higher polymer content is obtained for the initiator anchored $MWCNT_{BMS}^{95}$ than for $MWCNT_{FC}^{99}$, when the grafting takes place under similar reaction conditions. The observed discrepancies are believed to depend on the intrinsic characteristics of the carbon nanotubes used here. For example, in the case of the samples $PS_{19}^{3}MWCNT_{FC}^{99}$ and $PS_{34}^{7}MWCNT_{BMS}^{95}$ (entries 1 and 13), the polymer content for $MWCNT_{BMS}^{95}$ is twice of the one obtained for $MWCNT_{FC}^{99}$ under comparable reaction conditions. The interplay of two factors explains this difference. Firstly, the distribution of anchored initiator along the MWCNTs varies with the location of the structural defects, which is predetermined from the carbon nanotubes synthesis. If the initiator moieties are close to each other, coupling or deactivation reactions will compete with the propagation of the living chain. This could be related with the critical conversion of coupling (CCC),[6] where not just the electronic properties of the carbon nanotube may affect the

polymerization, but also the location of the growing chain could induce coupling reactions. Secondly, as discussed before, the viscosity of the dispersions containing $MWCNT_{BMS}^{95}$ is lower than the dispersion prepared with the $MWCNT_{FC}^{99}$ due to the presence of relative compact aggregates and shorter carbon nanotubes. For this reason the overall polymerization rate could be higher or a major reaction yield could be reached with the $MWCNT_{BMS}^{95}$-Br.

If the monomer to MWCNT weight ratio is kept constant, the amount of grafted polymer increases with the concentration of initiator anchored on $MWCNT_{BMS}^{95}$ and does not change for the initiator anchored on $MWCNT_{FC}^{99}$. The competition between polymer conversion, initiator concentration and dispersion of the MWCNTs might explain these results. Short polymer chains grafted from apparent shorter and more aggregated carbon nanotubes increase less dramatically the viscosity during the *grafting from* polymerization than apparent longer and less aggregated carbon nanotubes, as is the case of $MWCNT_{FC}^{99}$-Br. As a result, the grafting reactions on $MWCNT_{BMS}^{95}$-Br take place probably for prolonged times before the increase in viscosity decreases the propagation rate of the reaction, and these results in higher polymer contents. This behavior has been previously observed in the literature, although a clear correlation with the here presented results is not possible since no data is given regarding the length of the carbon nanotubes.[20]

The dispersion plays an important role on all the carbon nanotubes functionalization reactions. Prior to the grafting, both $MWCNT_{BMS}^{95}$-Br and $MWCNT_{FC}^{99}$-Br are dispersed in the monomer. In order to obtain optically homogeneous carbon nanotube dispersions before the start of the polymerization, the minimum feasible monomer-to-

nanofiller weight ratio found was 30 to 1; lower ratios lead to highly viscous solutions before the start of the reaction. In the case of the $MWCNT_{FC}^{99}$, the variation of the monomer-to-nanofiller weight ratio influences the content of grafted polymer. For example, increasing four times the monomer concentration with respect to $MWCNT_{FC}^{99}$-Br^{7} (entries 8 to 11, Table 4.3), the polystyrene weight fraction increases approx. 2.4 times. The low solution viscosity due to the high concentration of monomer at the beginning of the reaction enhances the access of the monomer to the propagating radical and extends the reaction time. The carbon nanotubes dispersion improves during the polymerization reaction due to the growing chains, but the viscosity rises due to the monomer consumption. Then, the reaction will be controlled until the dispersion is hindered by the monomer consumption, the surface confinement between carbon nanotubes will limit the propagation and coupling or disproportions might end the reaction. As the conversion of monomer advances, the viscosity rises and promotes the filler reaggregation, so that the deactivation of the growing radical is favored (as described above).

A common trend on the MWCNTs from both sources after ATRP reactions is the increase in grafted polymer content with the monomer concentration. The increase in polymer content with the monomer concentration has been also reported on $MWCNTs^{21}$ and other confined systems.[65]. These observations can be correlated to the transmission electron micrographs (inserts in Figure 4.8). If one assumes that the distribution of initiator moieties is homogeneous along the surface on both MWCNT sources, the polymer layer is relatively thinner for the $PS_{44}^{3}MWCNT_{FC}^{99}$ than for the sample $PS_{91}^{20}MWCNT_{BMS}^{95}$. This is in agreement with other systems, where the

polymer grafting depends on the nanoparticle surface area and its influence on the polymerization kinetics.[63]

Another possibility to control the polystyrene content in the $MWCNT_{FC}^{99}$ is by varying the length of the glycol spacer. As can be observed in Table 3.2 and Table 4.3, for comparable monomer to $MWCNT_{FC}^{99}$ weight fractions and initiator concentration, the polystyrene grafting content doubles when ethylene glycol and PEG_{400} are compared ($PS_9{}^1MWCNT_{FC}^{99}$ and $PS_{22}{}^2MWCNT_{FC}^{99}$) and increases four times when PEG_{200} is compared against PEG_{400} ($PS_{11}{}^1MWCNT_{FC}^{99}$ and $PS_{44}{}^3MWCNT_{FC}^{99}$). A polymer content over 80 wt % can be obtained with the $MWCNT_{FC}^{99}$ by choosing the right combination between glycol spacer, initiator concentration and monomer to carbon nanotube ratio (e.g., $PS_{85}{}^{24}MWCNT_{FC}^{99}$, entry 5, Table 4.3). From the obtained results one can deduce that the PEG_{400} chain length promotes the more stable dispersion under the described polymerization conditions. This spacer enhances the carbon nanotube dispersion and might increase the polymerization rate during the reaction.

4.3. Conclusions

Two commercially available multiwall carbon nanotubes were grafted with polystyrene after successive functionalization reactions. The *grafting from* polymerization of styrene was performed under atom transfer radical polymerization conditions. The purity and the dimension of the multiwall carbon nanotubes influence the grafted polystyrene content. The multiwall carbon nanotube with relative tighter aggregates and with apparent shorter length ($MWCNT_{BMS}^{95}$) showed a higher polystyrene weight content than the relative longer, less aggregated carbon nanotubes

($MWCNT_{FC}^{99}$), with comparable initiator concentrations. The presence of tight aggregates and shorter nanotubes decreases the viscosity of the dispersion during the functionalization reactions, which may enhance the propagation of the growing polymer chain before the polymerization slows down due to high monomer conversion. However, higher polymer contents can be achieved with the $MWCNT_{FC}^{99}$ with the right combination of poly(ethylene glycol) spacer, concentration of the anchored initiator, and monomer to carbon nanotube weight ratio.

4.4. References

1. Moniruzzaman, M.; Winey, K. I. Macromolecules 2006, 39, 5194-5205.
2. Gojny, F. H.; Schulte, K. Compos. Sci. Technol. 2004, 64, 2303-2308.
3. Sandler, J. K. W.; Kirk, J. E.; Kinloch, I. A.; Shaffer, M. S. P.; Windle, A. H. Polymer 2003, 44, 5893-5899.
4. Shi, Q.; Yang, D.; Su, Y.; Li, J.; Jiang, Z.; Jiang, Y.; Yuan, W. J. Nanopart. Res. 2007, 9, 1205-1210.
5. Kumar, N. A.; Ganapathy, H. S.; Kim, J. S.; Jeong, Y. S.; Jeong, Y. T. Eur. Polym. J. 2008, 44, 579-586.
6. Gao, C.; Muthukrishnan, S.; Li, W.; Yuan, J.; Xu, Y.; Muller, A. H. E. Macromolecules 2007, 40, 1803-1815.
7. Richard, C.; Balavoine, F.; Schultz, P.; Ebbesen, T. W.; Mioskowski, C. Science 2003, 300, 775-778.
8. Poland, C. A.; Duffin, R.; Kinloch, I.; Maynard, A.; Wallace, W. A. H.; Seaton, A.; Stone, V.; Brown, S.; MacNee, W.; Donaldson, K. Nat. Nanotechnol. 2008, 3, 423-428.
9. Kane, A. B.; Hurt, R. H. Nat. Nanotechnol. 2008, 3, 378-379.
10. Rausch, L. J.; Bisinger, E. C.; Sharma, A. Regul. Toxicol. Pharm. 2004, 40, 28-41.
11. Schipper, M. L.; Nakayama-Ratchford, N.; Davis, C. R.; Kam, N. W. S.; Chu, P.; Liu, Z.; Sun, X.; Dai, H.; Gambhir, S. S. Nat. Nanotechnol. 2008, 3, 216-221.
12. Gojny, F. H.; Wichmann, M. H. G.; Fiedler, B.; Kinloch, I. A.; Bauhofer, W.; Windle, A. H.; Schulte, K. Polymer 2006, 47, 2036-2045.
13. Sandler, J.; Shaffer, M. S. P.; Prasse, T.; Bauhofer, W.; Schulte, K.; Windle, A. H. Polymer 1999, 40, 5967-5971.
14. Sandler, J. K. W.; Pegel, S.; Cadek, M.; Gojny, F.; van Es, M.; Lohmar, J.; Blau, W. J.; Schulte, K.; Windle, A. H.; Shaffer, M. S. P. Polymer 2004, 45, 2001-2015.
15. Shim, M.; Shi Kam, N. W.; Chen, R. J.; Li, Y.; Dai, H. Nano Lett. 2002, 2, 285-288.
16. Tasis, D.; Tagmatarchis, N.; Bianco, A.; Prato, M. Chem. Rev. 2006, 106, 1105-1136.
17. Qin, S.; Qin, D.; Ford, W. T.; Resasco, D. E.; Herrera, J. E. Macromolecules 2004, 37, 752-757.
18. Qin, S.; Qin, D.; Ford, W. T.; Resasco, D. E.; Herrera, J. E. J. Am. Chem. Soc. 2004, 126, 170-176.
19. Kong, H.; Gao, C.; Yan, D. J. Am. Chem. Soc. 2004, 126, 412-413.
20. Baskaran, D.; Mays, J. W.; Bratcher, M. S. Angew. Chem., Int. Ed. 2004, 43, 2138-2142.
21. Kong, H.; Gao, C.; Yan, D. Macromolecules 2004, 37, 4022-4030.
22. Cheng, B.; Li, Y.; Shen, C. Polym. Prepr. (Am. Chem. Soc., Div. Polym. Chem.) 2004, 45, 653-654.

23. Kong, H.; Luo, P.; Gao, C.; Yan, D. Polymer 2005, 46, 2472-2485.
24. Baskaran, D.; Mays, J. W.; Bratcher, M. S. Polymer 2005, 46, 5050-5057.
25. Hong, C. Y.; You, Y. Z.; Pan, C. Y. Chem. Mater. 2005, 17, 2247-2254.
26. Yang, Y.; Xie, X.; Yang, Z.; Wang, X.; Cui, W.; Yang, J.; Mai, Y. W. Macromolecules 2007, 40, 5858-5867.
27. Li, J.; He, W.-D.; Yang, L.-P.; Sun, X.-L.; Hua, Q. Polymer 2007, 48, 4352-4360.
28. Wu, W.; Tsarevsky, Nicolay V.; Hudson, Jared L.; Tour, J. M.; Matyjaszewski, K.; Kowalewski, T. Small 2007, 3, 1803-1810.
29. Priftis, D.; Petzetakis, N.; Sakellariou, G.; Pitsikalis, M.; Baskaran, D.; Mays, J. W.; Hadjichristidis, N. Macromolecules 2009, 42, 3340-3346.
30. Kong, H.; Gao, C.; Yan, D. J. Mater. Chem. 2004, 14, 1401-1405.
31. Choi, J. H.; Oh, S. B.; Chang, J.; Kim, I.; Ha, C.-S.; Kim, B. G.; Han, J. H.; Joo, S.-W.; Kim, G.-H.; Paik, H.-j. Polym. Bull. 2005, 55, 173-179.
32. Gao, C.; Vo, C. D.; Jin, Y. Z.; Li, W.; Armes, S. P. Macromolecules 2005, 38, 8634-8648.
33. Hong, C. Y.; You, Y. Z.; Wu, D.; Li, Y.; Pan, C. Y. Macromolecules 2005, 38, 2606-2611.
34. Fragneaud, B.; Masenelli-Varlot, K.; Gonzalez-Montiel, A.; Terrones, M.; Cavaillé, J.-Y. Chem. Phys. Lett. 2006, 419, 567-573.
35. Matrab, T.; Chancolon, J.; L'Hermite, M. M.; Rouzaud, J.-N.; Deniau, G.; Boudou, J.-P.; Chehimi, M. M.; Delamar, M. Colloids Surf., A 2006, 287, 217-221.
36. Gao, C.; Li, W.; Morimoto, H.; Nagaoka, Y.; Maekawa, T. J. Phys. Chem. B 2006, 110, 7213-7220.
37. Li, W.; Gao, C.; Qian, H.; Ren, J.; Yan, D. J. Mater. Chem. 2006, 16, 1852-1859.
38. Chang, J. H.; Lee, Y. W.; Kim, B. G.; Kim, H.-K.; Choi, I. S.; Paik, H.-J. Compos. Interface 2007, 14, 493-504.
39. Liu, Y. L.; Chen, W. H. Macromolecules 2007, 40, 8881-8886.
40. Wu, H.-X.; Tong, R.; Qiu, X.-Q.; Yang, H.-F.; Lin, Y.-H.; Cai, R.-F.; Qian, S.-X. Carbon 2007, 45, 152-159.
41. Lei, Z.; Wei, X.; Zhang, L.; Bi, S. Colloids Surf., A 2008, 324, 131-136.
42. Xiao, Q.; He, S.; Liu, L.; Guo, X.; Shi, K.; Du, Z.; Zhang, B. Compos. Sci. Technol. 2008, 68, 321-328.
43. Chochos, C. L.; Stefopoulos, A. A.; Campidelli, S.; Prato, M.; Gregoriou, V. G.; Kallitsis, J. K. Macromolecules 2008, 41, 1825-1830.
44. Wang, T.-L.; Tseng, C.-G. J. Appl. Polym. Sci. 2007, 105, 1642-1650.
45. Chen, R. J.; Zhang, Y.; Wang, D.; Dai, H. J. Am. Chem. Soc. 2001, 123, 3838-3839.
46. Osswald, S.; Havel, M.; Gogotsi, Y. J. Raman Spectrosc. 2007, 38, 728-736.
47. Shanmugharaj, A. M.; Bae, J. H.; Lee, K. Y.; Noh, W. H.; Lee, S. H.; Ryu, S. H. Compos. Sci. Technol. 2007, 67, 1813-1822.
48. Sun, L.; Yang, J.-T.; Lin, G.-Y.; Zhong, M.-Q. Mater. Lett. 2007, 61, 3963-3966.
49. Xia, W.; Wang, Y.; Bergsträßer, R.; Kundu, S.; Muhler, M. Appl. Surf. Sci. 2007, 254, 247-250.
50. Kundu, S.; Wang, Y.; Xia, W.; Muhler, M. J. Phys. Chem. C 2008, 112, 16869-16878.
51. Forrest, G. A.; Alexander, A. J. J. Phys. Chem. C 2007, 111, 10792-10798.
52. Peng, F.; Zhang, L.; Wang, H.; Lv, P.; Yu, H. Carbon 2005, 43, 2405-2408.
53. Zhang, J.; Zou, H.; Qing, Q.; Yang, Y.; Li, Q.; Liu, Z.; Guo, X.; Du, Z. J. Phys. Chem. B 2003, 107, 3712-3718.
54. Ziegler, K. J.; Gu, Z.; Peng, H.; Flor, E. L.; Hauge, R. H.; Smalley, R. E. J. Am. Chem. Soc. 2005, 127, 1541-1547.
55. Breza, M. Chem. Phys. 2006, 330, 224-230.
56. Sano, M.; Kamino, A.; Okamura, J.; Shinkai, S. Langmuir 2001, 17, 5125-5128.
57. Liu, Y.-X.; Du, Z.-J.; Li, Y.; Zhang, C.; Li, C.-J.; Yang, X.-P.; Li, H.-Q. J. Polym. Sci., Part A: Polym. Chem. 2006, 44, 6880-6887.
58. Lin, Y.; Taylor, S.; Huang, W.; Sun, Y. P. J. Phys. Chem. B 2003, 107, 914-919.
59. Baskaran, D.; Mays, J. W.; Bratcher, M. S. Chem. Mater. 2005, 17, 3389-3397.

60. Yao, Z.; Braidy, N.; Botton, G. A.; Adronov, A. J. Am. Chem. Soc. 2003, 125, 16015-16024.
61. Fan, D.-Q.; He, J.-P.; Tang, W.; Xu, J.-T.; Yang, Y.-L. Eur. Polym. J. 2007, 43, 26-34.
62. Matyjaszewski, K.; Xia, J. Chem. Rev. 2001, 101, 2921-2990.
63. von Werne, T.; Patten, T. E. J. Am. Chem. Soc. 2001, 123, 7497-7505.
64. Matyjaszewski, K.; Miller, P. J.; Shukla, N.; Immaraporn, B.; Gelman, A.; Luokala, B. B.; Siclovan, T. M.; Kickelbick, G.; Vallant, T.; Hoffmann, H.; Pakula, T. Macromolecules 1999, 32, 8716-8724.
65. Moreno, J.; Sherrington, D. C. Chem. Mater. 2008, 20, 4468-4474.
66. Audouin, F.; Blas, H.; Pasetto, P.; Beaunier, P.; Boissière, C.; Sanchez, C.; Save, M.; Charleux, B. Macromol. Rapid Commun. 2008, 29, 914-921.

Chapter 5. Block Copolymer Nanocomposites based on $MWCNT_{BMS}^{95}$: Effect of the Functionalization of Multiwall Carbon Nanotubes on the Morphology of the Block Copolymer

5.1. Introduction

Polymers, more than any other class of materials, play an active role in the development of new technologies. Their importance will increase in the coming years in areas related with energy, sustainability, health care, security and informatics, defense and protection.[1] The physical properties of polymers can be controlled by combining different parameters, starting from the synthesis (e.g., monomers, chain architecture, functionality, etc.), to the processing (e.g., degree of crystallinity, geometry, compounding, orientation, etc.). Block copolymers based on polystyrene-*block*-polybutadiene-*block*-polystyrene (SBS) are clear examples of how the synthesis influences the physical properties of the polymers. The adjustment of the monomer sequence, the composition and the chain architecture lead to transparent SBS block copolymers with different degrees of toughness and stiffness.[2,3] Particularly, it is known that the deformation behavior of these type of block copolymers strongly depends on the microstructure of the polybutadiene block and the microdomain orientation of the block copolymer.[3-7]

Although the tuning of the properties of the (co)polymers broadens the range of applications of these materials, there are still requirements that are beyond their possibilities. In those cases, (co)polymers have been combined with fillers that seek to improve the properties of the final material, or simply to reduce cost of production. Typical examples can be found in the automotive and aircraft industries, where the

use of polymer based composites reduce considerable the weight, thus leading to energy and cost savings.

In the case of the carbon nanotubes, their impressive properties make them promising candidates for the design of a new generation of nanocomposites. Beside these properties, the aspect ratio and the chemical structure of the carbon nanotubes have led, for example, to variations in the glass transition, the crystallization and the melting behavior, in cases where homopolymers were used as matrices.[8-10] In the case of copolymers, the incorporation of the carbon nanotubes might induce changes on the morphology of the copolymer or, on the contrary, the morphology of the copolymer might influence the state of dispersion of the carbon nanotubes. Until now, attention has been brought to the relation between the dispersion of the carbon nanotubes and the mechanical or electrical properties of the nanocomposites[11,12] The assembly of carbon nanotubes in copolymer matrices has received less attention, mainly due to the high aspect ratio of the nanoparticle and its tendency to aggregate.[13] Recently, two works have been published related with the influence of surface functionalized carbon nanotubes on the morphology of block copolymer matrices; however, no clear data regarding the functionalization of the carbon nanotubes[14] and no clear evidences of the sel-assembly of the morphology of the block copolymer are given.[15] In this chapter, blends of a commercial polystyrene-*block*-polybutadiene-*block*-polystyrene block copolymer and $MWCNT_{BMS}$[95] with different polystyrene grafting content are reported. The morphology of the nanocomposites is analyzed by means of the effect of the polystyrene grafted from the $MWCNT_{BMS}$[95] during the microphase separation of the block copolymer and their influence on the orientation of the morphology when the nanocomposites are submitted to deformation.

5.2. Results and Discussion

5.2.1. Characteristics of the carbon nanotubes grafted with polystyrene

The characteristics of the polystyrene grafted multiwall carbon nanotubes can be appreciated in Table 5.1. The polystyrene thicknesses calculated from the TEM (t_{PS}) are below the theoretically expected values. The discrepancies with the calculations are may be related with the distribution of initiator groups and the conformation of the polymer chains along the carbon nanotubes. The effect of the initiator groups distributions has been previously reported on the grafting of poly(methyl methacrylate) and poly(*n*-butyl acrylate) from the surface of SWCNTs.[16,17] SFM measurements and computational modeling on different poly(*n*-butyl acrylate) grafted SWCNTs have suggested that the concentration of initiator groups on the surface of the carbon nanotubes might be strongly inhomogeneous along the length of the nanoparticle. TEM images presented in Chapter 4 have shown a relatively homogeneous coating of polystyrene for the samples $PS_{70}^{4}MWCNT_{BMS}^{95}$ and $PS_{91}^{20}MWCNT_{BMS}^{95}$, compared with $PS_{47}^{11}MWCNT_{BMS}^{95}$. In the case of the polymer grafted from carbon nanotubes, the conformation of the polymer chains is probably different from the one of a polymer chain in solution. The affinity between the benzene ring of the polystyrene and the graphene structure of the carbon nanotubes might lead also to the wrapping of the carbon nanotube by the polymer instead of the extension of the chain from the nanofiller. It has to be pointed out that the preparation of the dispersion (solvent, evaporation on the TEM grid) as well as the electron beam of the TEM may alter the reported values.

Table 5.1. Molecular and thermal characterization of the polystyrene grafted carbon nanotubes prepared by *grafting from* polymerization.

Sample	σ/a^2 (chains/nm^2)	f_{PS} (wt %)[a]	T_g (°C)	M_n (kg/mol)[a]	$\langle r^2\rangle_f^{1/2}$ (nm)[b]	d_t (nm)[c]	$2\langle s^2\rangle_o^{1/2}$ (nm)[d]	t_{PS} (nm)[e]
$PS_{47}{}^{11}MWCNT_{BMS}{}^{95}$	0.1	47.1	100.9	11.2	1.1	27.0	8.2	2.4 ± 0.7
$PS_{70}{}^{4}MWCNT_{BMS}{}^{95}$	2.9	70.4	107.0	3.9	0.6	9.4	4.8	1.3 ± 0.3
$PS_{91}{}^{20}MWCNT_{BMS}{}^{95}$	2.9	91.3	102.1	20.0	1.4	48.0	11.0	1.4 ± 0.4

a) determined by thermogavimetric measurements; b) root mean square end-to-end distance of a freely-jointed chain, $\langle r^2\rangle_f^{1/2} = n^{1/2}l$; c) estimation of the chain dimension in trans-trans conformation; d) real coil chain dimension $2\langle s^2\rangle^{1/2} = 4l[nC_\infty/6]^{1/2}$, $C_\infty = 9.85$[18] e) Thickness of the polystyrene *grafted from* the MWCNT calculated from the TEM images (see Figure 4.8).

The difference in the molecular weight of the grafted polystyrene can be appreciated by the variation in the glass transition temperature (T_g), as shown in Table 5.1. The $PS_{70}{}^{4}MWCNT_{BMS}{}^{95}$ has a relatively high T_g because the surface of the carbon nanotube restricts the mobility of the short polymer chain. For this reason, high energy absorption is required for the chain relaxation. The increase in the molecular weight of the polymer dissipates the effect of the anchoring of the polymer chain to the $MWCNT_{BMS}{}^{95}$ on the T_g.[19,20] The glass transition obtained in these cases is therefore comparable to the one corresponding to the nongrafted polystyrene.

The polymer grafted $MWCNT_{BMS}{}^{95}$ can be dispersed in the solvents used for the dissolution of polystyrene. However, some aggregates are observed in the dispersions, especially in the case of the $PS_{70}{}^{4}MWCNT_{BMS}{}^{95}$ and the $PS_{47}{}^{11}MWCNT_{BMS}{}^{95}$, i.e., the nanoparticles grafted with polystyrene of low molecular weight and low grafting content, respectively. Chapter 4 describes in detail the functionalization reactions made at the surface of the carbon nanotubes as a function of the characteristics of the nanoparticles. In the case of the $MWCNT_{BMS}{}^{95}$, the viscosity of the dispersions indicates that the nanoparticles form relative tight aggregates. For this reason it is

presumed that the *grafting from* polymerization reactions take place first at the surface of the aggregates and then the increase in the polymer chain length reduces the π-π stacking interactions between the graphitic layers of the carbon nanotubes. However, if the concentration of initiator moieties does not promote the polymer coating of individual carbon nanotubes or if the chain length of the grafted polymer does not drive away the carbon nanotubes, the nanoparticles will remain aggregated after the polymerization reaction. For these reasons, in order to reduce the quantity of aggregates in the nanocomposite films, the dispersions were sonicated and the aggregates separated by centrifugation before the casting of the film.

5.2.2. Morphology of the nanocomposites

Selected scanning electron micrographs of the different AS-SB_{26}/$MWCNT_{BMS}^{95}$ nanocomposites are shown in Figure 5.1. The carbon nanotubes are homogeneously dispersed in the AS-SB_{26} matrix even in the case of the pristine $MWCNT_{BMS}^{95}$. The arrows in Figure 5.1 indicate isolated or aggregates of carbon nanotubes present in the nanocomposites. Aggregation of the nanoparticles is difficult to detect within the evaluated images, just in the case of the nanocomposite based on $PS_{70}^{4}MWCNT_{BMS}^{95}$ some aggregates can be observed (Figure 5.1(d)). However, the transmission electron micrographs presented in Figure 5.2 show some differences on the dispersion of the MWCNTs as a function of the grafted polystyrene. For a better interpretation of the images, the polybutadiene phase has been stained with OsO_4 vapor. In the case of the AS-SB_{26}, the lamellae are randomly oriented along the polymer film (see Figure 5.2(a)). The domain periodicity of the AS-SB_{26} is 34 nm, as determined by SAXS, while the polystyrene lamellar thickness is 16 ± 1 nm, as determined by TEM measurements. These results are in agreement with the literature.[21,22] It can be

observed from Figure 5.2(b-e) that the pristine $MWCNT_{BMS}^{95}$ as well as the polymer grafted $MWCNT_{BMS}^{95}$ are randomly oriented along the block copolymer. In most of the evaluated regions, the carbon nanotubes are isolated, form groups of two or three nanotubes and, in seldom cases, some aggregates can be identified. The domain periodicities of the nanocomposites based on polystyrene grafted $MWCNT_{BMS}^{95}$ and $AS\text{-}SB_{26}$ are comparable to the ones described for the neat block copolymer. In the case of the pristine $MWCNT_{BMS}^{95}$ (see Figure 5.2(b)), most of the carbon nanotubes intersect the lamellar domains, and this indicates that the microphase separation of the block copolymer during the evaporation of the solvent does not seem to be affected by the presence of the $MWCNT_{BMS}^{95}$, and the carbon nanotubes do not show selectivity towards the polystyrene or the polybutadiene microdomains.

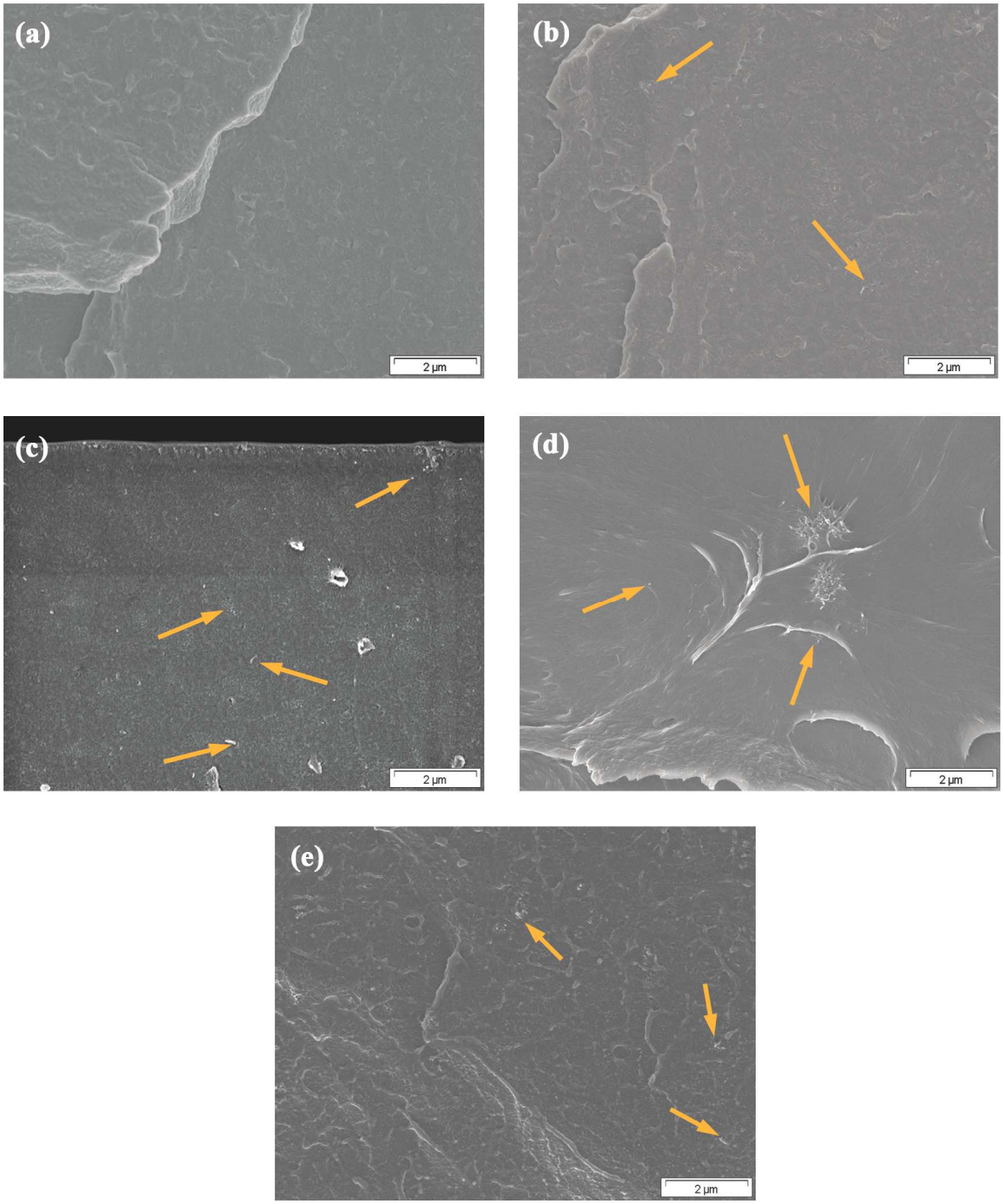

Figure 5.1. Selected scanning electron micrographs of the cryogenic fracture cross sections of: (a) AS-SB_{26}, (b) $MWCNT_{BMS}^{95}$/AS-SB_{26}, (c) $PS_{47}^{11}MWCNT_{BMS}^{95}$/AS-$SB_{26}$, (d) $PS_{70}^{4}MWCNT_{BMS}^{95}$/AS-$SB_{26}$ and (e) PS_{91}^{20} $MWCNT_{BMS}^{95}$/AS-SB_{26}. The content of the carbon nanotubes is approximately 1 wt %. The samples were sputtered with a layer of Au/Pd.

On the contrary, the TEM of the nanocomposites based on the polystyrene grafted $MWCNT_{BMS}^{95}$ show some differences in the morphology of the AS-SB_{26} in the proximities of the carbon nanotubes. In the case of the $PS_{47}^{11}MCWNT_{BMS}^{95}$ (see

Figure 5.2(c)), the carbon nanotubes locally distort the lamellar morphology. In the vicinity of the $PS_{47}{}^{11}MWCNT_{BMS}{}^{95}$, the lamellar domains of the block copolymer seem diffuse or partially deformed. The morphology of the nanocomposites prepared with $PS_{70}{}^{4}MCWNT_{BMS}{}^{95}$ (see Figure 5.2(d)) partially resembles the observations described in the two previous cases (pristine $MWCNT_{BMS}{}^{95}$ and the $PS_{47}{}^{11}MWCNT_{BMS}{}^{95}$): some carbon nanotubes bisect the lamellae, others distort the morphology locally (just in their vicinity). In the case of the nanocomposite based on $PS_{91}{}^{20}MWCNT_{BMS}{}^{95}$ (see Figure 5.2(e)), the morphology of the AS-SB_{26} locally resembles the contour of the $PS_{91}{}^{20}MWCNT_{BMS}{}^{95}$, which indicates that the $PS_{91}{}^{20}MWCNT_{BMS}{}^{95}$ locally templates the morphology of the AS-SB_{26}. This can be interpreted as follows: during the microphase separation of the AS-SB_{26} from solution, the polystyrene chains of the block copolymer interact favorably with the polystyrene grafted from the $PS_{91}{}^{20}MWCNT_{BMS}{}^{95}$. Therefore, the polystyrene chains in the vicinity of the $PS_{91}{}^{20}MWCNT_{BMS}{}^{95}$ segregate from the solution together with the anchored polystyrene chains and form a domain around the $PS_{91}{}^{20}MWCNT_{BMS}{}^{95}$. The polybutadiene chains consequently microphase separate next to the polystyrene lamellae. and the lamellar morphology of the block copolymer in the vicinity of the carbon nanotubes resembles then the contour of the filler. The process is repeated to a certain extend until the geometrical restriction given by the carbon nanotubes is lost. Farer away from the carbon nanotubes, the lamellae are randomly organized, as commonly observed in the case of the neat AS-SB_{26}. This behavior is similar to the results obtained on films based on polystyrene grafted organic clay and linear SBS prepared by roll casting. It was shown that the polystyrene grafted clay platelets are able to template the morphology of the block copolymer, even though the dimensions of the clay platelets exceed the thickness of the polystyrene lamellar phase.[23]

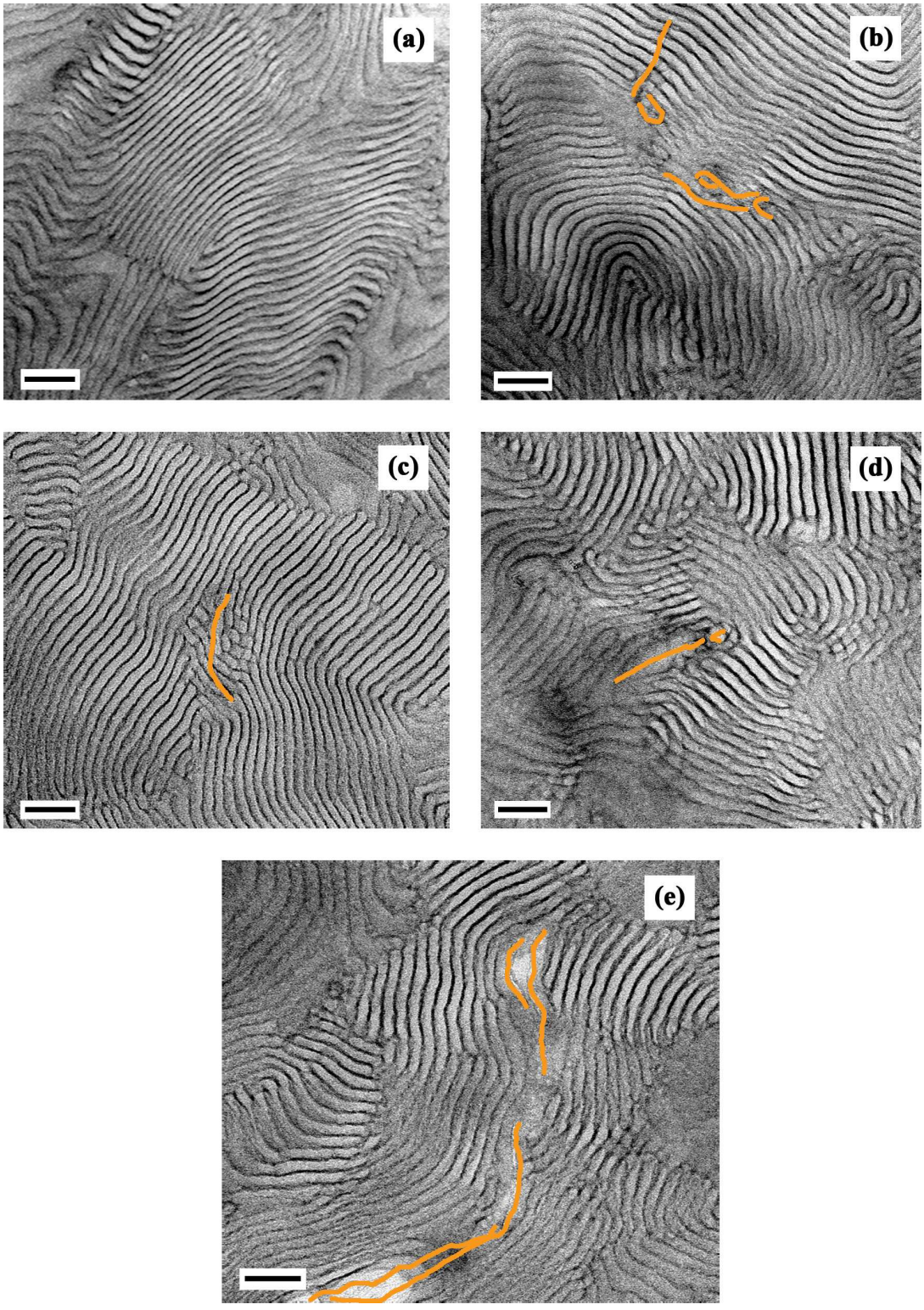

Figure 5.2. Selected transmission electron micrographs (stained with OsO_4; black: polybutadiene, gray: polystyrene) of: (a) AS-SB_{26}, (b) $MWCNT_{BMS}^{95}$/AS-SB_{26}, (c) $PS_{47}^{11}MWCNT_{BMS}^{95}$/AS-$SB_{26}$, (d) $PS_{70}^{4}MWCNT_{BMS}^{95}$/AS-$SB_{26}$ and (e) $PS_{91}^{20}MWCNT_{BMS}^{95}$/AS-$SB_{26}$. The carbon nanotubes are highlighted. Ultra thin sections were obtained from the nanocomposite films. Scale bar = 100 nm.

The sequestering of a MWCNT in a block copolymer phase has been previously reported in nanocomposites based on a high molecular weight polystyrene-*block*-polyisoprene diblock copolymer (SI) and polystyrene grafted MWCNTs.[14] The SI had a lamellar morphology, with a polystyrene lamellar thickness of approximately 150 nm. The TEM image can be appreciated in Chapter 2 (Figure 2.12). The TEM image showed that the polystyrene grafted MWCNT is placed at the center of the polystyrene lamellae phase. The sequestering of the polystyrene grafted MWCNTs in the polymer domain was attributed to the favorable interaction between the grafted polystyrene and the polystyrene chains in the block copolymer and to the polystyrene domain size, which is approximately three times the diameter of the MWCNT. Unfortunately, no information is given regarding the molecular weight and the grafting density of the polystyrene.[13]

In the case of the study presented in this chapter, the thickness of the lamellar domains in the AS-SB_{26} is comparable or smaller than the diameter of the pristine and polymer grafted $MWCNT_{BMS}^{95}$, which represents an entropic barrier for the incorporation of the $MWCNT_{BMS}^{95}$ into the polystyrene domain.[24] On the contrary, the selective interaction between the $PS_{91}^{20}MWCNT_{BMS}^{95}$ and the polystyrene chains of the AS-SB_{26} induce the microphase separation of the block copolymer, under the experimental conditions employed in this work. This behavior can be interpreted as a "wet brush" situation, i.e., the corona chains of the $MWCNT_{BMS}^{95}$ are swelled by the free block copolymer chains. However, according to the theory proposed by de Gennes,[25] this requires that the molecular weight of the grafted chains exceeds the molecular weight of the free chains in the copolymer. In order to have an idea about which brush regime is represented by the grafted polystyrene chains with respect to

the polystyrene block in the AS-SB_{26}[26] it is necessary to know the grafting density of the polystyrene chains on the carbon nanotube. The presence of different graphene layers forming the carbon nanotubes makes the determination of the grafting chain density more difficult than with SWCNTs.[17,27] Nevertheless, if considering the MWCNTs as straight cylinders it is possible to make a rough estimation of the grafting chain density. The estimation of the grafting chain density is described in the Appendix A, and the results are presented in Table 5.1. From the relation between the grafting chain density, the molecular weight of the grafted polymer and the molecular weight of the AS-SB_{26}, it can be assume that the carbon nanotubes and the block copolymer are more likely in a dry brush situation (dry brush long solvent for the pristine $MWCNT_{BMS}$[95], ideal mushrooms for PS_{47}[11]$MWCNT_{BMS}$[95] and ideal wet brush in the case of PS_{70}[4]$MWCNT_{BMS}$[95] and PS_{91}[20]$MWCNT_{BMS}$[95]).[26] This means that theoretically the nanoparticles will tend to aggregate in the AS-SB_{26} matrix. Contradictory to these calculations and despite the fact that the chemical structure of the carbon nanotubes (i.e. the π-π stacking interactions) induce the aggregation of the nanoparticles, the experimental evidences showed that the dispersions of pristine and polymer grafted $MWCNT_{BMS}$[95] in the AS-SB_{26} are acceptable.

It is important to mention at this point that the AS-SB_{26} is an asymmetric star block copolymer formed by a polybutadiene core and polystyrene arms of different lengths. The number of polystyrene arms and their molecular weights are unknown. This block copolymer is already a polymer brush and its interaction with a polymer coated nanoparticle (another brush) in solution and during the film casting could not be well described by the theories proposed for mixtures with homopolymers and maybe for block copolymers with a simpler architecture. Nevertheless, based on the

experimental evidences and results obtained with similar systems, some qualitative conclusions can be drawn.

Bates and co-workers[28] have found contradictory results in films (cast from solution) of polystyrene grafted silica nanospheres embedded in a linear polystyrene-*block*-polybutadiene block copolymer (SB), with a lamellar morphology. They observed that the dispersion of silica nanoparticles improves with the increase of the block copolymer molecular weight and with the decrease of the molecular weight of the polystyrene grafted from the silica nanoparticles, and that the polystyrene grafted silica nanospheres did not show selectivity towards the polystyrene or the polybutadiene lamellar domains in the SB. From the experimental evidences it was concluded that before the solvent evaporation takes place, the silica nanoparticles are homogeneously dispersed in the disordered block copolymer. During the evaporation of the solvent, the microphase separation of the block copolymer traps the nanoparticles in the nanocomposite, when the diameter of the polystyrene grafted silica is smaller than the domain size of the block copolymer. If the diameter of the polystyrene grafted silica is comparable or higher than the domain size of the block copolymer, the nanoparticles tend to aggregate during the microphase separation.

The considerations made in the case of the silica nanoparticles might be valid for the pristine and the polystyrene coated $MWCNT_{BMS}^{95}$ with the lowest grafting density (i.e.; $PS_{47}^{11}MWCNT_{BMS}^{95}$): the nanoparticles do not show preferences toward the polybutadiene or the polystyrene lamellae. Starting from a homogeneous dispersion, the carbon nanotubes are trapped in the block copolymer microstructure when the AS-SB_{26} microphase separate from solution. In the case of the $PS_{70}^{4}MWCNT_{BMS}^{95}$/AS-

SB_{26} and the $PS_{91}{}^{20}MWCNT_{BMS}{}^{95}$/AS-$SB_{26}$ nanocomposites, the situation could be more complicated. The molecular weight of the grafted polystyrene was calculated based on the weight loss and the initiator concentration at the surface of the carbon nanotubes. These values are an average of the molecular weight distribution of the corona chains; however, the molecular weight distribution of grafted chains along the carbon nanotubes depends on the location of the initiator moieties.[17] In those places where the molecular weight of the grafted chains and the polystyrene chains in the AS-SB_{26} fulfill a "wet-brush" situation, the favorable interaction between the polymer chains might induce the microphase separation of the AS-SB_{26} in the vicinity of the carbon nanotubes, taking the nanofillers as patterns for the shape of the lamellar domains. The film prepared using the $PS_{70}{}^{4}MWCNT_{BMS}{}^{95}$ showed that the microstructure of the AS-SB_{26} is "partially" template by the nanofiller. In the case of the $PS_{91}{}^{20}MWCNT_{BMS}{}^{95}$, the molecular weight distribution of grafted chains along the carbon nanotubes seems to better match with the polystyrene chains of the block copolymer. For this reason, the block copolymer microstructure copies the shape of the carbon nanotube during the microphase separation.

The analysis given below could lead to the conclusion that the dry-bush/wet-brush reasoning can be addressed, taking into account probable miscalculations regarding the molecular weight of the grafted polymer; however, the results obtained by Thomas and co-workers[23] on clay base nanocomposites might also lead to the assumption that the aspect ratio of the nanoparticle has an effect during the microphase separation of the block copolymer. It was reported that the clay grafted with low molecular weight polystyrene chains is able to template the microstructure of the polystyrene-*block*-polybutadiene-*block*-polystyrene copolymer. The results are

attributed to the good dispersion of the clay before the microphase separation of the block copolymer occurs, and for this reason the block copolymer microstructure is aligned with the clay sheets. A similar situation was obtained in the case of graphene sheet embedded in a polystyrene-*block*-polyisoprene-*block*-polystyrene copolymer.[29] In the case of the $MWCNT_{BMS}^{95}$ the shape of these nanoparticles makes energetically improbable that the block copolymer segregates the particle in the disordered state or during the microphase separation.[28] For this reason, the nanoparticles are trapped in the block copolymer microstructure. If the nanoparticles have certain affinity to any of the blocks, the polymer chains might use the surface of the nanofiller to reduce the energy associated to the microphase separation, without necessity of chain entanglements between grafted polymer chains and the polymer chains of the block copolymer.

5.2.3. Mechanical Properties of the nanocomposites

The results of the mechanical properties of the nanocomposites are not appreciably superior to the ones corresponding to the pristine AS-SB_{26}, as can be observed in Table 5.2. The Young modulus is slightly lower for the $MWCNT_{BMS}^{95}$/AS-SB_{26} nanocomposite compared with the block copolymer. The nanocomposite containing polystyrene grafted $MWCNT_{BMS}^{95}$ have Young moduli comparable to the one of AS-SB_{26} (within the experimental error), with slight improvement in yield strengths. The mechanical properties of such type of thermoplastic elastomers are known to depend on the block copolymer morphology.[30,31] The decrease of the elastic modulus in the case of the $MWCNT_{BMS}^{95}$/AS-SB_{26} can be caused by the disruption of the lamellar microstructure of the block copolymer and the poor load transfer between the filler and the matrix. In the case of the nanocomposites based on polystyrene grafted

$MWCNT_{BMS}^{95}$, although the carbon nanotubes locally templates the lamellar morphology of the AS-SB_{26}, the elastic modulus is not affected. The results might suggest that the concentration of pristine or polystyrene grafted $MWCNT_{BMS}^{95}$ used does not influence considerably the microstructure of the AS-SB_{26} in a way that the mechanical properties are governed by the filler. Similar results have been found for other nanocomposites prepared by film casting.[12,32,33] Lu et al.[12] found that the tensile strength does not improve in films based on linear polystyrene-*block*-polybutadiene-*block*-polystyrene and 3 wt % of MWCNT, and increases around 30 % with 7 wt % of MWCNT. They have also reported a moderate improvement in the tensile strength of the nanocomposites prepared by melt mixing. This behavior has been attributed to a better dispersion of MWCNTs in the block copolymer matrix and to the formation of covalent bonds between labile points in the MWCNT and the radicals formed on the polybutadiene block during the melt processing. A similar result has also been found on the behavior in the case of poly(ether-ester) elastomers loaded with SWCNT and MWCNT. In that case, it was also indicated that the influence of the nanofiller in the morphology of the polymer matrix and the orientation of the morphology of the nanocomposite are related to the mechanical properties.[32]

Table 5.2. Mechanical and thermal properties of the $MWCNT_{BMS}^{95}$/AS-SB_{26} nanocomposites.

Sample	E (MPa)	σ_y (MPa)	E' (25 °C) (MPa)[a]	E' (90 °C) (MPa)[a]	T_g (°C)
AS-SB_{26}	400 ± 20	13.3 ± 0.3	709	12	98.8
$MWCNT_{BMS}^{95}$ / AS-SB_{26}	370 ± 10	13.4 ± 0.4	577	18	99.1
$PS_{47}^{11}MWCNT_{BMS}^{95}$ / AS-SB_{26}	420 ± 20	13.6 ± 0.3	665	21	100.7
$PS_{70}^{4}MWCNT_{BMS}^{95}$ / AS-SB_{26}	400 ± 30	13.7 ± 0.1	685	19	101.1
$PS_{91}^{20}MWCNT_{BMS}^{95}$ / AS-SB_{26}	420 ± 10	13.9 ± 0.3	650	21	100.4

a) Measured at 0.01 rad/s

The stress-strain experiments were complemented with dynamical mechanical test at different temperatures. The storage modulus (*E'*) measured at 25 °C and 90 °C at a fixed frequency can be also appreciated in Table 5.2. At 25 °C, the polybutadiene is above its T_g while the polystyrene block is far below its T_g. The behavior of the block copolymer at this temperature can be interpreted as a combination of a rubbery phase (polybutadiene) and a rigid phase (polystyrene). The results obtained on the storage modulus at 90 °C are approximately one order of magnitude lower than at 25 °C. At 90 °C the polystyrene chains possess a higher mobility because the temperature of the measurement is close to the T_g of the polystyrene. Therefore, the chain relaxation of the AS-SB_{26} decreases compared to the experiments performed at 25 °C.

In the experiments conducted at 25 °C, the lowest *E'* is given by the $MWCNT_{BMS}^{95}$/AS-SB_{26} nanocomposite. The results obtained from the storage modulus at low frequencies are comparable to tendencies observed for the Young modulus of the stress-strain experiments. As already mentioned, the decrease in the elastic modulus and *E'* in the case of the $MWCNT_{BMS}^{95}$/AS-SB_{26} nanocomposite could be associated to the local disruption of the lamellar domains during the microphase separation or to unfavorable interaction between the nanofiller and the matrix.[12] There are no considerable differences in *E'* within the polystyrene functionalized $MWCNT_{BMS}^{95}$/AS-SB_{26} nanocomposites.

The *E´* of the AS-SB_{26} is below the values obtained for the nanocomposites at 90°C. Even though these experiments were performed below the glass transition of the polystyrene, the chain mobility of this block in the AS-SB_{26} increases and the storage modulus decreases dramatically. It seems that the increase in the chain mobility of the

polybutadiene and the polystyrene blocks in the AS-SB_{26} transfers more efficiently the load applied to the pristine and the polystyrene grafted $MWCNT_{BMS}$[95] than the chain relaxation of the AS-SB_{26} at 25 °C, independently of the fact that the microstructure of the AS-SB_{26} can be affected by the nanofiller (see previous section). The increase in the *E´* can be also interpreted as a consequence of the chemical affinity between the polystyrene block in the AS-SB_{26} and the graphite like structure of the carbon nanotubes. This affinity is enhanced with the grafting of polystyrene from the $MWCNT_{BMS}$[95]. Therefore, one can assume that, as well as with the stress-strain experiments, the storage modulus in these nanocomposites depends not only on the dispersion of the carbon nanotubes in the polymer matrix and the load transfer from the nanoparticles to the matrix, but also on the selectivity of the carbon nanotubes towards one of the components of the block copolymer.[4,34]

5.2.4. Thermal properties of the nanocomposites

The presence of the functionalized carbon nanotubes does not have a remarkable influence on the glass transition temperature (T_g) of these nanocomposites, specially when compared to other systems. The T_g increases approximately 1-2 °C with respect to the AS-SB_{26} matrix (see Table 5.2). The volume fraction of carbon nanotubes in the nanocomposites is too low to introduce a significant measurable effect. There are just a few examples that refer to changes in the glass transition temperature of nanocomposites based on thermoplastic polymers and carbon nanotubes. Wang and co-workers reported that the T_g of the poly(styrene-*co*-acrylonitrile) copolymer decreases with the addition of poly(methyl methacrylate) grafted MWCNTs, although the polymer grafted has a higher T_g and is miscible with the host matrix.[35] Other systems report important increments in T_g of the polymer (up to 40 °C, in some

cases). However, these increments are related with covalent bonding between the MWCNTs and the polymer matrices,[36,37] or to a combination between surface affinity of the MWCNTs and the preparation of the nanocomposite.[15,38]

5.2.5. Morphology of the nanocomposites: behavior of the carbon nanotubes in the block copolymer under an applied deformation

The effect of the $MWCNT_{BMS}$[95] on the morphology of the AS-SB_{26} was further investigated by simultaneous 2D-SAXS and stress-strain analyses. The orientation of the morphology of polystyrene-*block*-polybutadiene block copolymers has been well described by experiments performed on pre-oriented and unoriented films.[5,7] Representative 2D-SAXS patterns can be appreciated in Figure 5.3. When AS-SB_{26} is subjected to a continuous deformation as the one described in Figure 5.3, the deformation of the lamellar domains can be described by the evolution of the SAXS patterns: starting from a film consisting of randomly oriented lamellar grains, as evidenced by concentric rings in the scattering pattern and transmission electron micrographs, the stretching of the film promotes the deformation of the ring to an ellipsoidal shape with a compressed meridian axis and an expanded equatorial axis. The ellipsoid fragmentizes with increasing strain, forming a four point pattern that further elongates parallel to the equator, leading finally to a diffuse scattering profile. From the scattering profiles it can be corroborated that, during the first stages of the deformation, the lamellae with their normal parallel to the strain direction increase in periodicity. The scattering maxima on the equatorial axis do not change considerably, which indicates that the lamellae with their normal perpendicular to the straining direction are rather unaffected by the deformation process. The four point pattern found at higher strains is related with the tilting of the lamellae with respect to the strain direction. The further deformation of the film leads to the fragmentation of the

lamellar phases. At even higher deformations, the polystyrene layers fragmentize into isolated domains in a rubbery polybutadiene matrix.[5]

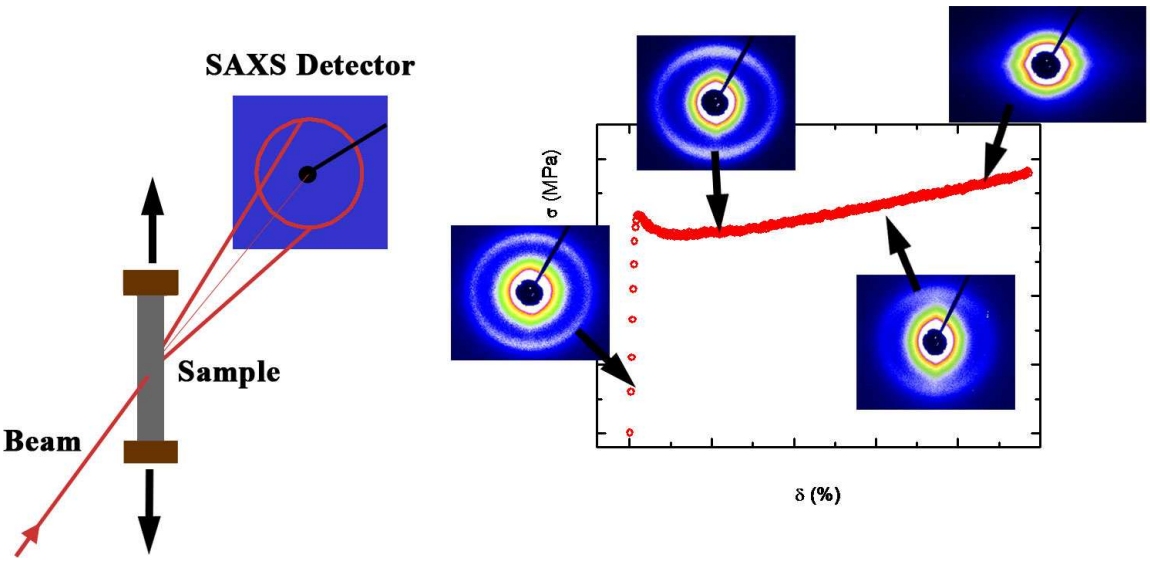

Figure 5.3. Representative sketch of the simultaneous 2D-SAXS/stress-strain measurements.

The effect of the carbon nanotubes on the domain orientation of the morphology of the block copolymer was quantified through the second coefficient of the Legendre polynomial (P_2, also called orientation factor), which is obtained from the scattering intensity ($I_q(\varphi)$)as a function of the azimuthal angle (φ)[39]

$$P_2 = \frac{3\langle \cos^2(\varphi)\rangle - 1}{2} \qquad \text{Eq. 5.1}$$

where

$$\langle \cos^2 \varphi \rangle = \frac{\int_{\alpha}^{\beta} I_q(\varphi) \cos^2 \varphi |\sin \varphi| d\varphi}{\int_{\alpha}^{\beta} I_q(\varphi) |\sin \varphi| d\varphi} \qquad \text{Eq. 5.2}$$

The orientation factor versus the strain for the different nanocomposites is plotted in Figure 5.4. The integrations of the scattering profiles were performed between φ = 90°

and φ = 270° in order to avoid any distortion caused by the beamstop.[40] It can be observed that, for all the nanocomposites as well as for the neat AS-SB_{26}, the orientation factor of the sample increases in the first stages of deformation, then decreases and reaches values close to 0. The behavior of P_2 is associated to the degree of orientation of the copolymer phases induced by an external stimulus. During the first stages of deformation, the periodicity of the lamellar domains increases and this is traduced as an increase in P_2. With the deformation of the film, the lamellar domains deform in a "zigzag" or "herringbone" structure (also known as "chevron" morphology)[5,7] which is related with the maximum orientation achieved by the copolymer. The decrease in P_2 is associated to the loss in domain periodicity due to the fragmentation of the polystyrene lamellae microdomains that are randomly dispersed in the polybutadiene matrix.

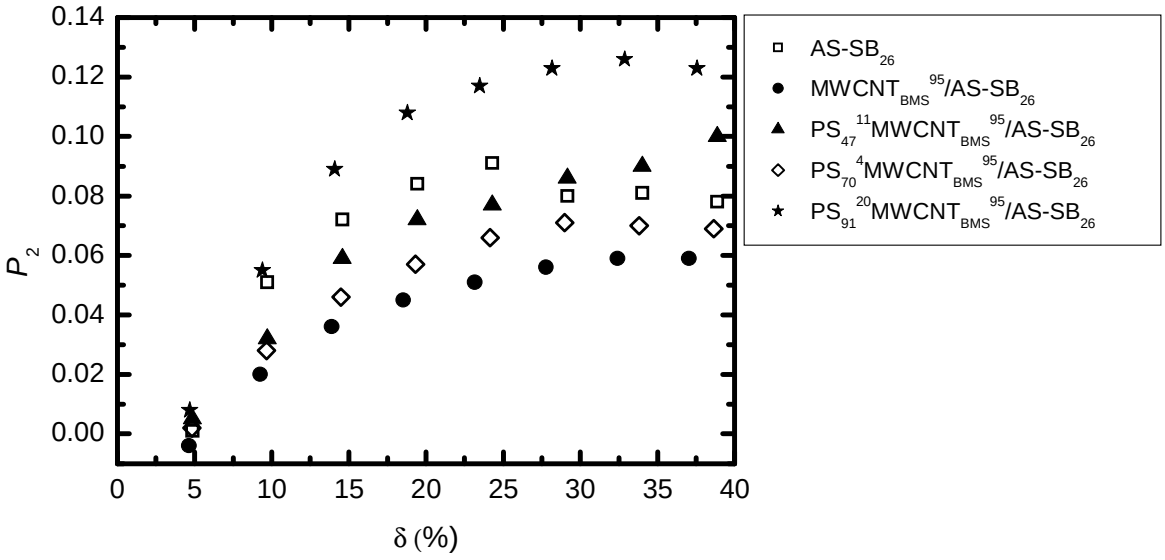

Figure 5.4. Orientation factor (P_2) versus δ (%) for the different $MWCNT_{BMS}^{95}$/AS-SB_{26} nanocomposites.

In the case of this study, the effect of the $MWCNT_{BMS}^{95}$ on the orientation of the block copolymer is taken into account until the maximum P_2 is reached. The plots of P_2 versus strain (δ) presented in Figure 5.4 show that the sample

$PS_{91}{}^{20}MWCNT_{BMS}{}^{95}$/AS-$SB_{26}$ reaches the higher P_2 followed by the values reached by $PS_{47}{}^{11}MWCNT_{BMS}{}^{95}$/AS-$SB_{26}$, AS-$SB_{26}$, $PS_{70}{}^{4}MWCNT_{BMS}{}^{95}$/AS-$SB_{26}$ and $MWCNT_{BMS}{}^{95}$/AS-SB_{26}. This behavior could be related with the influence of the carbon nanotubes on the development of the AS-SB_{26} morphology. In the case of the nanocomposite $PS_{91}{}^{20}MWCNT_{BMS}{}^{95}$/AS-$SB_{26}$, the TEM showed that the carbon nanotubes are able to template the morphology of the block copolymer (see Figure 5.2(e)). The lamellar microdomains in the proximity of a $PS_{91}{}^{20}MWCNT_{BMS}{}^{95}$ might be in consequence relatively longer and more regular than in the other cases. Then, when the sample is deformed, the lamellae close to the $PS_{91}{}^{20}MWCNT_{BMS}{}^{95}$ tend to orient according to the straining direction. This increases the value of P_2.

On the other hand, the TEM images showed that the carbon nanotubes in the $MWCNT_{BMS}{}^{95}$/AS-SB_{26} films bisect the lamellar domains of the block copolymer (see Figure 5.2(b)). These carbon nanotubes might change the distribution or size of the lamellar grains of the nanocomposite compared to the overall morphology of the neat block copolymer, and might be the reason for the fact that the orientation factor in this case is even lower than in the block copolymer.

The maximum P_2 obtained for the $PS_{70}{}^{4}MWCNT_{BMS}{}^{95}$/AS-$SB_{26}$ nanocomposite is higher than the one obtained for $MWCNT_{BMS}{}^{95}$/AS-SB_{26} but inferior than the value obtained for AS-SB_{26}. The orientation factor obtained for the blend between AS-SB_{26} and $PS_{47}{}^{11}MWCNT_{BMS}{}^{95}$ is slightly higher than the corresponding one for AS-SB_{26}. The behavior of these two nanocomposites, i.e., $PS_{70}{}^{4}MWCNT_{BMS}{}^{95}$/AS-$SB_{26}$ and $PS_{47}{}^{11}MWCNT_{BMS}{}^{95}$/AS-$SB_{26}$, is influenced by the content of polymer grafted from the carbon nanotubes and the chain density. In the case of the $PS_{47}{}^{11}MWCNT_{BMS}{}^{95}$ it

can be interpreted from the low maximum value of the P_2 that the interaction of these carbon nanotubes with the polymer matrix is not as favorable as in the case of the carbon nanotubes with higher grafting density, though the molecular weight of the grafted polymer is considerably higher than in $PS_{70}^{4}MWCNT_{BMS}^{95}$, which would have enhanced the chain entanglements with the polystyrene chain of the AS-SB_{26}. From the transmission electron micrograph it appears likely that the block copolymer is able to favorably interact with the $PS_{47}^{11}MWCNT_{BMS}^{95}$ but the nanofiller is not able to template the morphology of the block copolymer (see Figure 5.2(c)).

In order to understand the effect of the deformation on the orientation of the carbon nanotubes, the film morphology was analyzed after the stress-strain experiments. The TEM images of the $MWCNT_{BMS}^{95}$/AS-SB_{26} and the $PS_{91}^{20}MWCNT_{BMS}^{95}$/AS-$SB_{26}$ nanocomposites after the fracture of the films can be observed in Figure 5.5. It seems that, at higher strain levels, the carbon nanotubes tend to lay perpendicular to the strain direction in the nanocomposite containing $PS_{91}^{20}MWCNT_{BMS}^{95}$ (Figure 5.5(b)). On the contrary, in the case of the $MWCNT_{BMS}^{95}$/AS-SB_{26}, the carbon nanotubes are randomly oriented (Figure 5.5(a)).

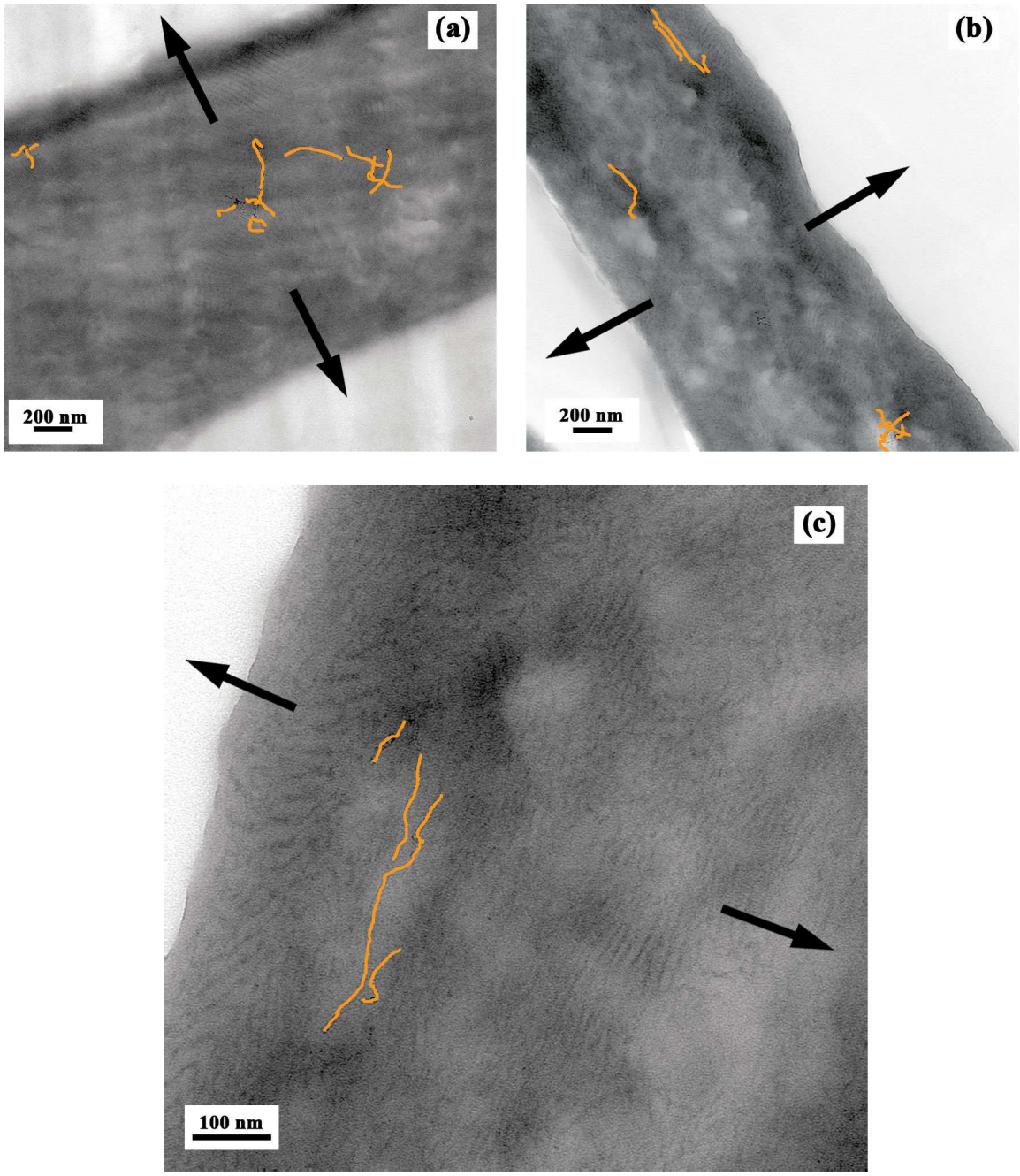

Figure 5.5. Transmission electron micrographs of (a) $MWCNT_{BMS}^{95}$/AS-SB_{26}, (b) and (c) $PS_{91}^{20}MWCNT_{BMS}^{95}$/AS-$SB_{26}$ after the stress-strain experiments. Ultra thin cuts were obtained from the films embedded in an epoxy resin. The samples are not stained. The arrows indicate the direction of the applied deformation.

If the alignment of the carbon nanotubes is assumed as a continuous process that starts from homogeneously distributed $PS_{91}^{20}MWCNT_{BMS}^{95}$, the preferential orientation of the $PS_{91}^{20}MWCNT_{BMS}^{95}$ might account for the high P_2 maximum during the first stages of the deformation. A model of this process is sketched in Figure 5.6. The

grafted polystyrene chains and the polystyrene block of the block copolymer form a continuous phase next to the carbon nanotube. When the nanocomposite is strained, the polymer chains try to align with the direction of the applied deformation. The chains grafted from the $PS_{91}{}^{20}MWCNT_{BMS}{}^{95}$ also orient parallel to the strain direction. As a consequence, the carbon nanotubes arrange perpendicularly to the direction of the deformation. The perpendicular orientation of the $PS_{91}{}^{20}MWCNT_{BMS}{}^{95}$ in the block copolymer matrix might account for the poor reinforcement of the nanofiller observed during the mechanical stress-strain or the dynamical mechanical experiments.

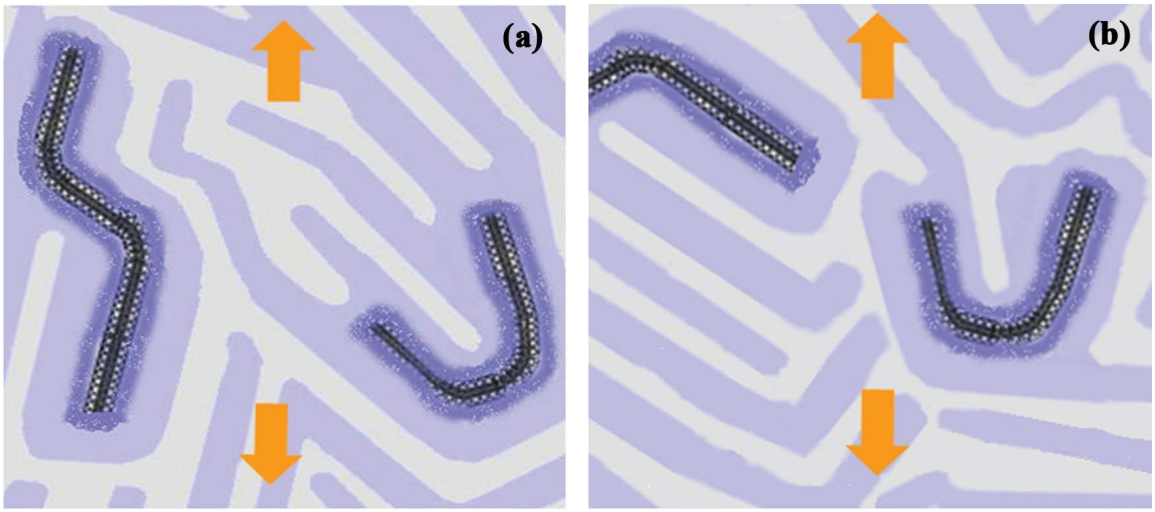

Figure 5.6. Sketch of the deformation process of the $PS_{91}{}^{20}MWCNT/AS\text{-}SB_{26}$ nanocomposites (a) before and (b) after the strain-stress experiments.

5.3. Conclusions

Nanocomposites based on as received $MWCNT_{BMS}{}^{95}$ or polystyrene grafted $MWCNT_{BMS}{}^{95}$ and $AS\text{-}SB_{26}$ were prepared by solution casting. The increase in the grafting density and molecular weight of the polystyrene grafted from the $MWCNT_{BMS}{}^{95}$ were observed to influence the morphology of the $AS\text{-}SB_{26}$. The highest influence was found in the case of the $PS_{91}{}^{20}MWCNT_{BMS}{}^{95}/AS\text{-}SB_{26}$, where the $PS_{91}{}^{20}MWCNT_{BMS}{}^{95}$ templates locally the lamellae morphology of the $AS\text{-}SB_{26}$,

so that the lamellae resemble the contour of the $PS_{91}^{20}MWCNT_{BMS}^{95}$. The mechanical properties of the block copolymer do not appreciably improve with the presence of the carbon nanotubes. The storage modulus at 90 °C slightly increases in the case of the polystyrene grafted $MWCNT_{BMS}^{95}$ based nanocomposites due to a better load transfer between the block copolymer and the functionalized carbon nanotubes. The $PS_{91}^{20}MWCNT_{BMS}^{95}$ increases the orientation factor of the AS-SB_{26}. Due to the polymer coating, the $PS_{91}^{20}MWCNT_{BMS}^{95}$ aligns perpendicular to the strain direction when the film is deformed. The results presented here demonstrate that the local orientation of nanofillers in an external field (here: mechanical force field) can be controlled by variation of the interaction between nanofiller and matrix. While in this study only the degree of polymerization and the polymer grafting density were varied in order to compatibilize the nanofiller with a similar matrix by entropic effects, also specific enthalpic interactions can be envisioned for such purposes, like hydrogen bonds, donor acceptor complexes, ionic interactions, etc.

5.4. References

1. Ober, C. K.; Cheng, S. Z. D.; Hammond, P. T.; Muthukumar, M.; Reichmanis, E.; Wooley, K. L.; Lodge, T. P. Macromolecules 2009, 42, 465-471.
2. Nestle, N.; Heckmann, W.; Steininger, H.; Knoll, K. Anal. Chim. Acta 2007, 604, 54-61.
3. Honeker, C. C.; Thomas, E. L. Chem. Mater. 1996, 8, 1702-1714.
4. Cohen, Y.; Albalak, R. J.; Dair, B. J.; Capel, M. S.; Thomas, E. L. Macromolecules 2000, 33, 6502-6516.
5. Fujimura, M.; Hashimoto, T.; Kawai, H. Rubber Chem. Technol. 1978, 51, 215-224.
6. Odell, J. A.; Keller, A. Polym. Eng. Sci. 1977, 17, 544-559.
7. Sakurai, S.; Aida, S.; Okamoto, S.; Ono, T.; Imaizumi, K.; Nomura, S. Macromolecules 2001, 34, 3672-3678.
8. Trujillo, M.; Arnal, M. L.; Muller, A. J.; Laredo, E.; Bredeau, S.; Bonduel, D.; Dubois, P. Macromolecules 2007, 40, 6268-6276.
9. Bose, S.; Bhattacharyya, A. R.; Kodgire, P. V.; Misra, A. Polymer 2007, 48, 356-362.
10. Lee, G.-W.; Jagannathan, S.; Chae, H. G.; Minus, M. L.; Kumar, S. Polymer 2008, 49, 1831-1840.
11. García-Gutiérrez, M. C.; Nogales, A.; Rueda, D. R.; Domingo, C.; García-Ramos, J. V.; Broza, G.; Roslaniec, Z.; Schulte, K.; Ezquerra, T. A. Compos. Sci. Technol. 2007, 67, 798-805.
12. Lu, L.; Zhou, Z.; Zhang, Y.; Wang, S.; Zhang, Y. Carbon 2007, 45, 2621-2627.

13. Bockstaller, M. R.; Mickiewicz, R. A.; Thomas, E. L. Adv. Mater. (Weinheim, Ger.) 2005, 17, 1331-1349.
14. Park, I.; Lee, W.; Kim, J.; Park, M.; Lee, H. Sensor Actuat B-Chem 2007, 126, 301-305.
15. Peponi, L.; Valentini, L.; Torre, L.; Mondragon, I.; Kenny, J. M. Carbon 2009, 47, 2474-2480.
16. Yao, Z.; Braidy, N.; Botton, G. A.; Adronov, A. J. Am. Chem. Soc. 2003, 125, 16015-16024.
17. Wu, W.; Tsarevsky, Nicolay V.; Hudson, Jared L.; Tour, J. M.; Matyjaszewski, K.; Kowalewski, T. Small 2007, 3, 1803-1810.
18. Brandrup, J.; Immergut, E. H.; McDowell, W. Polymer Handbook; Wiley: New York, 1975.
19. Kong, H.; Gao, C.; Yan, D. Macromolecules 2004, 37, 4022-4030.
20. Liu, Y. L.; Chen, W. H. Macromolecules 2007, 40, 8881-8886.
21. Adhikari, R.; Michler, G. H.; Knoll, K. Polymer 2004, 45, 241-246.
22. Adhikari, R.; Godehardt, R.; Lebek, W.; Goerlitz, S.; Michler, G. H.; Knoll, K. Macromol. Symp. 2004, 214, 173-196.
23. Ha, Y.-H.; Kwon, Y.; Breiner, T.; Chan, E. P.; Tzianetopoulou, T.; Cohen, R. E.; Boyce, M. C.; Thomas, E. L. Macromolecules 2005, 38, 5170-5179.
24. Bockstaller, M. R.; Kolb, R.; Thomas, E. L. Adv. Mater. (Weinheim, Ger.) 2001, 13, 1783-1786.
25. Gennes, P. G. D. J. Phys. France 1976, 37, 1445-1452.
26. Borukhov, I.; Leibler, L. Macromolecules 2002, 35, 5171-5182.
27. Qin, S.; Qin, D.; Ford, W. T.; Resasco, D. E.; Herrera, J. E. J. Am. Chem. Soc. 2004, 126, 170-176.
28. Lan, Q.; Francis, L. F.; Bates, F. S. J. Polym. Sci., Part B: Polym. Phys. 2007, 45, 2284-2299.
29. Peponi, L.; Tercjak, A.; Verdejo, R.; Lopez-Manchado, M. A.; Mondragon, I.; Kenny, J. M. J. Phys. Chem. C 2009.
30. Michler, G. H.; Adhikari, R.; Lebek, W.; Goerlitz, S.; Weidisch, R.; Knoll, K. J. Appl. Polym. Sci. 2002, 85, 683-700.
31. Adhikari, R.; Michler, G. H.; Lebek, W.; Goerlitz, S.; Weidisch, R.; Knoll, K. J. Appl. Polym. Sci. 2002, 85, 701-713.
32. Roslaniec, Z.; Broza, G.; Schulte, K. Compos. Interface 2003, 10, 95-102.
33. Shi, J.-H.; Yang, B.-X.; Pramoda, K. P.; Goh, S. H. Nanotechnology 2007, 18, 375704-375708.
34. Broza, G.; Schulte, K. Polym. Eng. Sci. 2008, 48, 2033-2038.
35. Wang, M.; Pramoda, K. P.; Goh, S. H. Polymer 2005, 46, 11510-11516.
36. Velasco-Santos, C.; Martinez-Hernandez, A. L.; Fisher, F. T.; Ruoff, R.; Castano, V. M. Chem. Mater. 2003, 15, 4470-4475.
37. Xiong, J.; Zheng, Z.; Qin, X.; Li, M.; Li, H.; Wang, X. Carbon 2006, 44, 2701-2707.
38. Meng, H.; Sui, G. X.; Fang, P. F.; Yang, R. Polymer 2008, 49, 610-620.
39. Böker, A.; Elbs, H.; Hansel, H.; Knoll, A.; Ludwigs, S.; Zettl, H.; Zvelindovsky, A. V.; Sevink, G. J. A.; Urban, V.; Abetz, V.; Muller, A. H. E.; Krausch, G. Macromolecules 2003, 36, 8078-8087.
40. Pople, J. A.; Hamley, I. W.; Fairclough, J. P. A.; Ryan, A. J.; Booth, C. Macromolecules 1998, 31, 2952-2956.

Chapter 6. Block Copolymer Nanocomposites based on $MWCNT_{FC}^{99}$: Effect of the Functionalization of the Multiwall Carbon Nanotubes and the film preparation on the Morphology and Properties of the Nanocomposites.

6.1. Introduction

The dimension of the fillers has a strong influence in their properties. Increase in the thermal transport or the mechanical properties are observed when micron size fillers are compared with their nanometer size analogous.[1,2] In the case of carbon nanotubes, beside the number of walls, the dimension and the regularity of the sp^2 carbon atoms strongly influence their properties.[3] Despite the benefits of the nanoparticles (including carbon nanotubes), their larger surface to volume ratio produces a strong state of aggregation within the particles. In this sense, different strategies have been used in order to homogeneously disperse the nanoparticles in solvents and especially in polymer matrices. Some of these strategies have been discussed in chapter 2.

Of particular interest is the dispersion of MWCNTs in block copolymer matrices, especially if the carbon nanotubes have favorable interaction with one of the microdomains. In the previous chapter, block copolymer nanocomposites based on $AS\text{-}SB_{26}$ and $MWCNT_{BMS}^{95}$ were prepared by film casting. The morphology, thermal and mechanical properties were discussed as a function of the polystyrene grafted content and the grafting density. It was found that the coated $MWCNT_{BMS}^{95}$s with the higher polystyrene grafted content and grafting density template locally the lamellar morphology of the $AS\text{-}SB_{26}$.

In this chapter, films of oxidized or polystyrene grafted $MWNCNT_{FC}^{99}$ and $AS\text{-}SB_{26}$ prepared at different casting temperatures are studied. Particular attention has been paid during the preparation of the nanocomposites, in order to avoid the presence of aggregates that could be formed during the synthesis or the functionalization of the carbon nanotubes. The effect of functionalization of the $MWNCNT_{FC}^{99}$ and the casting temperature on the morphology, the mechanical and the electrical conductivity properties of the $AS\text{-}SB_{26}$ nanocomposite will be discussed.

6.2. Results and Discussion

The nanocomposite films were prepared by film casting. Previous works has reported that the dispersion of carbon nanotubes in polymer matrices depends on the method of preparation of the nanocomposite. Homogeneous dispersion of pristine and functionalized carbon nanotubes in polymer matrices has been obtained through different methods which includes calendaring,[4] sonication,[5] melt[6-9] or high speed mixing.[10-12]

6.2.1. Characteristic of the carbon nanotubes after the oxidation and the *grafting from* polymerization reactions

In this work, the carbon nanotubes were dispersed in chloroform and then separated by centrifugation, previous to their blending with $AS\text{-}SB_{26}$. The experimental procedure is sketched in Figure 3.7. This procedure was adopted in order to decrease the quantity of carbon nanotubes bundles before the preparation of the nanocomposites. After the centrifugation step, the supernatant dispersions were carefully separated, filtrated and dried. The carbon nanotubes obtained from the supernatant dispersion could be redispersed in chloroform (or toluene) and formed an optically homogeneous and stable dispersion, after stirring for a few minutes. The

quantity of the carbon nanotubes recovered from the supernatant dispersion varies with the functionalization of the carbon nanotubes. The recovery values can be seen in Table 6.1. In chapter 5, the carbon nanotubes and the AS-SB_{26} were centrifuge before the film casting. This procedure sediments carbon nanotubes aggregates but also traces of AS-SB_{26} remains in the centrifuge tubes, which lead to inaccuracies on the final composition of the nanocomposites.

Table 6.1. Molecular and thermal characterization and recovery after the centrifugation of the dispersed nanoparticles of the acid treated and polystyrene grafted $MWCNT_{FC}^{99}$

	σ/a² (chains/nm²)	**PS** (wt %)	$\mathbf{M_n^{PS}}$ (kg/mol)[a]	$\boldsymbol{T_g^{PS}}$ (°C)	**recovery** (wt %)[b]
$^{oxid}MWCNT_{FC}^{99}$	--	--	--	n.a.	3.0
$PS_{14}{}^{2}MWCNT_{FC}^{99}$	0.20	14.1	2.2	--	6.5
$PS_{85}{}^{24}MWCNT_{FC}^{99}$	0.65	85.2	24.0	108.8	96.0

a) obtained from the TGA analysis;[13] b) recovery = (mass of the MWCNT dispersed in chloroform after ultracentrifugation/total mass of MWCNT) x 100; n.a. = not applicable

Chloroform was selected because it has a relative high density (1.48 g/cm^3).[14] When the pristine $MWCNT_{FC}^{99}$s are stirred in chloroform, the nanoparticle aggregates go to the surface of the chloroform after the stirring is stopped. If the dispersion of pristine $MWCNT_{FC}^{99}$ is centrifuge, the carbon nanotubes form a compact layer at the bottom of the centrifuge tube that can be removed with the help of a spatula. It was not possible to recover a quantifiable amount of pristine $MWCNT_{FC}^{99}$ from the supernatant dispersion. On the contrary, a small quantity of the $^{oxid}MWCNT_{FC}^{99}$ has been recovered from the supernatant dispersion after the centrifugation (Table 6.1). Infrared spectroscopy analysis has shown that, after the oxidation of the $MWCNT_{FC}^{99}$ with nitric acid, phenol and ester groups are formed. The oxidation treatment leads also to the degradation of amorphous carbon and catalyst remaining, as well as the disaggregation of carbon nanotubes ropes or bundles (see chapter 4). The

disaggregation of the carbon nanotubes improves their dispersion in chloroform; however, most of the $^{oxid}MWNCNT_{FC}^{99}$ sink after centrifugation.

Higher recovery yields were obtained in the case of the $MWCNT_{FC}^{99}$ grafted with polystyrene. The quantity of carbon nanotubes recovered from the supernatant increases with the grafting content and the molecular weight of the polystyrene. The quantity of carbon nanotubes recovered doubles the one corresponding to the $^{oxid}MWCNT_{FC}^{99}$ when 14 % wt of polystyrene with approximately 2.2 kg/mol are grafted from the $MWCNT_{FC}^{99}$. In the case of the $PS_{85}^{24}MWNCNT_{FC}^{99}$, the quantity of carbon nanotubes recovered is almost the complete amount dispersed in chloroform. The increment in the polymer grafting content and the molecular weight makes the carbon nanotubes more stable in organic solvents. This was previously discussed in chapter 4, as well as by other research groups.[15-17]

The centrifugation process aggregates and sediments large/heavy particles and leave small/light particles in the dispersion. In the case of the carbon nanotubes, the large/heavy particles should correspond to large/heavy bundles and the small/light should correspond to small/light bundles or isolated carbon nanotubes. The low recovery values of the sample $^{oxid}MWCNT_{FC}^{99}$ suggest that the dispersion is mainly composed of large/heavy ropes of carbon nanotubes. However, the centrifugation may lead to the aggregation of already dispersed $^{oxid}MWCNT_{FC}^{99}$.

The oxidation of the $MWCNT_{FC}^{99}$ probably does not avoid the coalescence of the carbon nanotubes due to the strong π-π stacking interactions within graphite layers. In the case of the $MWCNT_{FC}^{99}$ grafted with polystyrene, on one hand, the increase of the

weight percentage and the molecular weight of the polymer avoid coalescence of the carbon nanotubes during the centrifugation; on the other hand, the grafting of polymer from ropes or bundles of carbon nanotubes may increase the dispersibility of the aggregates. These aggregates might have remained in the supernatant dispersion after the centrifugation.

6.2.2. Optical dispersion of the carbon nanotubes in the nanocomposites: effect of the fractionation of the carbon nanotubes and the casting temperature

A fractionation of the carbon nanotubes was performed in order to avoid the presence of aggregates in the film. Though, reaggregation of the carbon nanotubes was evidenced upon solvent evaporation. For comparison, Figure 6.1 shows optical microscope images of films containing 0.1 wt % of the carbon nanotubes, prepared at different casting temperatures.

The optical micrographs clearly show the formation of aggregates on all the cast film, however, some differences on the dispersion of these aggregates as a function of the casting temperature can be addressed. Even though the dispersions in toluene look homogeneous before the film is cast, aggregates are formed during the solvent evaporation. Within the resolution of the optical microscope, the films with the best dispersion of aggregates are the ones prepared with $PS_{85}^{24}MWCNT_{FC}^{99}$, followed by the $PS_{14}^{2}MWCNT_{FC}^{99}$ and the $^{oxid}MWCNT_{FC}^{99}$. The dimensions of the aggregates observed in the nanocomposites containing $PS_{85}^{24}MWCNT_{FC}^{99}$ are on the order of 1 to 2 µm. These films are translucid to the naked eye and the aggregates are hardly identified. In the case of the samples prepared with $PS_{14}^{2}MWCNT_{FC}^{99}$, agglomerates from 1 µm up to 100 µm are observed. These aggregates are homogeneously

distributed along the films. In the case of the films containing $^{oxid}MWCNT_{FC}^{99}$, macroscopic aggregates (up to 1 mm) are randomly distributed in the AS-SB_{26}. These results are similar to the fractionation experiments described above: the better the affinity between substrate (AS-SB_{26}) and carbon nanotubes, the better the quality of the dispersion of the nanoparticles in the polymer.

The quality of the dispersion can be controlled by increasing the temperature of casting. The films cast at 60 °C presented more and bigger agglomerates than the films cast at 90 °C. This can be attributed to the aggregation of the nanoparticles in time: whereas the solvent is completely evaporated after approximately 30 minutes at 90 °C, the evaporation at 60 °C took approximately 12 hours. Therefore, the rate of evaporation as well as the affinity between the carbon nanotube and the polymer matrix determine the quality of the dispersion in the nanocomposite.

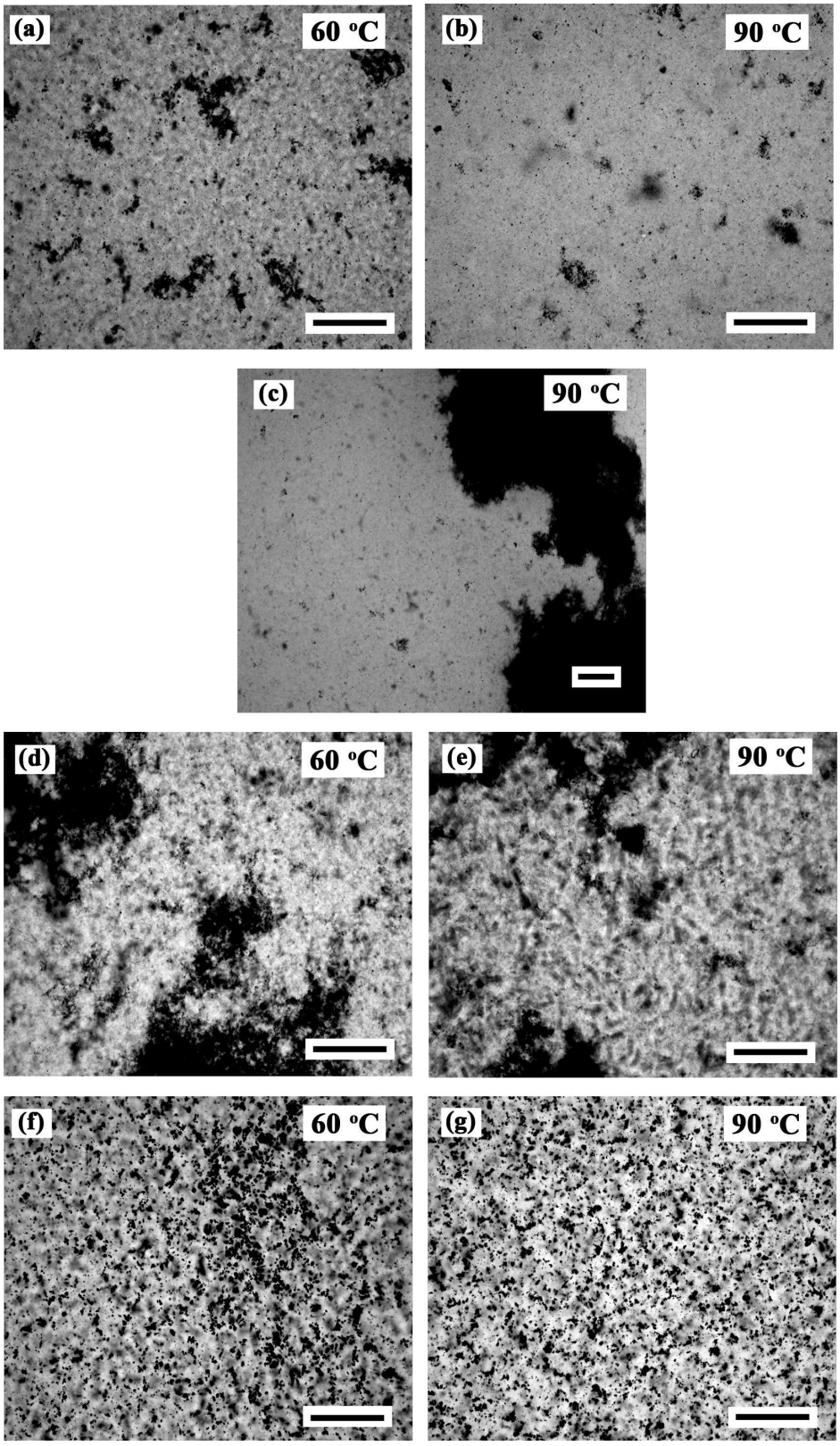

Figure 6.1. Optical microscopy images of the 0.1 wt % carbon nanotubes films prepared at different casting temperatures: (a), (b) and (c) $^{oxid}MWCNT_{FC}{}^{99}$/AS-SB_{26}; (d) and (e) $PS_{14}{}^{2}MWCNT_{FC}{}^{99}$/AS-$SB_{26}$; (f) and (g) $PS_{85}{}^{24}MWCNT_{FC}{}^{99}$/AS-$SB_{26}$. The casting temperatures are indicated on the images. Scale bar = 20 µm.

6.2.3. Thermal properties of the nanocomposites

Changes on the glass transition temperature (T_g) of the AS-SB_{26} have also been observed as a function of the casting conditions. The results obtained from the first heating run of the samples are presented in Table 6.2. The T_g of the polystyrene microphase of the AS-SB_{26} film cast at 90 °C is approximately 10 °C higher than the value obtained after the casting at 60 °C. The second heating run (after erasing the thermal history of the samples) showed glass transitions between 100 °C and 104 °C, independent of the carbon nanotube, the composition and the preparation method of the films.

Differences of the T_g of the polystyrene microphase were obtained also for the nanocomposites as a function of the casting temperature. It can be observed that the T_g of the polystyrene phase of the nanocomposites cast at 90 °C has a sharper transition, compared with the sample cast at 60 °C, which is broader. In the case of the films prepared at 90 °C, the T_g of the nanocomposites are slightly shifted to higher temperatures compared with the AS-SB_{26}. The samples containing 0.1 wt % of carbon nanotubes presented the highest T_g of the nanocomposites. This can be related with a better dispersion of the carbon nanotubes in the block copolymer and the favorable interaction between the stiff carbon nanotubes and the polystyrene chains in the block copolymer. This effect is pronounced in the case of the nanocomposite based in 0.1 wt% $PS_{14}{}^{2}MWCNT_{FC}{}^{99}$. The T_g decreases in the samples containing 0.5 wt % of carbon nanotubes. The increase of the quantity of carbon nanotubes favors the aggregation of the particles and hinders their mixing with the polystyrene microphases in the block copolymer.

Table 6.2. Glass transition temperatures of the polystyrene microphase of the AS-SB_{26} and its nanocomposites.

$T_{casting}$ = 60°C		
	1st run	**2nd run**
Sample	**T_g (°C)**	**T_g (°C)**
AS-SB_{26}	93.1	103.6
0.1 wt% $PS_{85}{}^{24}MWCNT_{FC}{}^{99}$ / AS-SB_{26}	88.7 108.6	103.8
0.5 wt% $PS_{85}{}^{24}MWCNT_{FC}{}^{99}$ / AS-SB_{26}	91.8	104.3
0.1 wt% $PS_{14}{}^{2}MWCNT_{FC}{}^{99}$ / AS-SB_{26}	93.4	103.6
0.5 wt% $PS_{14}{}^{2}MWCNT_{FC}{}^{99}$ / AS-SB_{26}	90.9 107.5	104.9
0.1 wt% $^{oxid}MWCNT_{FC}{}^{99}$ / AS-SB_{26}	92.8	101.9
0.5 wt% $^{oxid}MWCNT_{FC}{}^{99}$ / AS-SB_{26}	90.4 105.7	104.1
$T_{casting}$ = 90°C		
	1st run	**2nd run**
Sample	**T_g (°C)**	**T_g (°C)**
AS-SB_{26}	103.1	104.2
0.1 wt% $PS_{85}{}^{24}MWCNT_{FC}{}^{99}$ / AS-SB_{26}	106.3	103.5
0.5 wt% $PS_{85}{}^{24}MWCNT_{FC}{}^{99}$ / AS-SB_{26}	104.5	103.8
0.1 wt% $PS_{14}{}^{2}MWCNT_{FC}{}^{99}$ / AS-SB_{26}	107.7	104.1
0.5 wt% $PS_{14}{}^{2}MWCNT_{FC}{}^{99}$ / AS-SB_{26}	106.3	104.6
0.1 wt% $^{oxid}MWCNT_{FC}{}^{99}$ / AS-SB_{26}	105.3	100.4
0.5 wt% $^{oxid}MWCNT_{FC}{}^{99}$ / AS-SB_{26}	104.3	104.7

The T_g of the polystyrene microphase in the nanocomposites prepared at 60 °C presents an unusual behavior. The DSC curves corresponding to the first heating runs for the films prepared at 60 °C are presented in Figure 6.2. In the case of the nanocomposite that contains $^{oxid}MWCNT_{FC}{}^{99}$, the T_g increases approximately 10 °C with 0.5 wt % of filler, however, this value is inside the broad transition of the AS-SB_{26}. No changes were observed in the case of the nanocomposite containing 0.1 wt % of $PS_{14}{}^{2}MWCNT_{FC}{}^{99}$ and 0.5 wt % of $PS_{85}{}^{24}MWCNT_{FC}{}^{99}$. On the contrary, two T_g's were observed for the films having 0.5 wt % of $PS_{14}{}^{2}MWCNT_{FC}{}^{99}$ and 0.1 wt % of $PS_{85}{}^{24}MWCNT_{FC}{}^{99}$. The first transition is located in the range of the T_g of the AS-

SB_{26} and the second at approximately 10 °C higher than the first one. These two transitions could indicate the existence of two regions in the nanocomposite, one dominated by the AS-SB_{26} and another where the polystyrene chains in the block copolymer and the carbon nanotubes have favorable interactions as the one explained in chapter 5, increasing the glass transition of the polymer due to the presence of the stiff nanofiller.

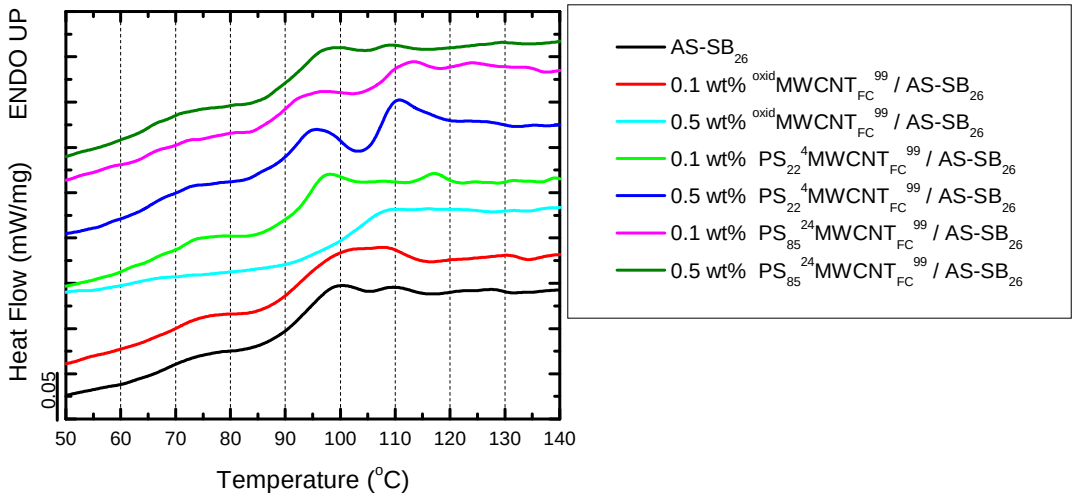

Figure 6.2. Differential scanning calorimetry scans (first heating runs, 20°C/min, N_2) of the nanocomposites films prepared at 60 °C.

6.2.4. Morphology of the AS-SB_{26} : effect of the casting temperature

The difference in the glass transition temperature of the AS-SB_{26}'s could be consequence of the block copolymer morphology after the microphase separation from solution. Selected transmission electron micrographs of the AS-SB_{26} as a function of the casting temperature can be observed in Figure 6.3. The AS-SB_{26} has a lamellar morphology independent of the casting temperature. However, the polystyrene lamellar thickness distribution presents some peculiarities as a function of the casting temperature. The polystyrene lamellae of the film cast at 60 °C presents a typical Gaussian distribution centered at 20.5 ± 0.3 nm. The lamellar thickness

distribution of the block copolymer cast at 90 °C shows a bimodal behavior. There are two populations of lamellar thicknesses of the block copolymer, one centered at 20.2 ± 0.2 nm and a second located at 15.6 ± 0.3 nm. This suggests that the morphology formed in this case is farer away from the equilibrium morphology than in the case of the films casted at 60°C. The presence of two lamellae populations indicates that the morphology of the AS-SB_{26} cast at 90 °C is more disordered than in the case of the film prepared at 60 °C. The faster casting of the AS-SB_{26} may have lead to regions where the polystyrene and the polybutadiene chains were not able to completely separate in microphases during the solvent evaporation (unfortunately, these regions are difficult to identify in the transmission electron micrographs). Therefore, the polystyrene lamellar domains are less isolated from each other and, as a consequence, the glass transition temperatures are located at temperatures typical for the homopolymers.

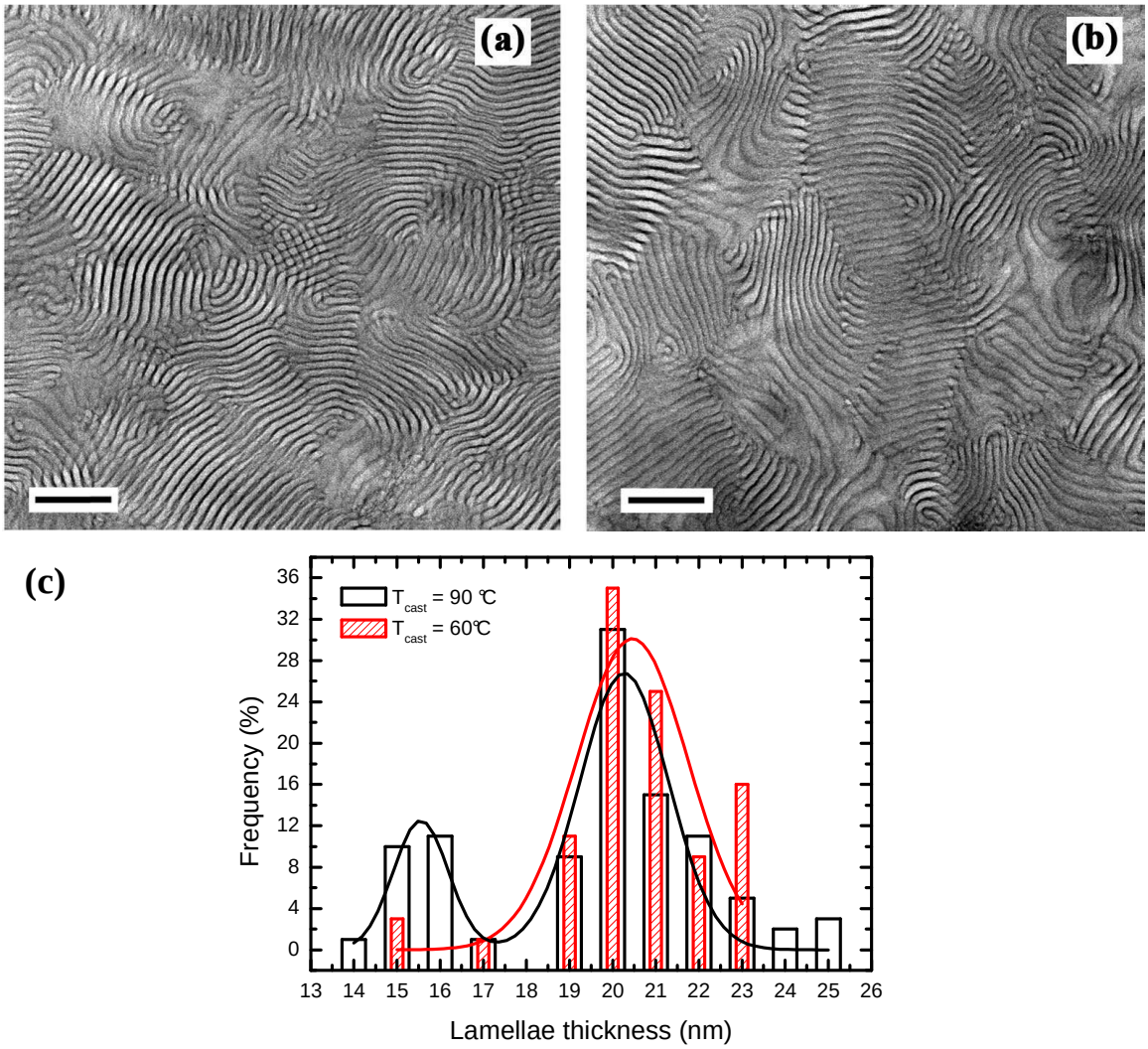

Figure 6.3. Transmission electron micrographs (stained with OSO_4; black; polybutadiene, gray; polystyrene) of the AS-SB_{26} cast at (a) 60 °C and (b) 90 °C. Ultra thin sections were obtained at approximately -120 °C. Scale bar = 200 nm. (c) Lamellae thickness distribution of the AS-SB_{26} at the indicated casting temperatures. The solid lines are the Gaussian distribution estimations of the lamellae thickness.

6.2.5. Mechanical properties of the nanocomposites

In addition, it is known that the mechanical properties of these particular block copolymers depend on the chain architecture, the morphology of the block copolymer, and the preparation.[18,19] The presence of a mixed phase between polybutadiene and polystyrene and a lamellar population of thinner thickness may affects the mechanical performance of the block copolymer. The casting temperature has a negative influence on the properties of the block copolymer. The results from the mechanical

tests can be appreciated in Table 6.3. The elastic modulus and the elongation at break of the neat AS-SB_{26} cast at 60 °C increases approximately 14% and 12%, respectively, compared to the film prepared at 90 °C.

Table 6.3. Mechanical properties of the nanocomposite as a function of the casting temperature.

$T_{casting}$ = 60°C			
Sample	***E*** **(MPa)**	**σ_b (MPa)**	**ε_b (%)**
AS-SB_{26}	590 ± 20	22 ± 2	370 ± 40
0.1 wt% $^{oxid}MWCNT_{FC}^{99}$ / AS-SB_{26}	610 ± 10	21 ± 1	320 ± 20
0.5 wt% $^{oxid}MWCNT_{FC}^{99}$ / AS-SB_{26}	640 ± 30	20 ± 1	320 ± 20
0.1 wt% $PS_{14}^{2}MWCNT_{FC}^{99}$ / AS-SB_{26}	580 ± 30	21 ± 2	370 ± 40
0.5 wt% $PS_{14}^{2}MWCNT_{FC}^{99}$ / AS-SB_{26}	630 ± 10	19 ± 1	320 ± 20
0.1 wt% $PS_{85}^{24}MWCNT_{FC}^{99}$ / AS-SB_{26}	580 ± 10	21 ± 1	340 ± 50
0.5 wt% $PS_{85}^{24}MWCNT_{FC}^{99}$ / AS-SB_{26}	580 ± 20	17 ± 1	260 ± 60
$T_{casting}$ = 90°C			
Sample	***E*** **(MPa)**	**σ_b (MPa)**	**ε_b (%)**
AS-SB_{26}	510 ± 20	20 ± 2	330 ± 50
0.1 wt% $^{oxid}MWCNT_{FC}^{99}$ / AS-SB_{26}	530 ± 30	19 ± 3	300 ± 70
0.5 wt% $^{oxid}MWCNT_{FC}^{99}$ / AS-SB_{26}	580 ± 30	16 ± 4	200 ± 100
0.1 wt% $PS_{14}^{2}MWCNT_{FC}^{99}$ / AS-SB_{26}	500 ± 20	20 ± 1	360 ± 30
0.5 wt% $PS_{14}^{2}MWCNT_{FC}^{99}$ / AS-SB_{26}	540 ± 20	18 ± 2	300 ± 70
0.1 wt% $PS_{85}^{24}MWCNT_{FC}^{99}$ / AS-SB_{26}	480 ± 20	19 ± 1	370 ± 40
0.5 wt% $PS_{85}^{24}MWCNT_{FC}^{99}$ / AS-SB_{26}	520 ± 10	18 ± 2	270 ± 50

The results corresponding to the mechanical properties of the nanocomposites are also given in Table 6.3. It can be observed that the elastic modulus of the nanocomposites slightly improves in a few cases. The elastic modulus on the AS-SB_{26} reinforced with 0.1 wt % of polystyrene grafted $MWCNT_{FC}^{99}$ does not change, no matter the temperature treatment.

The yield strength and the deformation at yield are around 14 MPa and 7 %, respectively, independent of the sample studied (results not shown). The behavior of the AS-SB_{26} at the yielding point depends on the sample preparation. For example, according to the literature, samples prepared by injection molding form neck and break at relative low deformation strains during the tensile test while samples prepared by solution casting do not form neck and the elongation at break is clearly larger than in the former case. Both samples have lamellae morphology, but in the case of the injected block copolymer, the lamellae are oriented in the flow direction, while in the solvent cast case the lamellae are randomly distributed.[19] It seems that in the present case the carbon nanotubes do not affect the deformation mechanism of the block copolymer.

The elastic moduli of the AS-SB_{26} reinforced with 0.5 wt % of the nanofillers present some differences depending on the casting temperature. The nanocomposites containing 0.5 wt% of $^{oxid}MWCNT_{FC}^{99}$ and 0.5 wt% of $PS_{14}^{2}MWCNT_{FC}^{99}$ cast at 60 °C and 90 °C bear the major increase in Young modulus compared to the AS-SB_{26}. No variations on the elastic modulus of the samples $PS_{85}^{24}MWCNT_{FC}^{99}$/AS-$SB_{26}$ were observed. The dispersion of the carbon nanotubes in the AS-SB_{26} is of paramount importance to understand these behaviors. Scanning electron microscopy images are presented in Figure 6.4. For a better identification of the carbon nanotubes using the microscope, images were taken to the samples containing 0.5 wt % of the nanofiller, however, similar conclusion regarding the dispersion can be made independent of the composition. The micrographs showed an improvement of the dispersion of single carbon nanotubes (isolated nanoparticles) with the increase of the casting temperature and the polystyrene content on the $MWCNT_{FC}^{99}$. The size and

concentration of aggregates of carbon nanotubes decreases with the increase of the casting temperature. These observations are in agreement with the ones made on the macroscopic aggregates observed by optical microscopy. In the case of the samples with 0.1 wt % of oxidized or polymer grafted $MWNCNT_{FC}^{99}$, although agglomerates are present, especially in the nanocomposite based on the $^{oxid}MWCNT_{FC}^{99}$, their size or concentration do not have an effect on the elongation at break.

As can be seen from Table 6.3, the increase of weight content of carbon nanotube decreases the elongation at break; especially for the samples containing 0.5 wt % of $^{oxid}MWCNT_{FC}^{99}$ and $PS_{85}^{24}MWCNT_{FC}^{99}$. The optical and scanning electron microscopy images showed marked differences of the dispersion of aggregates or isolated carbon nanotubes in these samples. For the nanocomposites containing $^{oxid}MWCNT_{FC}^{99}$, it is clear that the presence of macroscopic size aggregates causes the elongation at break of the sample to decrease dramatically. In the case of the nanocomposites prepared with $PS_{85}^{24}MWCNT_{FC}^{99}$, the decrease on the elongation at break might be due to aggregation of the nanoparticles during the grafting reaction, caused by coupling reactions between grafted polymer radicals. These nanoparticles are difficult to separate during the centrifugation because of the crosslinked corona polymer chains. Another explanation could be that the deformation of the nanocomposites containing $PS_{85}^{24}MWCNT_{FC}^{99}$ follows a microvoid formation mechanism in the surrounding of the $PS_{85}^{24}MWCNT_{FC}^{99}$ aggregates, due to a low cavitation stress of the polybutadiene phase compared with the polystyrene phase and the carbon nanotubes. This mechanism was described by Michler and co-workers[20] for a similar block copolymer with polystyrene inclusions. This mechanism is

possible if the interface between the carbon nanotubes and the block copolymer are intimately interconnected.

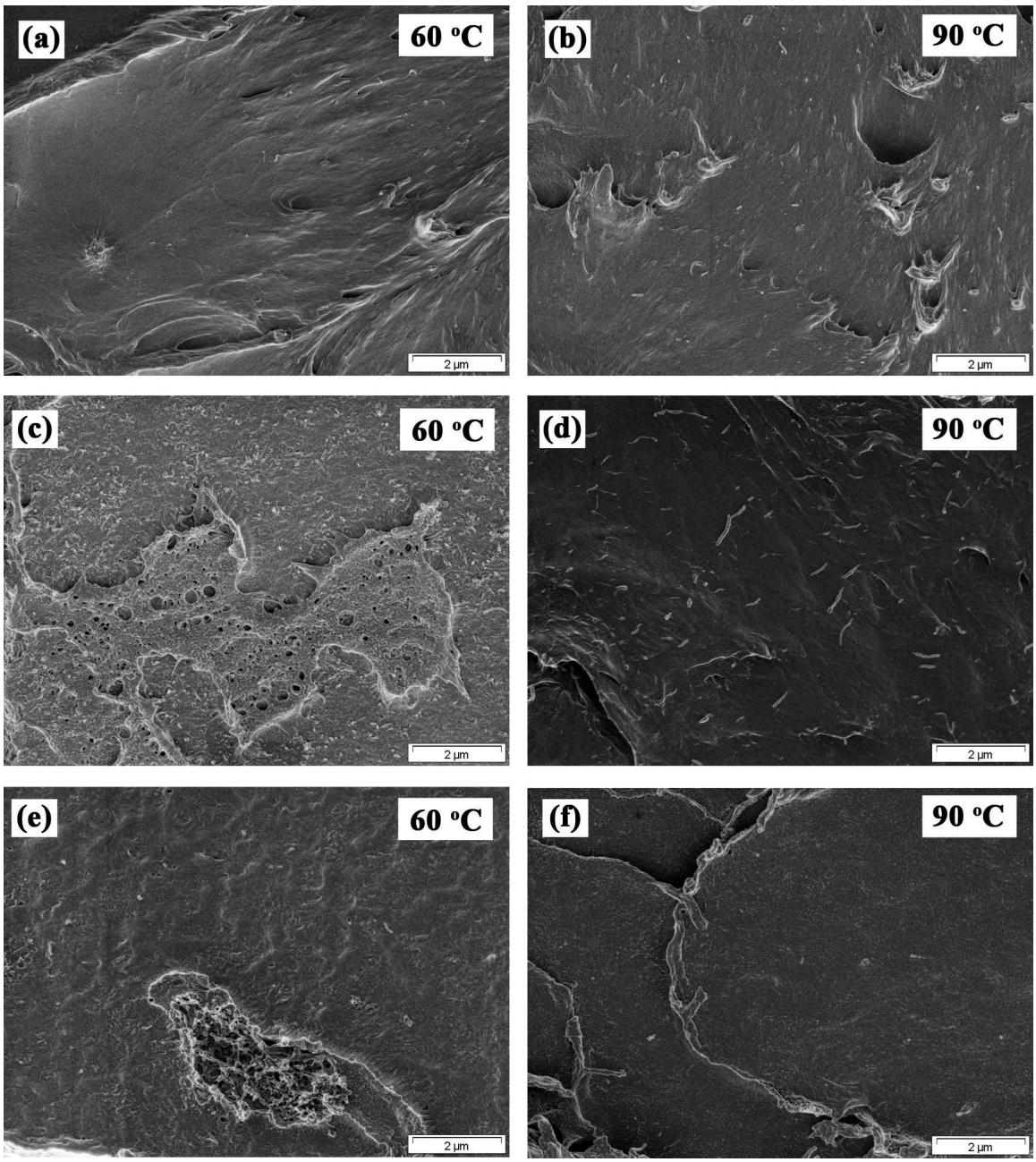

Figure 6.4. Selected scanning electron micrographs of the cryogenic fracture cross sections of the 0.5 wt % carbon nanotubes/AS-SB_{26} films prepared at different casting temperatures: (a) and (b) $^{oxid}MWCNT_{FC}{}^{99}$; (c) and (d) $PS_{14}{}^{2}MWCNT_{FC}{}^{99}$; (e) and (f) $PS_{85}{}^{24}MWCNT_{FC}{}^{99}$; The casting temperatures are indicated on the images.

Surprisingly, the nanocomposites with the poorest dispersion presented the higher values of the elastic modulus. The increase in the Young modulus of polymer

composites depends on the load transfer of the reinforcement to the matrix. It seems that the aggregates of carbon nanotubes can transfer the load more efficiently than the dispersed carbon nanotubes. A more detailed analysis regarding the dispersion quality and the load transfer of the polymer coated carbon nanotubes in homopolymers and block copolymers is necessary, and a broader spectrum of mixing conditions and carbon nanotubes loadings have to be considered.

The grafting of polystyrene from the surface of the carbon nanotubes seeks to promote a favorable interaction between the nanoparticles and the polystyrene microdomains in the AS-SB_{26}, besides the improvement in the dispersion of the nanoparticles during the casting of the films. The selective reinforcement of the polystyrene microdomains in the block copolymer pretended to increase the strength of the AS-SB_{26} without decreasing its elongation, which is dominated by the polybutadiene microphase. Surprisingly, although the elongation at break of the nanocomposites based in the polymer coated $MWCNT_{FC}^{99}$ are relative higher than for the $^{oxid}MWCNT_{FC}^{99}$, the elastic moduli of the nanocomposites are below the theoretical predictions.

6.2.6. Morphology of the nanocomposites: effect of the carbon nanotubes in the block copolymer microstructure

The selective incorporation of nanoparticles in the microphase of a block copolymer results from the interplay between the selectivity of the nanoparticle towards one microdomain (this represent an enthalpic barrier), and the relation between the size of the nanoparticle and the size of the microdomain (this represents an entropic barrier). The selective incorporation of nanoparticles in a block copolymer domain has been observed for sphere like nanoparticles when they are directly synthesized within one

domain of the block copolymer matrix,[21-24] or by direct blending of the block copolymer with surface functionalized nanoparticles that have certain compatibility with one microdomain.

The high aspect ratio, the irregular shape, and the tendency to aggregate make more complicate the inclusion of the carbon nanotubes in one microdomain of a block copolymer. Heretofore, the synthesis of carbon nanotubes in one microdomain of a block copolymer matrix is impossible due to the conditions necessary for the synthesis. The only example reported in the literature regarding the selective sequestering of a polymer grafted carbon nanotubes in a block copolymer matrix was reported by Park et al,[25] however, as it was previously described, no further conclusions or comparison can be made because no data of the functionalization of the carbon nanotubes and the blending conditions were described.

In the last chapter the influence of the $PS_{91}^{20}MWCNT_{BMS}^{95}$ in the morphology of the AS-SB_{26} was described. The $PS_{91}^{20}MWCNT_{BMS}^{95}$s were able to "locally" template the lamellar morphology of the AS-SB_{26} during the casting of the films from solution. This template effect is similar to the one described in the case of surfactant functionalized SWCNTs,[26] and for other high aspect ratio nanoparticles like clay[27,28] or graphene sheets[29] in linear block copolymer matrices.

As in the case of the $MWCNT_{BMS}^{95}$, the diameter of the $MWCNT_{FC}^{99}$ is comparable to the lamellar thickness of the polystyrene in the AS-SB_{26}. while the length of the $MWCNT_{FC}^{99}$ is several orders of magnitude larger than the microdomain size. The TEM images of the different nanocomposites can be appreciated in Figure 6.5. The

behavior of the $^{oxid}MWCNT_{FC}^{99}$ is similar to the one obtained for the pristine $MWCNT_{BMS}^{95}$, the carbon nanotubes are not selective to the polystyrene neither to the polybutadiene.

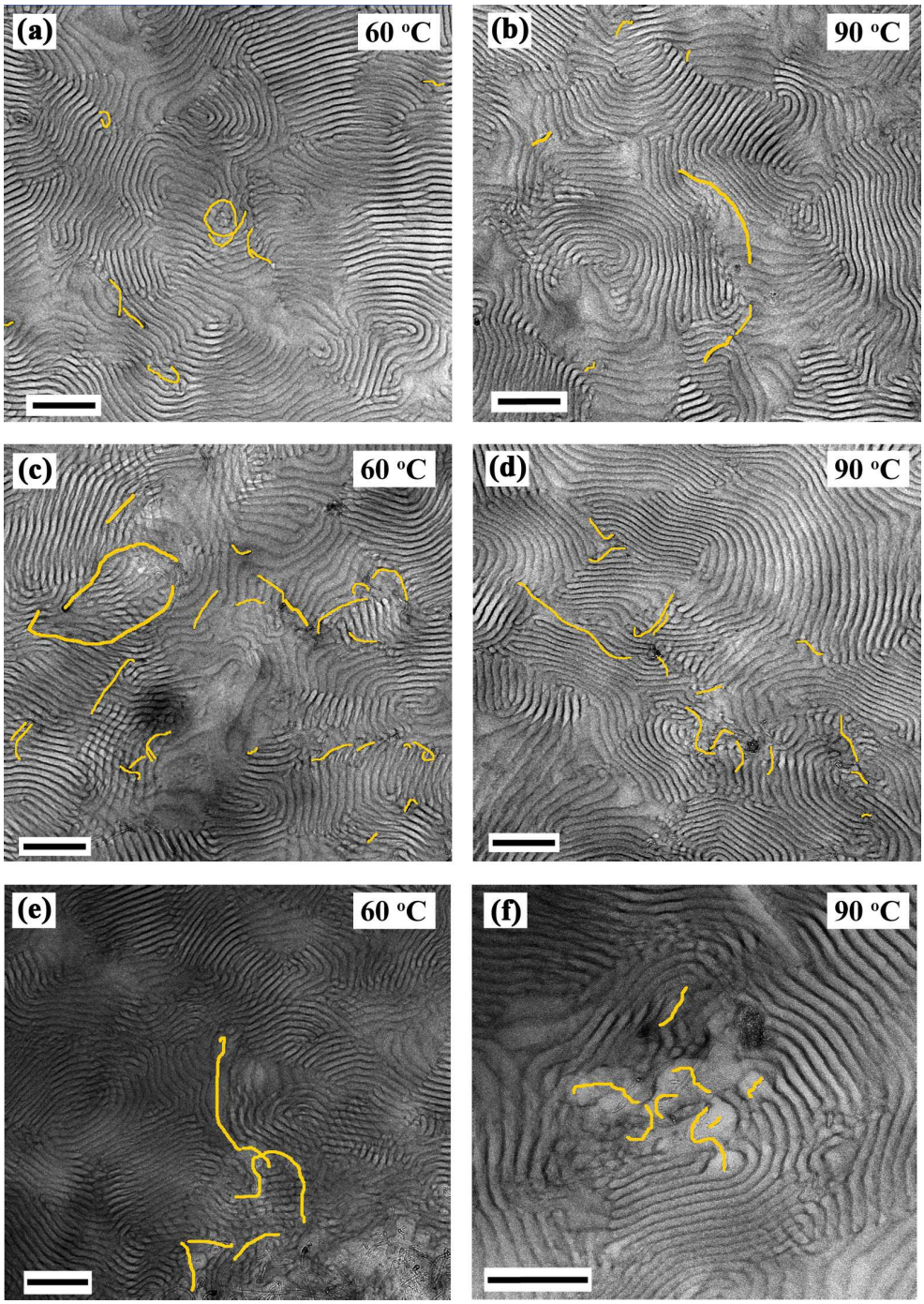

Figure 6.5. Transmission electron micrographs (stained with OSO_4; black; polybutadiene, gray; polystyrene) of the 0.1 wt % carbon nanotubes/AS-SB_{26} films prepared at different casting temperatures: (a) and (b) $^{oxid}MWCNT_{FC}^{99}$; (c) and (d) $PS_{14}{}^{2}MWCNT_{FC}^{99}$; (e) and (f) $PS_{85}{}^{24}MWCNT_{FC}^{99}$. Ultra thin sections were obtained at approximately -120 °C. The casting temperatures are indicated on the images. Scale bar = 200 nm.

The optical and scanning electron microscope images have shown a better dispersion of aggregates and isolated $PS_{14}{}^{2}MWCNT_{FC}{}^{99}$ in the AS-SB_{26} compared with the $^{oxid}MWCNT_{FC}{}^{99}$ due to the polymer coating. Though, no selective interaction with the polystyrene lamellar microphases is observed, the dispersion of the $PS_{14}{}^{2}MWCNT_{FC}{}^{99}$ is similar than the $^{oxid}MWCNT_{FC}{}^{99}$ in the TEM images. This behavior could be understood as a consequence of the relative low molecular weight, grafting content and grafting chain density of the polystyrene in the $PS_{14}{}^{2}MWCNT_{FC}{}^{99}$ (see Table 6.1), compared with the nanocomposites based on $PS_{47}{}^{11}MWCNT_{BMS}{}^{95}$ and $PS_{70}{}^{4}MWCNT_{BMS}{}^{95}$ presented in chapter 5, where the higher molecular weight, grafting content and grafting chain density of the polymer coating favors the interaction of the carbon nanotubes with the polystyrene lamellar microphase.

The increase in the concentration of initiator anchored to the surface of the $MWCNT_{FC}{}^{99}$ leads to grafted polystyrene chains with higher molecular weight (under the experimental conditions described in chapter 4), as is the case of the $PS_{85}{}^{24}MWCNT_{FC}{}^{99}$. The TEM images of the nanocomposites based on $PS_{85}{}^{24}MWCNT_{FC}{}^{99}$ (Figure 6.5(e) and (f)) showed that the carbon nanotubes are surrounded by the polystyrene microphase of the AS-SB_{26}. This demonstrates that, compared with other types of nanofiller,[27,29] the characteristics of the polymer coating at the surface of the carbon nanotubes is an important factor for the favorable interaction of the nanofiller with the AS-SB_{26}. However, the “local” template effect on the morphology is not observed, as in the case of the $PS_{91}{}^{20}MWCNT_{BMS}{}^{95}$ presented in chapter 5. The content and the molecular weight of the polystyrene grafted from the $PS_{85}{}^{24}MWCNT_{FC}{}^{99}$ and the $PS_{91}{}^{20}MWCNT_{BMS}{}^{95}$ are comparable, but

the grafting chain density of the former is approximately 4.5 times lower. The grafting chain density is an indication of the distribution of the polymer chains along the carbon nanotube. In the case of the $PS_{85}^{24}MWCNT_{FC}^{99}$ the polymer coating is may be less regular than in the case of the $PS_{91}^{20}MWCNT_{BMS}^{95}$. This difference could lead to lesser chain entanglements between the corona chains and the polystyrene blocks in the AS-SB_{26}, which induces the inclusion of the carbon nanotube within polystyrene lamellae but not the template effect observed when the $PS_{91}^{20}MWCNT_{BMS}^{95}$ was used (Figure 5.2(e)). The morphology of the nanocomposite based on $PS_{85}^{24}MWCNT_{FC}^{99}$ is comparable to the image obtained with $PS_{70}^{4}MWCNT_{BMS}^{95}$ (Figure 5.2(d)). If the intrinsic characteristics of the carbon nanotubes are not heavily considered ($MWCNT_{FC}^{99}$ vs. $MWCNT_{BMS}^{95}$), these results demonstrate that for the selective interaction between the carbon nanotubes and one microphase of a block copolymer it is necessary to control not just the molecular weight of the grafted polymer but also the grafting chain density.

6.2.7. Electrical properties of the nanocomposites

The electrical properties of the nanocomposite films have been studied by means of the AC conductivity. The increase in the electrical conductivity of a polymer due to the incorporation of conductive fillers depends on the aspect ratio of the filler, their interaction with the polymer host and their dispersion throughout the sample.[9] Figure 6.6 shows log-log plots of the specific AC conductivities as a function of the frequency for the different nanocomposites. In Figure 6.6(c) the average values at a frequency of 1 MHz can be appreciated. The behavior obtained for the AS-SB_{26} is typical for a dielectric material, where the electrical conductivity increases linearly with the frequency.

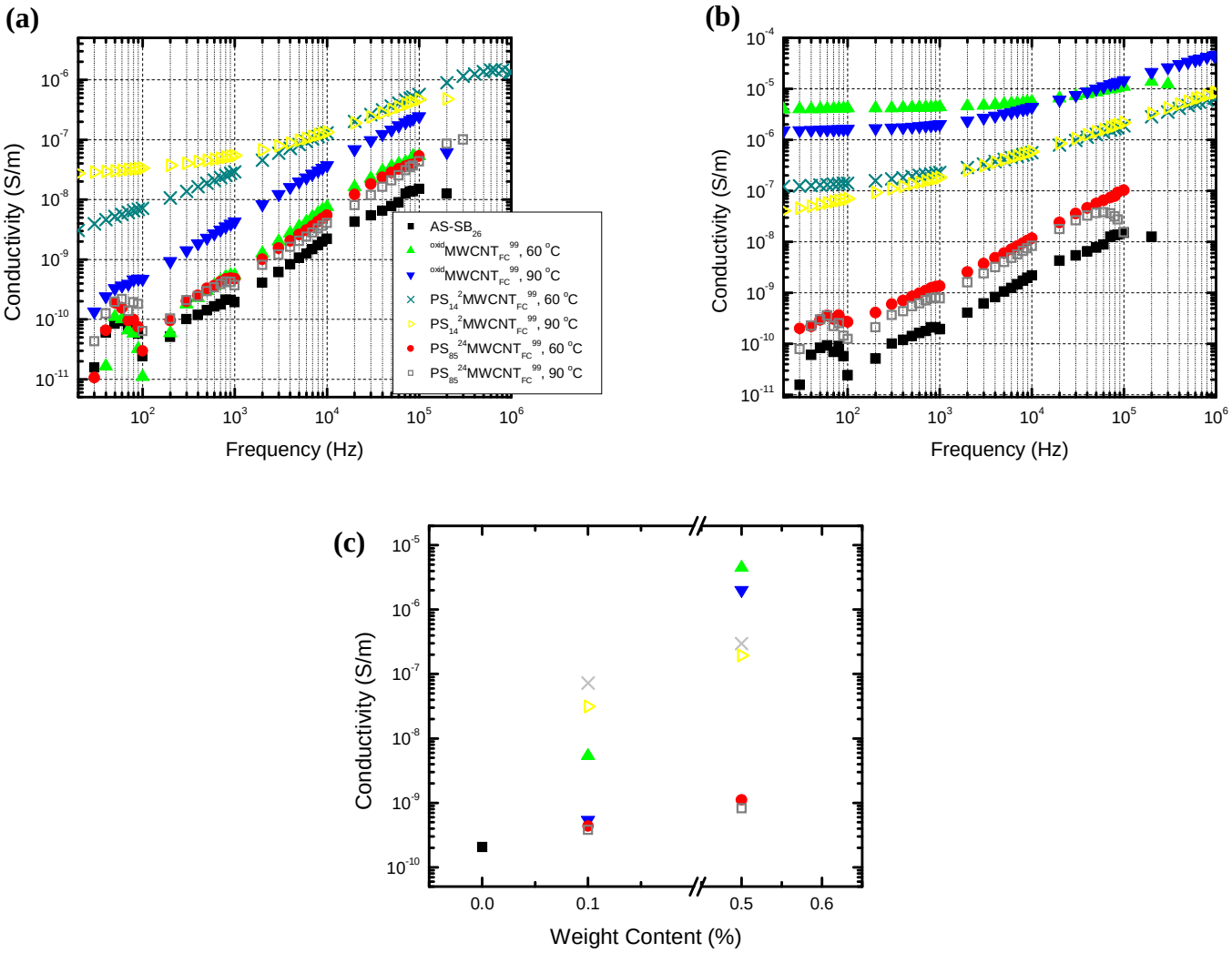

Figure 6.6. Electrical conductivities measurements of the samples containing (a) 0.1 wt% and (b) 0.5 wt% of the different functionalized $MWCNT_{FC}^{99}$. (c) Electrical conductivities at 1 x 10^3 Hz, filled points indicate the films casted at 60 °C, contour points represent the films casted at 90 °C.

As can be observed in Figure 6.6, values where the nanocomposites can be considered as electrical conductors (> ~10^{-3} S/m) were not obtained among the samples studied; however, electrical conductivity values reaching percolation transition regions were obtained. The AC conductivity at the percolation transition region is equal to the DC conductivity up to a characteristic frequency, above which the conductivity linearly increases with the frequency.[30] Variations in the electrical conductivity of the nanocomposites were observed depending of the functionalization of the carbon nanotubes.

The electrical conductivity showed a discrete variation with the temperature of the casting just for the case of the samples containing 0.1 wt % $^{oxid}MWCNT_{FC}^{99}$. In this sample, the decrease of the casting temperature to 60 °C increased the electrical conductivity in approximately one decade with respect to the sample prepared at 90 °C. In both cases, the electrical conductivity of the nanocomposites is below the percolation threshold. For this reason, the discrete increase could be related with negligible differences regarding the dispersion of the carbon nanotubes in the film.

If the nanocomposites with nanofiller content of 0.1 wt % are considered, the nanocomposites based on $PS_{14}{}^{2}MWCNT_{FC}^{99}$ showed an increment of 2.5 decades on the electrical conductivity compared to the AS-SB_{26}. This is the highest value obtained among these samples. The formation of a percolation network is a three dimensional event. For this reason, the theories related on this matter are developed considering the volume fraction of the filler in the host matrix. Though, the volume of the carbon nanotubes is difficult to measure due to the difficulties of the determination of the exact dimensions and the presence of defects on the graphitic structure, especially in the commercial product.[31] The volume fraction can be roughly estimated using the equation proposed by Thostenson et al.[32] for the determination of the density of multiwall carbon nanotubes. In the case of the $MWCNT_{FC}^{99}$, the density is approximately 1.8 g/cm^3. Then, the volume fraction of the sample containing 0.1 wt % of $MWCNT_{FC}^{99}$ is around 0.06 vol%.

Electrical conductive nanocomposite containing comparable carbon nanotube contents have been obtained in the case of epoxy base nanocomposite.[4,11] In the case of thermoplastic based nanocomposites, Poetschke et al.[9] have found electrical

percolation values of around 1.5 wt % for polyamide 6 reinforced with multiwall carbon nanotubes, whereas Saeed and co-workers have reported similar results in poly(ε-caprolactone) reinforced also with multiwall carbon nanotubes.[33] In all the mentioned cases, the dispersion of the multiwall carbon nanotubes in the polymer matrices was achieved using high shear mixing or the in-situ polymerization of the monomer in the presence of the dispersed nanoparticles. In the case presented here, the dispersion of the carbon nanotubes depends on the interaction between the nanofiller and the block copolymer during the solvent casting. The correct combination between the characteristics of the polymer grafted from the surface of the carbon nanotubes and the content of the filler could lead to the preparation of electrical conductive nanocomposites using more efficient compounding methods.

The increase in the polystyrene grafting content leads to a decrease in the electrical conductivity of the nanocomposites. Although the polymer grafted from the carbon nanotubes improves their distribution in the AS-SB_{26}, the polymer coating insulates the nanoparticles. This assumption is corroborated when the nanocomposites with 0.5 wt % content of carbon nanotubes are compared. While the $^{oxid}MWCNT_{FC}^{99}$ and the $PS_{14}^{2}MWCNT_{FC}^{99}$ showed increase in the electrical conductivity of 4 and almost 3 decades, respectively, the values obtained for the $PS_{85}^{24}MWCNT_{FC}^{99}$ are similar to the ones reported for the nanocomposites that contain 0.1 wt % of the nanoparticles.

6.3. Conclusions

Nanocomposites based on acid treated and polystyrene grafted $MWCNT_{FC}^{99}$ and commercial block copolymer (AS-SB_{26}) were prepared by film casting. The dispersion of the nanoparticles improves with the increase in molecular weight and grafting content of the polystyrene from the carbon nanotube, as well as with the

increase of the casting temperature. The carbon nanotubes grafted with the higher content of polystyrene ($PS_{85}^{24}MWCNT_{FC}^{99}$) showed the best dispersion in the AS-SB_{26} among the samples evaluated. Additionally, evidences of favorable interactions between the $PS_{85}^{24}MWCNT_{FC}^{99}$ and the the AS-SB_{26} were observed, but not as in the previous chapter ($PS_{91}^{20}MWCNT_{BMS}^{95}$/AS-$SB_{26}$ nanocomposite). The chain grafting density, the molecular weight of the grafted polymer and difference in length and curvature of the carbon nanotubes seem to play an important role on the self-assembly of these nanocomposites. The enhancement on the dispersion of the carbon nanotubes does not improve the mechanical properties of the nanocomposites. It seems that the load transfer of dispersed carbon nanotubes in this thermoplastic elastomer is not efficient in the range of compositions studied. The nanocomposites with the worse dispersion showed the highest Young moduli of this work, which leads to conclude that the load transfer within aggregated nanoparticles is more efficient than in the dispersed case. The electrical conductivity of the AS-SB_{26} is also influenced by the dispersion and polymer coating of the $MWCNT_{FC}^{99}$. The blend containing carbon nanotubes with a moderate grafting content and a low polystyrene molecular weight ($PS_{14}^{2}MWCNT_{FC}^{99}$) showed an increase in the electrical conductivity at lower weight percent than the $^{oxid}MWCNT_{FC}^{99}$. The improvement on the dispersion of the carbon nanotubes due to the polymer coating enhances the electrical conductivity of the nanocomposite. However, the polymer coating characteristics have to be controlled in order to avoid the insulation of the carbon nanotube as in the case of the $PS_{85}^{24}MWCNT_{FC}^{99}$/AS-$SB_{26}$ nanocomposites. This method of preparation of nanocomposite represents a new alternative for the design of new materials with controlled nanostructures.

6.4. References

1. Vollath, D. Nanomaterials, An Introduction to Synthesis, Properties and Applications; Wiley-VCH Verlag GmbH & Co. KGaA: Weinheim, 2008.
2. Dresselhaus, M.; Endo, M. In Carbon Nanotubes: Synthesis, Structure, Properties and Applications; Springer Berlin / Heidelberg, 2001, p 11-28.
3. Forró, L.; Schönenberger, C. In Carbon Nanotubes: Synthesis, Structure and Applications; Springer Berlin / Heidelberg, 2001, p 329-391.
4. Gojny, F. H.; Wichmann, M. H. G.; Fiedler, B.; Kinloch, I. A.; Bauhofer, W.; Windle, A. H.; Schulte, K. Polymer 2006, 47, 2036-2045.
5. Yuen, S.-M.; Ma, C.-C. M.; Lin, Y.-Y.; Kuan, H.-C. Compos. Sci. Technol. 2007, 67, 2564-2573.
6. Broza, G.; Schulte, K. Polym. Eng. Sci. 2008, 48, 2033-2038.
7. Wu, H.-X.; Tong, R.; Qiu, X.-Q.; Yang, H.-F.; Lin, Y.-H.; Cai, R.-F.; Qian, S.-X. Carbon 2007, 45, 152-159.
8. Bellayer, S.; Gilman, J. W.; Eidelman, N.; Bourbigot, S.; Flambard, X.; Fox, D. M.; De Long, H. C.; Trulove, P. C. Adv. Funct. Mater. 2005, 15, 910-916.
9. Pötschke, P.; Bhattacharyya, A. R.; Janke, A. Eur. Polym. J. 2004, 40, 137-148.
10. Sandler, J.; Shaffer, M. S. P.; Prasse, T.; Bauhofer, W.; Schulte, K.; Windle, A. H. Polymer 1999, 40, 5967-5971.
11. Sandler, J. K. W.; Kirk, J. E.; Kinloch, I. A.; Shaffer, M. S. P.; Windle, A. H. Polymer 2003, 44, 5893-5899.
12. Moniruzzaman, M.; Du, F.; Romero, N.; Winey, K. I. Polymer 2006, 47, 293-298.
13. Gao, C.; Vo, C. D.; Jin, Y. Z.; Li, W.; Armes, S. P. Macromolecules 2005, 38, 8634-8648.
14. Smallwood, I. M. Handbook of Organic Solvent Properties; Elsevier, 1996.
15. Baskaran, D.; Mays, J. W.; Bratcher, M. S. Angew. Chem., Int. Ed. 2004, 43, 2138-2142.
16. Kong, H.; Gao, C.; Yan, D. J. Am. Chem. Soc. 2004, 126, 412-413.
17. Kong, H.; Gao, C.; Yan, D. Macromolecules 2004, 37, 4022-4030.
18. Adhikari, R.; Godehardt, R.; Lebek, W.; Goerlitz, S.; Michler, G. H.; Knoll, K. Macromol. Symp. 2004, 214, 173-196.
19. Adhikari, R.; Michler, G. H.; Huy, T. A.; Ivan'kova, E.; Godehardt, R.; Lebek, W.; Knoll, K. Macromol. Chem. Phys. 2003, 204, 488-499.
20. Michler, G. H.; Adhikari, R.; Lebek, W.; Goerlitz, S.; Weidisch, R.; Knoll, K. J. Appl. Polym. Sci. 2002, 85, 683-700.
21. Bockstaller, M. R.; Lapetnikov, Y.; Margel, S.; Thomas, E. L. J. Am. Chem. Soc. 2003, 125, 5276-5277.
22. Bockstaller, M. R.; Thomas, E. L. Phys. Rev. Lett. 2004, 93, 166106.
23. Mendoza, C.; Gindy, N.; Gutmann, J. S.; Frömsdorf, A.; Förster, S.; Fahmi, A. Langmuir 2009, 25, 9571-9578.
24. Mendoza, C.; Pietsch, T.; Gindy, N.; Fahmi, A. Adv. Mater. (Weinheim, Ger.) 2008, 20, 1179-1184.
25. Park, I.; Lee, W.; Kim, J.; Park, M.; Lee, H. Sensor Actuat B-Chem 2007, 126, 301-305.
26. Peponi, L.; Valentini, L.; Torre, L.; Mondragon, I.; Kenny, J. M. Carbon 2009, 47, 2474-2480.
27. Ha, Y.-H.; Kwon, Y.; Breiner, T.; Chan, E. P.; Tzianetopoulou, T.; Cohen, R. E.; Boyce, M. C.; Thomas, E. L. Macromolecules 2005, 38, 5170-5179.
28. Ha, Y.-H.; Thomas, E. L. Macromolecules 2002, 35, 4419-4428.
29. Peponi, L.; Tercjak, A.; Verdejo, R.; Lopez-Manchado, M. A.; Mondragon, I.; Kenny, J. M. J. Phys. Chem. C 2009.
30. Jang, P. G.; Suh, K. S.; Park, M.; Kim, J. K.; Kim, W. N.; Yoon, H. G. J. Appl. Polym. Sci. 2007, 106, 110-116.
31. Lu, Q.; Keskar, G.; Ciocan, R.; Rao, R.; Mathur, R. B.; Rao, A. M.; Larcom, L. L. J. Phys. Chem. B 2006, 110, 24371-24376.
32. Thostenson, E. T.; Chou, T.-W. J. Phys. D: Appl. Phys. 2003, 36, 573-582.
33. Saeed, K.; Park, S.-Y. J. Appl. Polym. Sci. 2007, 104, 1957-1963.

Chapter 7. Summary

One of the aims of this work was the identification of the factors that affect the grafting of polymer from the surface of commercially available MWCNTs. The grafting of polystyrene from the surface of two commercially available MWCNTs was performed under atom transfer radical polymerization conditions after successive functionalization reactions. The purity, the state of aggregation and the size of the MWCNTs were found to influence the content of grafted polystyrene. The multiwall carbon nanotube with lower purity, relative shorter length and higher state of aggregation ($MWCNT_{BMS}^{95}$) showed higher grafting efficiencies along all the surface functionalization reactions than the $MWCNT_{FC}^{99}$, i.e., the one with higher carbon purity and relative longer lengths.

The presence of compact aggregates was found to decrease the viscosity during the reactions, which increases the yield of the polymerization reaction but the grafting at the surface of aggregates is favored. As a consequence, high polymer grafting contents are relatively easy to obtain with the $MWCNT_{BMS}^{95}$, but probably there is a high amount of aggregates coated with polymer. In the case of the $MWCNT_{FC}^{99}$, the nanoparticle length and the looseness of the bundles promote the disaggregation of the nanoparticles during the functionalization reaction. This leads to the increase of the viscosity of the media and decreases the yield of the reaction. However, higher polymer content can be achieved with the $MWCNT_{FC}^{99}$ when the right combination of length of glycol spacer, concentration of the anchored initiator and monomer to carbon nanotube weight ratio are employed.

These studies demonstrate that there is a correlation between the characteristics of the carbon nanotubes and the polymer grafting. Parameters like the carbon purity, the length and the state of aggregation of the carbon nanotubes are important to determine the extent of the polymer grafting. Though, the functionalization could be adjusted in order to obtain the desired degree of functionalization and molecular weight of the grafted polymer.

Nanocomposites based on pristine MWCNTs, pre-functionalized and polymer grafted MWCNTs and the block copolymer AS-SB_{26} were prepared by film casting from solution. The dispersion of the nanoparticles improves with the increase in molecular weight and grafting content of the polystyrene from the carbon nanotube. In the case of the system prepared with the polymer grafted $MWCNT_{FC}^{99}$, the nanoparticle dispersion was also enhanced by the increase of the casting temperature. For the nanocomposite based on the $MWCNT_{BMS}^{95}$, the mechanical properties of the block copolymer do not appreciably improve by compounding with polymer grafted carbon nanotubes at ambient temperature. The storage modulus at 90 °C slightly increases in the case of the polystyrene grafted $MWCNT_{BMS}^{95}$ based nanocomposites due to a better load transfer between the block copolymer and the functionalized nanotubes. In the case of the $MWCNT_{FC}^{99}$, the enhancement of the dispersion of the carbon nanotubes does not improve the mechanical properties of the nanocomposites at ambient temperature. It seems that the load transfer from the polymer matrix to the dispersed carbon nanotubes in this thermoplastic elastomer is not efficient under the compounding conditions employed in the range of composition evaluated.

The increase in the grafting density and molecular weight of the polystyrene grafted from the $MWCNT_{BMS}^{95}$ and the $MWCNT_{FC}^{99}$ influences the morphology of the AS-SB_{26}. In the case of the nanocomposite based on $PS_{91}^{20}MWCNT_{BMS}^{95}$ and AS-SB_{26}, the $PS_{91}^{20}MWCNT_{BMS}^{95}$ "locally" templates the lamellae morphology of the AS-SB_{26}, so that the lamellae resemble the contour of the $PS_{91}^{20}MWCNT_{BMS}^{95}$. A similar observation was obtained for the nanocomposite containing $PS_{85}^{24}MWCNT_{FC}^{99}$, however, comparatively a lower quantity of lamellae adapts to the shape of the $PS_{85}^{24}MWCNT_{FC}^{99}$. The difference could be related with the lower grafting density of the polystyrene and with the difference in length and the curvature of the nanotubes, the longer the nanotube the more irregular is the contour length.

The orientation of the nanocomposite under a linear deformation was observed for the samples containing $MWCNT_{BMS}^{95}$. The $PS_{91}^{20}MWCNT_{BMS}^{95}$ increases the orientation factor of the AS-SB_{26}. Due to the polymer coating, the $PS_{91}^{20}MWCNT_{BMS}^{95}$ align perpendicular to the strain direction. With this study it could be demonstrated that the local orientation of nanofillers in an external field (here: mechanical force field) can be controlled by variation of the interaction between nanofiller and matrix.

The studies on the electrical conductivity of the nanocomposites based on AS-SB_{26} and $MWCNT_{FC}^{99}$ demonstrate that the dispersion and polymer coating of the nanofiller influence the properties of the nanocomposite. The blend containing carbon nanotubes with a moderate grafting content and a low polystyrene molecular weight ($PS_{14}^{2}MWCNT_{FC}^{99}$) showed an increase in the electrical conductivity at lower weight

percentage than the $^{oxid}MWCNT_{FC}^{99}$. The improvement on the dispersion of the carbon nanotubes due to the polymer coating improves the electrical conductivity of the nanocomposite compared with the neat AS-SB_{26}, at lower loadings than the oxidized nanofillers. However, the polymer coating characteristics have to be controlled in order to avoid the insulation of the carbon nanotube as in the case of the $PS_{85}^{24}MWCNT_{FC}^{99}$.

The synthetic strategies presented in this work open the gate to further developments in the functionalization of various kinds of nanofillers, besides carbon nanotubes also inorganic materials like silica, or organic ones like the upcoming cellulose nanofibers. Besides functionalization with homopolymers, also the attachment of block copolymers to appears possible, which should allow for the adjustment of transfer of properties (e.g. electrical, mechanical or thermal properties) between matrix and filler. To some extent, the systems presented in this thesis contained already a short elastomeric oligo(ethylene oxide) block between carbon nanotube and the polystyrene, Also the attachment of different types of polymers to the same nanofiller for the adjustment of interfacial properties (useful in multiphase polymer blends), or the attachment of polymers with functional groups for further reactions (useful, for example, in melt blending) are possible future developments which will potentially lead to new nanocomposites with tailored properties.

Chapter 8. Acknowledgement

I would like to express my deep appreciation to Prof. Dr. Volker Abetz for giving me the opportunity to develop this dissertation and form part of the Institute of Polymer Research in GKSS Research Centre during these years. He was always eager to discuss and focus the most foolish ideas that sometimes I said. His support and initiative to start from the scratch this new topic in our Institute was the key for the success of this work. I am also very grateful to Dr. Adriana Boschetti-de-Fierro. Although she is the department leader of the department since two years, she guide and support this work from the very beginning. Her ideas and point of view were always of great importance and are mirrored on the dissertation. Many thank also to Dr. Michaël Alexandre, his patience and philosophy of work were extremely important during the experimental part of this work..

I would also like to thank Dr. Sérgio Funari, Dr. Stephan Roth and Dr. Andreas Timmann for their support during the X-ray measurements. Especially at this point I would like to greatly acknowledge Adriana and Daniel. The time in HASYLAB was one of the most exhausting moments during this dissertation but working with friends make the time always enjoyable.

GKSS Research Centre, the financial support by the 7th Framework Programme of the European Commision (HARCANA (NMP3-LA-2008-213277)) and the project CarboFunk (an Innocent initiative), and the fellowship given by the DAAD-HGF are greatly acknowledged.

Many thank to all the colleagues in the department “PMM” and in the groups where I have worked during these years, specially to Clarissa, Heinrich, Muni, Shahid, Golda, Nahide, Christian, Allen, Andreas, Marcio, Thea, Kristina, Karen, Sabrina, Berthold, Silvio, Brigitte, Maren, Petra, Susanne, Silke, Carsten, Holger, Regina, Aragon, Katrin, Peter and Nico for all the discussions, the inputs, the support, the good coffee and cake times, and the patience to teach me a bit of German.

I will not have enough time to give back all the help and support that my wife, friends and family gave me during these years, without them, none of these could have been possible.

APPENDIX A. Estimation of the chain grafting density from the concentration of initiator groups attached at the carbon nanotubes.

The concentration of initiator groups is not a common reference used to describe the grafting of nanoparticles with polymer corona chains. Instead, the grafting chain density is commonly used, as it was reviewed in Chapter 5. Unfortunately, the presence of different graphene layers forming the multiwall carbon nanotubes makes the determination of the grafting chain density more difficult than in the case of the SWCNTs. Nevertheless, the grafting chain density (σ/a^2) can be estimate if one assumes that this value is proportional to the concentration of initiator groups at the surface of the carbon nanotubes.

$$\frac{\sigma}{a^2} \propto \left[MWCNT_x^y - Br\right]$$

one can calculate the concentration of initiator groups at the surface of the carbon nanotubes as a function of the volume of the nanofillers knowing the density of the carbon nanotubes (equation A.1) and assuming that the carbon nanotubes are straight cylinder (Figure A.1) as

$$\left[MWCNT_x^y - Br\right]/V_{MWCNT} = \left[MWCNT_x^y - Br\right] * \rho_{MWCNT} \qquad \text{Eq. A.1}$$

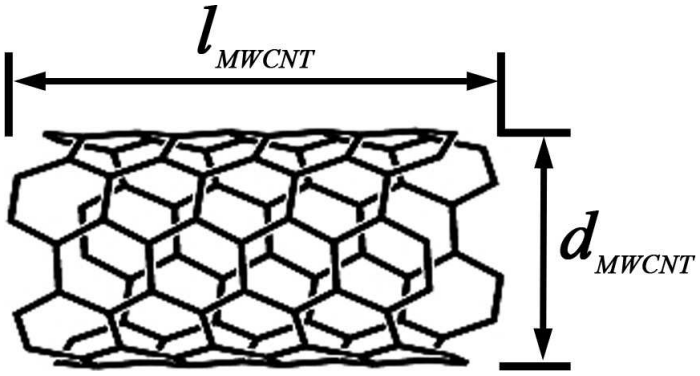

Figure A.1. Model of carbon nanotubes.

Then, assuming that the volume (V_{MWCNT}) and the surface (S_{MWCNT}) of the carbon nanotubes can be expressed as

$$V_{MWCNT} = \frac{\pi d_{MWCNT}^2}{4} l_{MWCNT} \qquad \text{Eq. A.2}$$

$$S = \pi * d_{MWCNT} * l_{MWCNT} \qquad \text{Eq. A.3}$$

The number of initiator groups per unit of surface that are equivalent to the grafting chain density can be calculate then as follow

$$\frac{\sigma}{a^2} = \frac{\left[MWCNT_x^y - Br\right] * \rho_{MWCNT} * N_A * V_{MWCNT}}{S} \qquad \text{Eq. A.4}$$

substituting in equation A.4 the equations A.2 and A.3,

$$\frac{\sigma}{a^2} = \frac{\left[MWCNT_x^y - Br\right] * \rho_{MWCNT} * N_A * \frac{\pi d_{MWCNT}^2}{4} l_{MWCNT}}{\pi d_{MWCNT} * l_{MWCNT}} \qquad \text{Eq. A.5}$$

and eliminating the common variables, one obtains finally

$$\frac{\sigma}{a^2} = \frac{\left[MWCNT_x^y - Br\right] * \rho_{MWCNT} * N_A * d_{MWCNT}}{4} \qquad \text{Eq. A.6}$$

The grafting chain density is then independent of the length of the carbon nanotubes.

List of Publications

1. Albuerne, J.; Marquez, L.; Mueller, A. J.; Raquez, J. M.; Degee, Ph.; Dubois, Ph.; Castelletto, V.; Hamley, I. W.; "Nucleation and Crystallization in Double Crystalline Poly(*p*-dioxanone)-*b*-poly(ε-caprolactone) Diblock Copolymers", *Macromolecules* **2003**, 36(5), 1633-1644.
2. Mueller, A. J.; Albuerne, J.; Marquez, L.; Raquez, J. M.; Degee, Ph.; Dubois, Ph.; Hobbs, J.; Hamley, I. W.; "Self-nucleation and crystallization kinetics of double crystalline poly(*p*-dioxanone)-*b*-poly(ε-caprolactone) diblock copolymers", *Faraday Discussions* **2004**, 128(Self-Organising Polymers), 231-252.
3. Sabino, M. A.; Albuerne, J.; Mueller, A. J; Brisson, J.; Prud'homme, R. E.; "Influence of in vitro hydrolytic degradation on the morphology and crystallization behavior of poly(*p*-dioxanone), *Biomacromolecules* **2004**, 5(2), 358-70.
4. Mueller, A. J.; Albuerne, J.; Esteves, L. M.; Marquez, L.; Raquez, J. M.; Degee, Ph.; Dubois, Ph.; Collins, S.; Hamley, I. W.; "Confinement effects on the crystallization kinetics and self-nucleation of double crystalline poly(*p*-dioxanone)-*b*-poly(ε-caprolactone) diblock copolymers", *Macromolecular Symposia* **2004**, 215(Proceedings of the 2003 International Symposium on Ionic Polymerization and Related Processes), 369-382.
5. Mueller, A. J.; Albuerne, J.; Marquez, L.; Raquez J. M.; Degee, Ph.; Dubois, Ph.; Hobbs, J.; Hamley, I. W.; "Self-nucleation and crystallization kinetics of double crystalline poly(*p*-dioxanone)-*b*-poly(ε-caprolactone) diblock copolymers", *Faraday discussions* **2005**, 128, 231-252.
6. Albuerne, J.; Marquez, L.; Mueller, A. J.; Raquez, J. M.; Degee, Ph.; Dubois, Ph.; "Hydrolytic degradation of double crystalline PPDX-*b*-PCL diblock copolymers", *Macromolecular Chemistry and Physics* **2005**, 206(9), 903-914.
7. Albuerne, J.; Boschetti-de-Fierro, A.; Simon, P. F. W.; Abetz, V.; "Modification of polymeric surfaces for the improvement of thermoplastic composites", *Polymer Preprints* (American Chemical Society, Division of Polymer Chemistry) **2006**, 47(2), 557-558.
8. Boschetti-de-Fierro, A.; Fierro, D.; Albuerne, J.; Funari, S. S.; Abetz, V.; "Thermal monitoring of morphology in triblock terpolymers with

crystallizable blocks", *Journal of Polymer Science, Part B: Polymer Physics* **2007**, 45(23), 3197-3206.

9. Lorenzo, A. T.; Arnal, M. L.; Albuerne, J.; Mueller, A. J.; "DSC isothermal polymer crystallization kinetics measurements and the use of the Avrami equation to fit the data: Guidelines to avoid common problems", *Polymer Testing* 2007, 26(2), 222-231.
10. Loos, M.; Albuerne, J.; Gomes, D.; "Herstellung von Kompositen aus Polyoxadiazol-Polymeren", *German Patent Application* **DE 10 2008 027 499.2**.
11. Albuerne, J.; Boschetti-de-Fierro, A.; Abetz, V.; "Modification of Multiwall Carbon Nanotubes by Grafting from Controlled Polymerization of Styrene: Effect of the Characteristics of the Nanotubes", *Journal of Polymer Science, Part B: Polymer Physics*, **submitted**.
12. Selvaraj, M. Albuerne, J.; Boschetti-de-Fierro, A.; Abetz, V.; "Functionalization of Carbon Materials using Diels-Alder Reaction", *Macromolecular Rapid Communications*, **submitted**.